CARBONACEOUS ADSORBENTS AS COATINGS FOR ULTRAFILTRATION MEMBRANES

A Thesis
Presented to
the Graduate School of
Clemson University

In Partial Fulfillment
of the Requirements for the Degree
Master of Science
Environmental Engineering and Earth Sciences

---

by
Jaclyn R. Ellerie
May 2012

Accepted by:
Dr. David Ladner, Committee Chair
Dr. Tanju Karanfil
Dr. Cindy Lee

ABSTRACT

The feasibility of using adsorptive carbonaceous coatings on ultrafiltration (UF) membranes was evaluated by quantifying atrazine and methylene blue removal capabilities in addition to flux reductions associated with adsorbent applications. Various alternative adsorbents were incorporated in this study, including multi-walled carbon nanotubes (MWCNTs), nano-graphene platelets (NGPs), and superfine powdered activated carbon (S-PAC), for comparison with a more traditional material, powdered activated carbon (PAC). All adsorbents except S-PAC were associated with filtration flux reductions of less than 5% after application as a membrane coating during constant pressure tests, and flux recovery after membrane backwashing was greater than 88% for all materials and masses tested.

For removal of methylene blue in a lab-scale UF system, S-PAC showed fast adsorption kinetics and a steep breakthrough curve. It is likely that the mesopore volume and large external surface area available for adsorption contributed to this phenomenon. MWCNTs were inferior to PAC for overall methylene blue removal, which may be attributable to their lower surface area, extensive aggregation, and lack of micropores. The breakthrough was slower with adsorption occurring in a stirred vessel configuration than through adsorption in a carbon coated membrane, but overall contaminant removal was roughly equivalent in both cases. With atrazine as the second model contaminant, S-PAC and NGPs were the most efficient for rapid adsorption, while MWCNTs and PAC had slower kinetics. Using a stirred vessel setup rather than the coated membrane resulted

in lower retention of atrazine for all adsorbents, which is in contrast with the methylene blue results.

The homogeneous surface diffusion model (HSDM) for packed-column adsorption was applied to the membrane coating results, with significant deviations noted. The deviations likely resulted in part from inaccurate estimation of the surface diffusion coefficient, since adjustment of this parameter in the model yielded well-fitted curves. The linear driving force (LDF) model showed better accuracy, though this model was considered empirical. Considering the minimal flux reduction associated with adsorbent application on the membrane as well as contaminant removal capabilities, membrane coatings have the potential to be a transformative technology for water treatment.

DEDICATION

I would like to dedicate my thesis to my family, who have always been supportive of my endeavors.

ACKNOWLEDGEMENTS

I would like to acknowledge my advisor, Dr. David Ladner, who was willing to meet with me on a weekly basis to discuss my results and future experiments. I would also like to acknowledge Dr. Tanju Karanfil and Dr. Cindy Lee for their willingness to be members of my committee.

NGPs and MWCNTs used in this project were supplied by Dr. Karanfil, and S-PAC and PAC were provided by Dr. Detlef Knappe at North Carolina State University. Pore size measurements were obtained by Dr. Qiliang Wang, and the data for the carbon-membrane cross-linking portion of this project were collected by Ashton Schultz, a participant in the Advanced Functional Membranes REU Program.

TABLE OF CONTENTS

Page

Table of Contents (Continued)

Page

Table of Contents (Continued)

Page

Table of Contents (Continued)

Page

LIST OF TABLES

LIST OF FIGURES

List of Figures (Continued)

Figure Page

List of Figures (Continued)

Figure Page

List of Figures (Continued)

Figure Page

LIST OF SYMBOLS AND ABBREVIATIONS

Abbreviations

ATR	Attenuated Total Reflectance
BBOT	2,5-bis-(5-tert-Butylbenzoxazolyl)-thiophene
BET	Brunauer-Emmett-Teller
CNTs	Carbon Nanotubes
CSTR	Completely Stirred Tank Reactor
CUR	Carbon Usage Rate
DOM	Dissolved Organic Matter
FTIR	Fourier Transform Infrared Spectroscopy
GAC	Granular Activated Carbon
HSDM	Homogeneous Surface Diffusion Model
IUPAC	International Union of Pure and Applied Chemistry
LDF	Linear Driving Force (model)
lmh	Liters per meter squared per hour ($L/m^2/h$)
MCL	Maximum Contaminant Level
MV	Molar Volume
MW	Molecular Weight
MWCNTs	Multi-walled Carbon Nanotubes
N/A	Not Applicable
NDMA	*N*-nitrosodimethylamine
NGPs	Nano-graphene Platelets

PAC	Powdered Activated Carbon
PAC/UF	Powdered Activated Carbon/Ultrafiltration
pH_{pzc}	Point of zero charge pH
PolyDADMAC	Polydiallyldimethylammonium Chloride
PVDF	Polyvinylidene Difluoride
SEM	Scanning Electron Microscope
S-PAC	Superfine Powdered Activated Carbon
SVF	Specific Volume Filtered
SWCNTs	Single-walled Carbon Nanotubes
UF	Ultrafiltration
UV/Vis	Ultraviolet/Visible (spectroscopy)

Symbols

A	Absorbance
C	Liquid-phase concentration
C_e	Liquid-phase concentration at equilibrium
C_0	Initial liquid-phase concentration
$\bar{c}$	Dimensionless liquid-phase concentration
$\bar{c}_s$	Dimensionless liquid-phase concentration at particle surface
d	Membrane diameter
d_p	Particle diameter
D_l	Liquid-phase diffusion coefficient

D_p	Pore diffusion coefficient
D_s	Solid-phase diffusion coefficient
h	Height of carbon layer
J	Flux
J_0	Reference flux through an uncoated membrane
k_f	Film transfer coefficient
K_F	Freundlich constant
K_L	Langmuir constant
M	Number of collocation points in carbon layer
m_0	Mass of carbon
m_1	Mass of carbon required for a membrane monolayer
N	Number of collocation points in adsorbent particle
n	Freundlich constant
P	Pressure
q	Solid-phase concentration
$\bar{q}$	Dimensionless solid-phase concentration
q_e	Solid-phase concentration in equilibrium with C_0
q_0	Langmuir constant
r	Radial position
$\bar{r}$	Dimensionless radial position
R	Equilibrium parameter
R_c	Carbon layer resistance

R_m	Membrane resistance
Re	Reynolds number
t	Time
t_0	Characteristic time
T	Dimensionless time
V	Volume of the carbon layer (with interstitial voids)
V_p	Volume of adsorbent particles (without interstitial voids)
v_s	Superficial velocity
z	Axial position
$\overline{z}$	Dimensionless axial position
ε	Adsorbent layer porosity
ε_p	Intraparticle porosity
η	Feed solution viscosity
ρ	Apparent particle density of adsorbent
ρ_s	Solution density
ϕ	Correlation parameter
τ	Residence time in carbon layer

CHAPTER ONE

INTRODUCTION

A study in the 1990s highlighted the long-range transport of heavy metals, radionuclides, and organic contaminants of industrial and agricultural origin. Such transport has led to the detection of these species in the air, snow, and sea water of remote Arctic areas (*1*). Based on these findings, it is unlikely that there remains any liquid surface water on this planet unaffected by anthropogenic chemicals. In fact, a recent study in the United States revealed the presence of herbicides, steroids, flame retardants, pharmaceuticals, and plasticizers in drinking water sources, with a median of four different contaminants detected at each sampling site (*2*).

Although contaminant concentrations in drinking water typically do not exceed the microgram-per-liter level, the long-term effects on humans exposed to low-level water contamination are not known with certainty. Results from animal testing require high-to-low dose extrapolations and other approximations when estimating effects on humans. Nonetheless, extensive data indicate the carcinogenicity of many organic contaminants, and detections in drinking water have in the past exceeded maximum contaminant levels (MCLs) set by the EPA (*3*). For example, atrazine, an herbicide that has been found to have endocrine-disrupting properties, has exceeded its MCL of 3 μg/L at a Midwestern treatment plant on at least one occasion (*4*).

As the detection limits of analytical instruments decrease, new pollutants become identifiable in source and treated water. Despite improvements in detection, many commercially available chemicals remain free of any control measures, with only

approximately 1% of chemicals regulated in any part of the world (*5*). Consequently, improvements to water treatment technologies are desirable for reducing the prevalence of regulated and unregulated contaminants in drinking water, thereby improving public health.

Powdered activated carbon (PAC) has been coupled with ultrafiltration (UF) processes in drinking water treatment for the removal of contaminants. PAC has been selected for this purpose because its large surface area, on the order of several hundred meters squared per gram, provides an extensive number of adsorption sites, in particular for hydrophobic organic contaminants. However, new carbonaceous materials with potential adsorptive capabilities have been developed in recent years and merit study for application to membrane systems. This project examined the advantages and drawbacks of three novel adsorbents and differing UF system setups, considering contaminant removal effectiveness as well as flux reduction and flux recovery characteristics.

CHAPTER TWO

BACKGROUND

2.1 Activated Carbon

2.1.1 Origins and Production

According to the International Union of Pure and Applied Chemistry (IUPAC), activated carbon is "a porous carbon material, a char which has been subjected to reaction with gases, sometimes with the addition of chemicals before, during, or after carbonization to increase its adsorptive properties" (*6*). Carbonization is the use of pyrolysis to transform organic material to elemental carbon, which occurs through a multitude of reactions. The resulting char is then "activated" by thermal or chemical mechanisms, though a combination of the two may be employed to achieve a desirable level of porosity (*7*). Thermal activation consists of partial oxidation with high-temperature carbon dioxide, air, or steam to create a microporous structure, while agents such as zinc chloride and phosphoric acid may be used in chemical activation.

As a result of activation, unique surface characteristics arise on the carbon. Typical raw materials include coal, wood, and coconut shells, but in recent years other materials, such as newspapers and corncobs (*8, 9*), have been converted to activated carbons with the intent of utilizing waste products as adsorbents.

2.1.2 Applications

The uses for activated carbon span many industries, and applications exist for both gas and liquid-phase processes. Primarily employed for contaminant removal, it may be found in cigarette filters, fish tank filters, and household filters for faucets. On an

industrial scale, it is used for purification in refineries and as a catalyst (*7*). However, Figure 2.1 shows that water treatment facilities are the main destination for activated carbon produced in the United States.

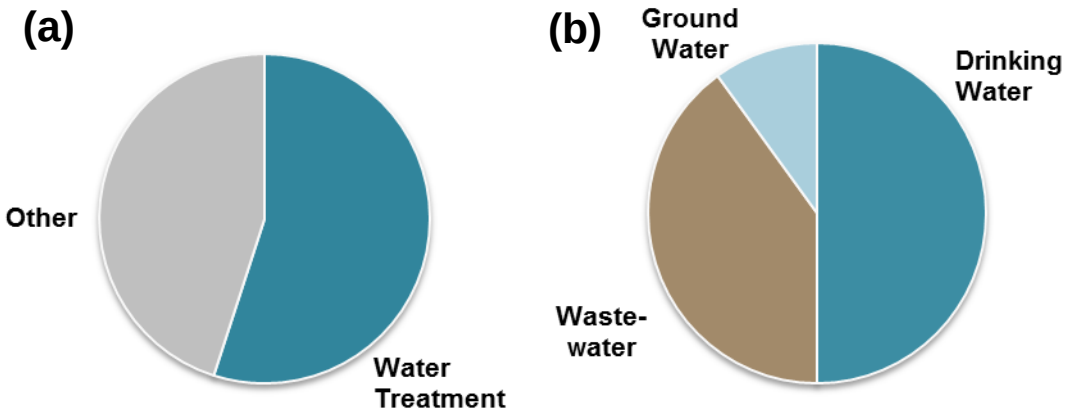

Figure 2.1. (a) The distribution of activated carbon applications in the United States, and (b) the distribution of activated carbon applications in water treatment. Based on data presented in ref. [7].

Typical forms of activated carbon utilized in water treatment include granular activated carbon (GAC), with a particle size of 1-2 mm, and PAC, with a particle size up to about 150 µm. The usefulness of activated carbon for adsorption of contaminants stems from its extensive surface area, which is in the approximate range of 800-1000 m^2/g. It is mainly applied for organic pollutant removal from water, though it is also implemented for odor, taste, and color refinement (*7*, *10*).

2.1.3 Factors Influencing Adsorption

The ability for an activated carbon to remove a pollutant from a water supply depends on characteristics of the adsorbent, target contaminant, and solution, which are

summarized in Table 2.1. How the adsorbent interacts with the target contaminant and other components of the solution governs the adsorption capacity as well as kinetics.

Table 2.1. Factors Influencing Adsorption on Activated Carbon (*7*)

Adsorbent Characteristics	Adsorbate Characteristics	Solution Characteristics
○ Porosity (interparticle and intraparticle) ○ Surface chemistry ○ Surface area ○ Particle size	○ Dimensions and molar volume ○ Polarity ○ Concentration ○ pK_a	○ pH ○ Water hardness ○ Temperature ○ Ionic strength ○ Competing species (i.e. organic matter)

The pore structure of the carbon is important to consider because the adsorbate molecules may be influenced by size exclusion, and different pore sizes are associated with different adsorption energies. Macropores, which are classified as those having diameters greater than 50 nm, are poorly suited for adsorption compared to mesopores, ranging from 2 nm to 50 nm, and micropores, which are less than 2 nm (*10*). Adsorption in micropores is associated with the greatest adsorption energy, since the confined space allows several points of contact (*11*). The optimal pore size is dependent upon characteristics of the adsorbing molecule, including dimensions and geometry. For example, the optimal pore size for adsorption of atrazine, an herbicide that contaminates drinking water, is 10-20 Å (1-2 nm), which falls under the classification of secondary micropores (*12*).

There are two distinct descriptors for porosity: intraparticle and interparticle. Voids inside an individual carbon particle constitute intraparticle porosity. The packing of the particles in an adsorbent bed or layer influences the fraction of interparticle voids

relative to the total bed volume. Interparticle porosity is relevant to GAC columns as well as PAC coating applications, the focus of this project. Because larger voids indicate a longer diffusion distance necessary for contaminant-adsorbent contact, a high interparticle porosity is associated with slower adsorption. Although interparticle porosity is independent of adsorbent particle size, the particle size influences adsorption kinetics and, to a lesser extent, adsorption capacity at equilibrium (*13*).

Surface chemistry and surface area are additional characteristics that result from the choice of raw material and activation process. Numerous functional groups may be present in activated carbons, some of which are depicted in Figure 2.2. Carbonaceous materials are hydrophobic, but oxygen groups at the surface reduce hydrophobicity, leading to enhanced sorption of water molecules. Water molecules may form three-dimensional, hydrogen-bonded clusters at the surface (*14*). Although oxygenated groups constitute only a small fraction of the adsorbent surface, their affinity for water molecules has been shown to reduce sorption capabilities for the target contaminant. One study concluded that adsorbents with higher surface acidities are associated with reduced adsorption of hydrophobic organic contaminants, a phenomenon that originates with increased polarity at the carbon surface (*15*).

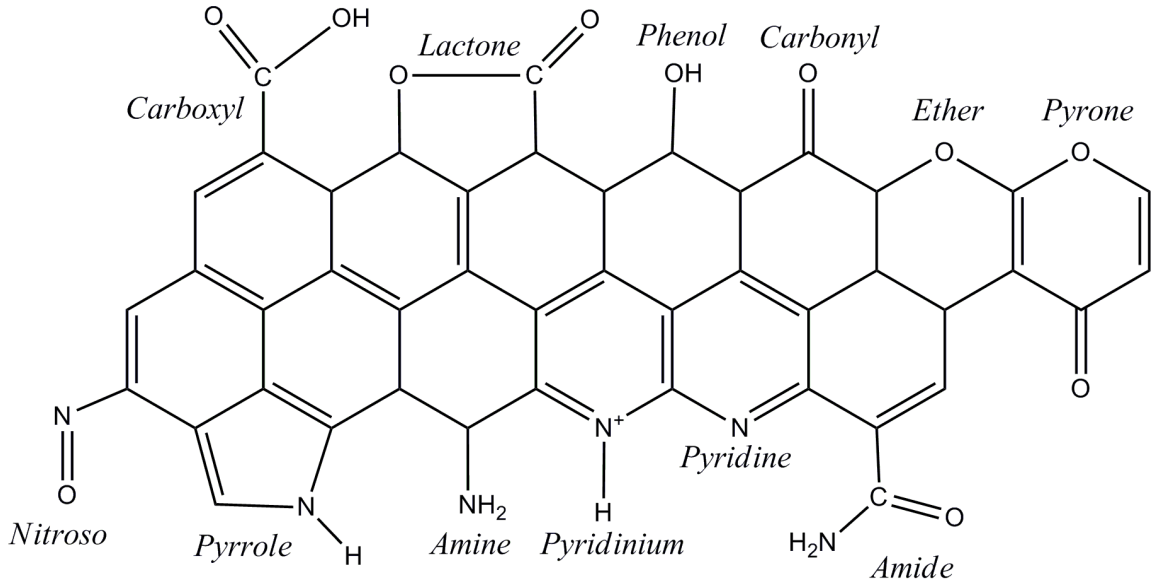

Figure 2.2. Examples of oxygen and nitrogen-containing functional groups on an activated carbon surface. Adapted from ref. [7] and [10].

Research has shown that activated carbons contain ionic groups, which include calcium, sulfate, and phosphate (*16*). Sulfur and phosphorus have also been described as heteroatoms in the carbon structure. Furthermore, specific surface modifications may be employed to impart desired surface qualities on the adsorbent. Techniques for the evaluation of surface chemistry, which include elemental analysis and FTIR (*17*), may offer information about specific functional groups and elements present, and net external charge may be determined using zeta potential measurements. The pH at which the net surface charge is zero is termed the point of zero charge, or pH_{pzc} (*18*); the net surface charge is negative or positive at pH values higher or lower than pH_{pzc}.

Properties of the target contaminant are important for predicting adsorption on a particular adsorbent. If a contaminant molecule is not able to enter small pores because of size exclusion, the accessible surface area and adsorption capacity of the adsorbent

decrease (*7*, *19*). The polarity of the adsorbate determines the magnitude of the forces associated with adsorption, which occurs through London dispersion forces, specifically dipole and induced dipole. In addition, aromatic compounds can undergo π-π interactions with the carbon surface (*7*).

If the contaminant has a pK_a that falls in the pH range of the water in contact with the adsorbent, then the protonation and deprotonation associated with pH changes may influence how well the contaminant is retained at the carbon surface. One last important factor is contaminant concentration. The isotherm for the contaminant of interest provides information about the adsorption capacity at different concentrations. As concentration increases, adsorption capacity increases. However, the effect of increased adsorption capacity with increasing concentration may not be noticeable with small variations in concentration, and adsorption capacity is essentially constant at higher concentrations.

In addition to pH and concentration, there exist many different solution characteristics that have the potential to influence adsorption. Most of these characteristics pertain to the presence of other species in the solution. For example, natural organic matter (NOM) sorbs to activated carbon and is ubiquitous in natural waters. Consequently, it competes with the target contaminant for adsorption sites on the carbon surface. In addition to the issue of competitive adsorption, NOM can have a pore-blocking effect, thereby hindering the effectiveness of contaminant removal (*20*). However, some activated carbon adsorption efforts are specifically directed at the removal of dissolved organic matter (DOM). Studies have shown that the effectiveness for adsorption of DOM on GAC increases with increasing ionic strength, which was

thought to be a result of a decrease in effective molecular size for the DOM. In particular, divalent ions such as calcium were shown to have a greater effect than monovalent ions (*21*).

2.1.4 Regeneration

Contaminants adhere to carbon surfaces through physical adsorption, a reversible process, so regeneration is feasible. However, regeneration of PAC is not usually considered economically advisable (*11*), so most regeneration efforts are directed at GAC. The carbon may be exposed to high temperatures to promote volatilization of sorbed chemicals and decomposition of sorbed organic matter, though this process can result in 8-15% adsorbent loss (*7*). Other options include steam, solvents, or other chemicals that are applied to react with and eliminate a specific adsorbate from the surface. Lastly, digestion by microorganisms is less energy and resource intensive than the other methods (*11*), potentially converting toxic adsorbates to benign substances. However, this technique requires optimization and control of the environmental conditions needed to ensure colony growth, including temperature and pH.

2.2 Alternative Adsorbents

Throughout this text, the term “alternative adsorbents” is used as a descriptor for recently developed materials that are under study to act as substitutes for PAC in adsorption processes. This designation includes three carbon-based materials analyzed in this project: superfine powdered activated carbon (S-PAC), multi-walled carbon nanotubes (MWCNTs), and nano-graphene platelets (NGPs).

2.2.1 Superfine Powdered Activated Carbon

With the proper equipment, PAC can be ground into S-PAC, which is characterized by a submicron particle size. The fraction and size of macropores is likely to be lower on S-PAC than on PAC because of the large reduction in particle size. Faster adsorption kinetics is cited as the main motivation for the application of S-PAC to water treatment (*22*), as verified using dissolved organic carbon and trace organic contaminants (*23*).

2.2.2 Carbon Nanotubes

Described as "helical microtubules of graphitic carbon," CNTs were brought to attention through their production at a laboratory scale in 1991 (*24*). MWCNTs consist of concentric tubes that have diameters typically in the range of 2-25 nm and lengths of several micrometers, while an SWCNT consists of a single microtubule of diameter 1-2 nm (*25*).

Adsorption between the walls of an individual multi-walled tube is unlikely because the gaps are not sufficiently large for the entrance of a contaminant (*26*). However, CNT aggregation is extensive, and the voids created by the aggregates can act as pores for adsorption (*27*). Consequently, adsorption may occur on the external surface of CNTs, the inner wall of the center tube, or in the pores formed from aggregation. Aggregation is accompanied by a decrease in surface area, however, and it is described as an unfavorable phenomenon (*28*). As with activated carbon adsorbents, some surface chemistry may be observable on CNTs. Alternatively, specific surface functionalization may be imparted by exposure to oxidizing agents such as HNO_3, H_2O_2, or $KMnO_4$,

though this type of alteration has been shown to reduce adsorption capabilities for hydrophobic contaminants (*29*).

2.2.3 Graphene

Like CNTs, graphene is a hydrophobic material with graphitic properties; it consists of carbon atoms arranged hexagonally into sheets of single-atom thickness (*30*). One form of graphene, NGPs, have nanoscale thicknesses and diameters of several micrometers. While graphene has potential applications in electronics (*30*), its usefulness as an adsorbent has been investigated in a few recent studies (*31, 32*). Adsorption mechanisms on graphene are similar to those for CNTs, except that the available surface area and pore structure formed through aggregation are different because of its sheet-like primary morphology.

2.3 Adsorbent/Membrane Systems

Carbonaceous adsorbents have been integrated into water treatment systems in a variety of ways. Flow-through columns with residence times of several minutes may include GAC as a substrate, while PAC may be integrated in the water treatment process through addition at a specified point to impart a desired residence time.

2.3.1 Conventional PAC/UF

One use for PAC in a treatment system involves addition to a mixed tank preceding a filter, such as a UF membrane, in a process called PAC/UF, which is shown in Figure 2.3. The membrane is typically a polymeric material, which for UF has a pore size range of approximately 0.01-0.2 μm (*33*). Because of the larger pore size compared to nanofiltration and reverse osmosis, most organic molecules are not sufficiently

retained by the membrane. However, it is useful for preventing larger particles, such as viruses and macromolecules, from entering the effluent. Microfiltration (MF) and UF systems are becoming more prominently used in water treatment as capital costs decrease and flexibility for implementation improves. In 2000, there were 110 new installations for membrane treatment systems, following an upward trend (*33*).

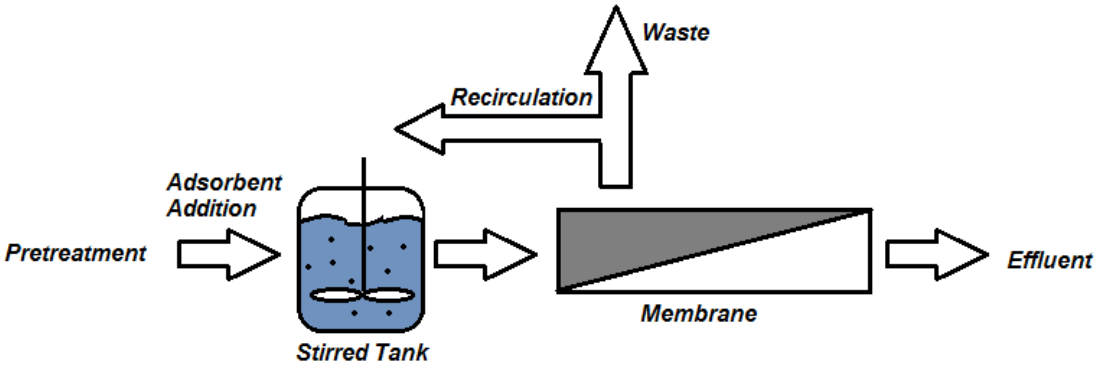

Figure 2.3. Schematic of a PAC/UF treatment plant implementing a stirred tank for adsorption. Adapted from ref. [34].

One advantage of PAC/UF is that a low pressure, on the order of 15 psi (*33*), may be used, corresponding to a reduced energy requirement compared to reverse osmosis for example, which runs at 800-1000 psi. A notable characteristic of PAC/UF is the accumulation of PAC particles on the membrane to form a layer (*35*). In cross-flow filtration, the layer has been observed to reach a maximum thickness, after which PAC deposition equals removal due to the fluid flow (*36*). Backwashing is applied every 30-90 minutes to remove foulants from the system and regenerate PAC (*37*), and chlorine may be used during backwashing to impede bacterial growth on the membrane (*38*). However, chlorine may negatively impact adsorption capabilities by oxidizing the carbon surface.

A survey of membranes for trace contaminant removal at the nanogram-per-liter level confirmed that UF is not suitable for most pollutants, though retention up to 90% was noted for steroidal compounds (*39*). The retention of the target compounds was probably a result of adsorption on the membrane polymer, which would eventually reach capacity. Conversely, a removal of 50% or more was measured for 58 out of 65 tested compounds when PAC was incorporated in the filtration setup at a dose of 5 mg/L (*39*). One commercial PAC/UF application is termed CRISTAL® (Combination of Reactors, Including Membrane Separation Treatment and Adsorption in Liquid), which has been implemented at treatment plants in France to alleviate problems with taste and odor, organic micropollutants, and halogenated compounds, issues that were not adequately addressed with GAC columns (*40*).

2.3.2 Alternative PAC/UF: Membrane Coatings

The setup utilized in this project implements an intentionally applied adsorbent layer on the membrane, which would be represented by Figure 2.4 for a full-scale system. In this proposed setup, the adsorbent is added after a backwashing cycle directly to the influent water preceding the membrane, rapidly forming a coating without interruption in the filtration process.

One objective of this project is an evaluation of the adsorption kinetics for each of the two PAC-membrane systems: the membrane coating and the stirred vessel approach described in the previous section. An immediately discernible advantage of the membrane coating technique is the elimination of the need for an adsorption tank, as the intent is to form the membrane coating rapidly after the addition of the adsorbent to the

system. The absence of the adsorption tank reduces the amount of space needed for the UF system and also decreases energy requirements because the need for stirring is eliminated.

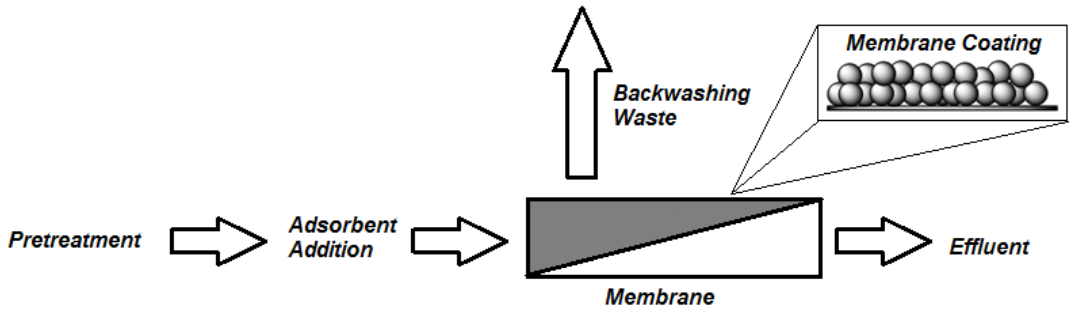

Figure 2.4. Schematic of a full-scale treatment plant implementing membrane coatings.

While membrane fouling is a concern with the carbon layer, PAC particles are often large enough to prevent a significant flux reduction (*36*). In fact, a reduction of membrane fouling has been observed with PAC coated membranes, since the adsorbent layer prevents some foulants in the influent water from reaching the membrane (*41-42*). This constitutes a key advantage of the carbon layer. However, there are some conflicting reports in the literature, with some studies indicating that hydrophobic membranes may be fouled by PAC (*43*). Ensuring compatibility of the adsorbent and membrane is an important consideration for the design of PAC-membrane systems.

One study showed that S-PAC coatings tested on a lab scale exhibited better atrazine adsorption kinetics compared with PAC and also prevented biopolymer foulants from reaching the membrane (*23*). Other research for wastewater treatment has shown that PAC coatings applied to hollow-fiber microfiltration membranes decrease flux reductions (*44*).

An additional incentive for the use of membrane coatings is related to the dependence of adsorption capacity on bulk liquid concentration. With the membrane coating technique, the adsorbent is in contact with the contaminant at concentrations present in the feed solution, as shown in Figure 2.5a. However, with the stirred vessel approach, the adsorbent is in contact with a solution of reduced contaminant concentration as the adsorbate molecules are being removed from solution in the enclosed vessel (Figure 2.5b). Analysis of an adsorption isotherm, such as that in Figure 2.5c, shows that as equilibrium concentration increases, adsorption capacity increases, a characteristic that is most prominent at low concentrations that would be typical of a water treatment scenario. Consequently, the possibility of an increased adsorption capacity for membrane coatings is a key feature of the technique.

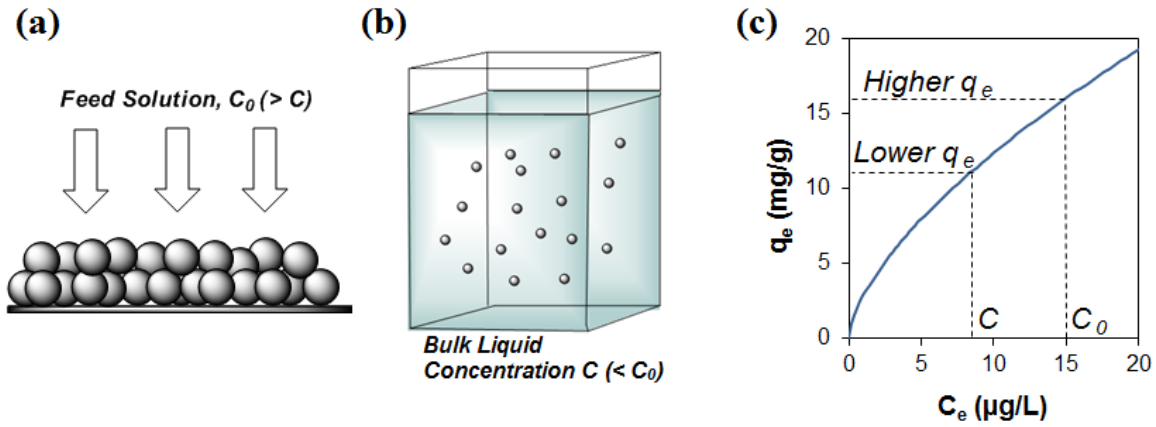

Figure 2.5. Illustrations of the stirred tank (a) and membrane coating (b) configurations, with a corresponding hypothetical isotherm (c). *C* represents the concentration of the solution in contact with the adsorbent particles in the stirred tank setup, while C_0 is the feed solution concentration. Figures not drawn to scale.

In addition to carbon-based membrane coatings, polymeric materials have also been studied for membrane applications. The application of poly(ether ether ketone) to a nanofiltration membrane was shown to reduce fouling by creating a nearly neutral overall surface charge that resulted from having a negatively charged polymeric coating on a positively charged membrane (*45*).

Polydiallyldimethylammonium chloride (polyDADMAC), a positively charged polymeric coagulant, was selected for this project to be tested as an adsorbent-membrane cross-linker. The polymer was applied to the membrane before the carbon was added, with the intent of improving adsorbent adherence. Previous research has shown that polyDADMAC binds strongly to the negatively charged substrate montmorillonite (*46*). A similar effect was anticipated to occur between the polymer coating and the carbonaceous adsorbents, which have negative net surface charges. However, one disadvantage for the use of polyDADMAC is its potential to form *N*-nitrosodimethylamine (NDMA), a probable carcinogen that has been shown to be generated during chloramination in water treatment processes using polyDADMAC (*47*).

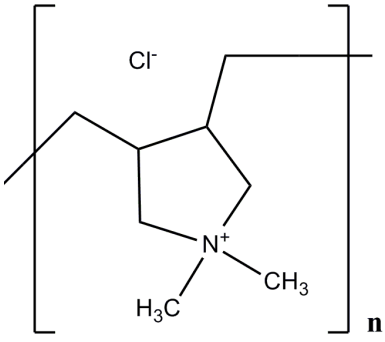

Figure 2.6. Molecular structure of polyDADMAC.

2.4 Modeling Carbon Layer Adsorption

Several mathematical models have been developed for adsorption processes on activated carbon in fixed beds (*48, 49*). It was thought that these models would be applicable to thin-layer carbon coatings, which can be described as short carbon columns. Consequently, the homogeneous surface diffusion model (HSDM) and linear driving force (LDF) model, which are applicable to fixed bed adsorption, were selected for evaluation in this project. The adsorption process underlying these models consists of several stages. The contaminant first needs to diffuse through the liquid phase towards the adsorbent particle. It then must be transported through the liquid film surrounding the particle, and finally undergo intraparticle surface diffusion to reach an internal adsorption site (*50*).

2.4.1 Estimation of Parameters

Important parameters that must be incorporated in the models are detailed in Table 2.2, along with equations used to approximate them. The film transfer coefficient, k_f, and the surface diffusion coefficient, D_s, are the most difficult parameters to accurately quantify (*50*). The Sontheimer correlation, used as an approximation of D_s, is described by Sontheimer as "crude" (*10*). This parameter is assumed to be constant, with no variability resulting from differences in surface concentration (*50*). The Wilke-Chang method is well known for approximating liquid phase diffusion and was used in this modeling effort (*51*). Other parameters, such as isotherm coefficients (Section 5.2) and particle size (Section 5.1.1), were experimentally determined.

Table 2.2. Methods for Estimating Model Parameters

Parameter	Relevant Equation(s)	Assignment of Variables
Liquid Diffusion [a]	$D_l = 1.17x10^{-16}\frac{T\sqrt{2.6MW}}{\eta MV^{0.6}}$ (1)	○ D_l = liquid diffusion coefficient (m^2/s) ○ MW = molecular weight of solvent (g/mol) ○ MV = molar volume of solute (m^3/kmol) ○ T = temperature (K) ○ η = solution viscosity (kg/(m·s))
Film Transfer [b]	$\mathrm{Re} = \frac{\rho_s d_p v_s}{\eta(1-\varepsilon)}$ (2) $Sc = \frac{\eta}{\rho_s D_l}$ (3) $k_f = \frac{2.4v_s\,\mathrm{Re}^{-0.66}}{Sc^{0.58}}$ (4)	○ d_p = particle diameter ○ k_f = film transfer coefficient ○ Re = Reynolds number ○ Sc = Schmidt number ○ v_s = superficial velocity ○ ε = adsorbent bed porosity ○ ρ_s = solution density
Surface Diffusion [c]	$D_s = \frac{5D_l\varepsilon_p C_0}{q_e\rho}$ (5)	○ C_0 = feed solution concentration ○ D_s = surface diffusion coefficient ○ q_e = solid-phase concentration in equilibrium with C_0 ○ ε_p = intraparticle porosity ○ ρ = apparent particle density
Interparticle Porosity	$\varepsilon = \frac{V - V_p}{V}$ (6)	○ V = volume of adsorbent bed ○ V_p = volume of adsorbent particles

[a] Ref. [52]. [b] Ref. [53]. [c] Ref. [10].

2.4.2 Homogeneous Surface Diffusion Model

The HSDM is a mechanistic model that has been successfully applied to fixed-bed column adsorption (*54, 55*). It assumes that adsorbent particles are homogeneous and spherical, though in reality the adsorbent exhibits pore size heterogeneity (*50*). The model is based on an assumption that the adsorbate is transported along the pore walls to

adsorption sites in the particle. A final assumption is an equilibrium state between liquid and solid-phase concentration along the particle surface (*56*).

Equations for solid and liquid-phase concentrations must be solved simultaneously to determine the permeate concentration at a particular time during the filtration. Solid-phase diffusion is predicted by Fick's Law, and the material balances for the solid phase and liquid phase, respectively, are written in simplified form as

$$\frac{\partial \overline{q}}{\partial T} = \frac{D_s \tau \rho q_e (1-\varepsilon)}{\varepsilon C_0 (d_p/2)^2} \frac{1}{\overline{r}^2} \frac{\partial}{\partial \overline{r}} \left(\overline{r}^2 \frac{\partial \overline{q}}{\partial \overline{r}} \right) \tag{7}$$

$$\frac{\partial \overline{c}}{\partial \overline{z}} + \frac{\varepsilon C_0}{\rho q_e (1-\varepsilon)} \frac{\partial \overline{c}}{\partial T} + \frac{\partial}{\partial T} \left(3 \int_0^1 \overline{q} (\overline{r}^2) d\overline{r} \right) = 0 \tag{8}$$

in which D_s = surface diffusion coefficient, τ = hydraulic residence time, d_p = carbon particle diameter, ρ = apparent particle density, C_0 = initial feed solution concentration, q_e = solid-phase concentration in equilibrium with initial feed solution concentration, ε = interparticle porosity, $\overline{r}$ = dimensionless position in carbon particle, $2r/d_p$, $\overline{q}$ = dimensionless solid-phase concentration, T = dimensionless time, $t\varepsilon C_0/(\tau\rho q_e(1-\varepsilon))$, $\overline{c}$ = dimensionless concentration, c/C_0, and $\overline{z}$ = dimensionless position in fixed bed (*48*).

Several initial conditions and boundary conditions need to be fulfilled. Initial concentrations are set at zero, and the change in solid-phase concentration, $\partial \overline{q} / \partial \overline{r}$, at the particle center is assumed to be zero throughout the filtration. One final boundary condition at the particle surface is given as

$$\frac{k_f \tau (1-\varepsilon)}{\varepsilon \, \mathrm{Re}} (\overline{c} - \overline{c}_s) = \frac{\partial}{\partial T} \int_0^1 \overline{q} (\overline{r}^2) d\overline{r} \tag{9}$$

in which k_f = film transfer coefficient, Re = Reynolds number, and $\bar{c}_s$ = dimensionless liquid-phase concentration at the particle surface. Tests must be conducted to determine the best-fit isotherm correlation, such as the Langmuir or Freundlich equation, and the parameter $\bar{c}_s$ is eliminated by rearranging the isotherm expression and substituting in Equation 9.

Equations 7 through 9 constitute a system of partial differential equations that must be solved numerically. Two equation simplification methods can be used: finite difference and orthogonal collocation. Orthogonal collocation has been shown to be the more viable method for solution of the system of differential equations, since finite difference exhibits instability and convergence problems (*55*). A system of algebraic equations has been developed as an empirical simplification of the HSDM, but the approximation is valid only for sufficiently long contact times (*57*), which are not achieved in thin-layer coatings.

The orthogonal collocation method was derived from the method of weighted residuals, in which a trial function is chosen to evaluate the system of equations at set points, which have residuals of zero (*58*). As the number of collocation points increases to infinity, the approximated solution converges to the exact solution. The values of the collocation points derived from Legendre polynomials are tabulated in the literature, along with the corresponding coefficients for the simplified differential equations (*59*). The orientations of the collocation points in the fixed bed and adsorbent particle are clarified in ref. [60], and application of the orthogonal collocation method to Equations 7 through 9 is detailed in ref. [55].

2.4.3 Linear Driving Force Model

The LDF model is based on the premise that the difference between liquid-phase concentration at the particle surface and adsorbed concentration serves as a driving force for adsorption (*49*). Two versions of the model have been developed. For adsorption scenarios that involve mass transfer dominated by surface diffusion, the LDFQ model is applicable. In cases for which film transfer to the particle surface is the primary limiting factor, the LDFC model may be more suitable. The models have been applied successfully to experimental results in both gas and liquid phases (*49, 61-64*), and applying both models to a single data set reveals which mechanism is dominant.

The LDFC model may be solved to determine at what time a certain effluent concentration is reached:

$$t = t_0 + \frac{\rho q_e}{k_f C_0}\left(1 - \frac{R\ln(1-\bar{c}) - \ln\bar{c}}{1-R}\right) \tag{10}$$

t represents the time corresponding to an effluent concentration of $\bar{c}$, while t_0 is the characteristic time, or the time at which the effluent concentration is 1-$\bar{c}$. R is an equilibrium parameter that may be obtained using the correlation

$$R = \frac{1}{1 + K_L C_0} \tag{11}$$

in which K_L is the Langmuir constant extracted from isotherm data. Using a linear regression on a plot of t versus the expression in parentheses in Eq. 10, fitted parameters may be identified and used to apply the model. Consequently, the model functions as an empirical means of identifying the primary adsorption mechanism.

The LDFQ model is available in two forms. Eq. 12 below utilizes a surface diffusion coefficient, D_s, while Eq. 13 incorporates the pore diffusion coefficient, D_p. Both versions include a correlation parameter, ϕ, which is ideally equal to one:

$$t = t_0 + \frac{d_p^{\,2}}{60\phi D_s}\left(\frac{R}{1-R}\ln\bar{c} - \frac{1}{1-R}\ln(1-\bar{c}) - 1\right) \tag{12}$$

$$t = t_0 + \frac{\rho q_e d_p^{\,2}}{60\phi D_p C_0}\left(\frac{R}{1-R}\ln\bar{c} - \frac{1}{1-R}\ln(1-\bar{c}) - 1\right) \tag{13}$$

As with the LDFC model, parameters needed for the model may be determined by a linear regression with the experimental data.

2.5 Flux Reductions and Recoveries

A portion of this project was dedicated to assessing and modeling the flux reductions associated with the application of a carbon layer on the membrane. The general flux equation for filtrations is

$$J = \frac{\Delta P}{\eta(R_m + R_c)} \tag{14}$$

in which J is the flux, ΔP is the transmembrane pressure, η is the viscosity of the feed solution, R_m is the membrane resistance, and R_c is the resistance contribution from the carbon layer (*65*). For the dead-end setup employed in this project, the Kozeny-Carman model was used for determining the resistance to flow caused by the carbon layer, which can be described as

$$R_c = \frac{180(1-\varepsilon)^2 h}{d_p^{\,2}\varepsilon^3} \tag{15}$$

in which ε is the porosity in the layer, h is the height of the layer, and d_p is the adsorbent particle diameter.

There are three factors that contribute to flux reduction by foulants (*33*). Pore constriction refers to adsorption of the foulant in the membrane pores, and pore blocking renders pores inaccessible to fluid flow at the membrane surface. Cake formation describes the accumulation of a foulant layer on the membrane. An evaluation of the decrease in flux associated with application of the adsorbent layer on the membrane is necessary to draw conclusions about the additional energy that would be required to maintain a constant volumetric effluent output.

Based on the model, PAC coatings with thicknesses on the micrometer scale are not predicted to decrease flux appreciably during constant pressure filtrations. However, S-PAC particles with sizes comparable to the membrane pore size are susceptible to cake formation as well as pore clogging and may significantly reduce the flux.

CHAPTER THREE

RESEARCH OBJECTIVES

This project was designed with the intent of evaluating the organic contaminant removal capabilities of carbon coatings and determining the effect that coatings have on filtration efficiency. Specifically, the objectives were as follows:

(1) ***Compare the suitability of different carbonaceous materials for adsorption of methylene blue and atrazine in membrane coatings***. In particular, the potential for alternative and novel adsorbents to act as substitutes for PAC in water treatment systems was of interest.

(2) ***Determine the effect of varying filtration parameters on contaminant retention*.** Feed solution concentration, flux, and carbon dose were altered sequentially to elucidate the influence of these parameters on adsorption kinetics in the carbon layer.

(3) ***Use a stirred vessel setup for comparison with the coated membrane approach***. In water treatment plants, incorporation of a stirred tank ahead of the UF membrane is a more traditional method for contaminant adsorption on carbon, and it is desirable to study the usefulness of this setup alongside the coated membrane system.

(4) ***Develop a predictive model for contaminant adsorption in the carbon layer.*** This aspect of the project could be useful for calculating the carbon dose required to maintain the permeate concentration below a maximum contaminant level (MCL) for a specified filtration period.

(5) ***Evaluate the contribution to membrane resistance resulting from application of a carbon coating and determine the extent of flux recovery.*** These characteristics are key to ascertaining the amount of energy required to maintain the flow rate as well as determining the extent of irreversible membrane fouling caused by small adsorbent particles.

(6) ***Attempt to improve coating adherence to the membrane with the use of polyDADMAC***. This material was selected for its coagulation properties. Improving adhesion to the membrane is especially relevant if the coated membrane method is to be applied to cross-flow systems.

(7) ***Evaluate the advantages and disadvantages of the different adsorbents.*** Considering adsorption kinetics based on breakthrough curves as well as isotherm and flux characteristics, the materials can be assessed for their expected usefulness in water treatment.

CHAPTER FOUR

MATERIALS AND METHODS

4.1 Adsorbents

Coal-based WPH and F400 activated carbons (Calgon Carbon Corporation) were used in this project. S-PAC was produced from the WPH PAC in a wet-mill micro-grinding process at Netzsch Premier Technologies. F400 GAC was used to verify that the HSDM works for fixed column adsorption. For some of the filtrations, the F400 GAC was ground and sieved using 230/400 and 100/120 mesh sizes to produce two size fractions. MWCNTs and NGPs were purchased from Nanostructured and Amorphous Materials, Inc. and Angstron Materials, respectively. All adsorbents were weighed on a microgram balance (Mettler Toledo MX5) in powder form and then soaked in 2 mL of distilled or deionized water overnight before use in a filtration.

4.1.1 Particle and Pore Size Characterizations

Images of PAC on a hemocytometer were obtained under a light microscope (Zeiss Axioskop 2) and analyzed with a MATLAB program that was designed to determine the particle size distribution (PSD). A total of 20-25 images were analyzed for each carbon type, and some representative images of the particles are included in Figures A-1 through A-4. The program used to find the PSDs is in Appendix B-1. It functions by determining the visible area in pixels of each particle, which is then converted into particle volume based on a pixel-to-micrometer calibration that assumes spherical geometry. Particles are then sorted into size ranges, and a PSD plot is made. The PSD for S-PAC was obtained using a particle size analyzer (Brookhaven Instruments Corp.

90Plus) because the particles were too small to be viewed with the microscope. To promote disaggregation of particles, the S-PAC was sonicated for 10 minutes prior to analysis in a bath sonicator (Branson 2510) at 130 W. The pore size distributions were obtained with nitrogen gas adsorption at 77 K using density functional theory (Micromeritics ASAP 2020), and surface areas were calculated from the Brunauer-Emmett-Teller (BET) equation.

4.1.2 FTIR Spectroscopy and Oxygen Analysis

To assist with surface chemistry characterization, the activated carbon adsorbents were analyzed with a Thermo Scientific Nicolet 6700 Fourier transform infrared (FTIR) spectrometer using attenuated total reflectance (ATR). Diffuse reflectance is more suitable for activated carbons because of their high radiation absorption characteristics (*7*), but this technique was not available. Resolution was set at 4 cm^{-1} with 256 scans, and adsorbents were dried for 3 hours in a 105°C oven prior to analysis.

An elemental analyzer (Flash EA 1112) was used for the determination of oxygen content. A mass of approximately 1 mg was weighed and transferred to a silver cup for each adsorbent, though for the low-density NGPs only 0.2 mg could be contained in the cup. Instrument calibration was completed with the use of a 2,5-bis-(5-tert-Butylbenzoxazolyl)-thiophene (BBOT) standard (CE Elantech Inc.) with a 7.43% oxygen content, and samples were run in duplicate.

4.1.3 Zeta Potential Measurements

Adsorbent masses of 10 mg were measured on a microgram balance, transferred to vials with 10 mL of deionized water, and allowed to equilibrate overnight. MWCNTs,

S-PAC, and NGPs were sonicated for 10 minutes prior to analysis. Zeta potentials were measured with a ZetaPALS (Phase Analysis Light Scattering) program (Brookhaven Instruments Corp. 90Plus). The instrument was set to convert mobility to zeta potential using the Smoluchowski method, which was selected because the mixtures were aqueous.

4.1.4 Electron Microscope Imagery

A small mass of each adsorbent was deposited on 0.1 μm pore size hydrophilic PVDF membranes. S-PAC, MWCNTs, and NGPs were sonicated for 10 minutes prior to deposition on the membranes. After sputter coating the samples with gold, images were obtained using a Hitachi TM3000 scanning electron microscope (SEM); these images are shown in Figure A-5 and A-6. Additional images, which may be seen in Figures A-7, A-8, and A-9 were generated with a Hitachi SU6600 SEM using platinum surface coatings. Despite the use of sonication, the MWCNTs and NGPs displayed extensive aggregation.

4.2 Adsorbates

A survey of water treatment techniques for the elimination of chloro-s-triazines showed that, with the exception of activated carbon adsorption, the compounds were not readily removed by conventional treatment processes (*66*). Furthermore, the authors claimed that comparatively high doses of PAC were needed to decrease concentrations appreciably. Atrazine, a member of the chloro-s-triazine class, was selected for this project to evaluate the effectiveness of membrane coatings with the intent of improving its retention in simulated water treatment systems. In addition, methylene blue was selected as a second model contaminant for comparison with atrazine. Methylene blue

has been studied for PAC-membrane adsorption processes because of its ease of detection and ability to adsorb well to activated carbon.

The molecular structures of the target contaminants are shown in Figure 4.1, and various chemical and physical properties are included in Table 4.1. Methylene blue is a cationic dye, and atrazine is an herbicide. These chemicals adsorb fairly well to activated carbon, a trait that may result in part from their aromatic structures and corresponding ability to undergo π-π interactions with adsorbents. Both chemicals have very low pK_a values. This indicates that in the pH range used in the filtrations, which was varied from 5.5 to 7.0, both chemicals were in base form.

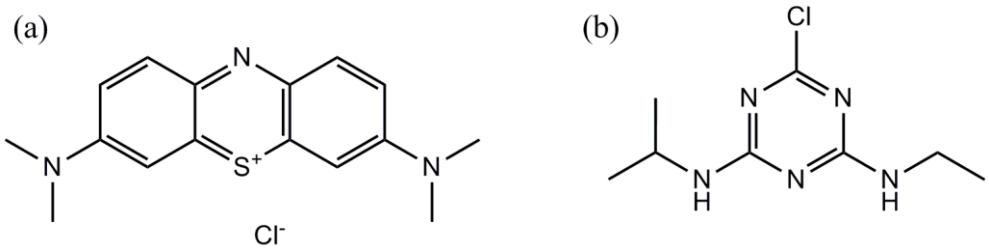

Figure 4.1. Molecular structures of methylene blue (a) and atrazine (b).

Table 4.1. Adsorbate Properties

Compound	Chemical Formula	Dimensions (Å)	MW (g/mol)	Molecular Volume [b] (m^3/kmol)	pK_a	Solubility in Water (g/L)	log K_{ow}
Atrazine	$C_8H_{14}ClN_5$	9.6×8.4×3 [a]	215.7	0.247	1.95 [c]	0.03 [e]	2.75 [e]
Methylene Blue	$C_{16}H_{18}H_3S Cl{\cdot}3H_2O$	14.3×6.1×4 [a]	373.9	0.374	< 1 [d]	40 [f]	3.56 [g]

[a] Ref. [67]. [b] Estimated using Le Bas method (*52*). [c] Ref. [68]. [d] Ref. [69]. [e] Ref. [70]. [f] Ref. [71]. [g] Estimated using atom/fragment contribution method (*72*).

Methylene blue was purchased from Mallinckrodt, Inc. Instead of using a stock solution and diluting to make the feed solution, a separate mass of solid methylene blue

was used to make the feed solution for each filtration. Radiolabeled atrazine was purchased from American Radiolabeled Chemicals, Inc., and used in conjunction with non-labeled atrazine from Accustandard, to enable detection with a liquid scintillation counter. Two batches of atrazine were used. The first had a specific activity of 10 mCi/mmol, and the second was 160 mCi/mmol. The stock solution with an activity of 10 mCi/mmol was prepared with a labeled to non-labeled atrazine ratio of 1:2, while the 160 mCi/mmol solution was not diluted with the non-labeled atrazine. Instead, the feed solutions for individual filtrations were adjusted with the non-labeled atrazine in a 1:29 ratio. The stock solutions were prepared in ethanol, and aliquots were transferred to distilled or deionized water to make feed solutions.

4.3 Adsorption Experiments

4.3.1 Coated Membrane Filtrations

The lab-scale dead-end UF setup, shown in Figure 4.2, consisted of an 800-mL pressure vessel (Millipore) that held the feed solution, a 16-mL capacity membrane cell (Millipore) containing the UF membrane and mesh support material, glassware for permeate collection, and a balance connected to a computer to monitor the flux. Pressure for the filtrations was supplied by a nitrogen tank connected to the pressure vessel. The membranes (Millipore VVLP) were hydrophilic PVDF with a pore size of 0.1 μm and diameter of 2.5 cm (2.1-cm active diameter when installed in the filtration cell). Membranes were soaked in distilled or deionized water overnight before use in filtrations.

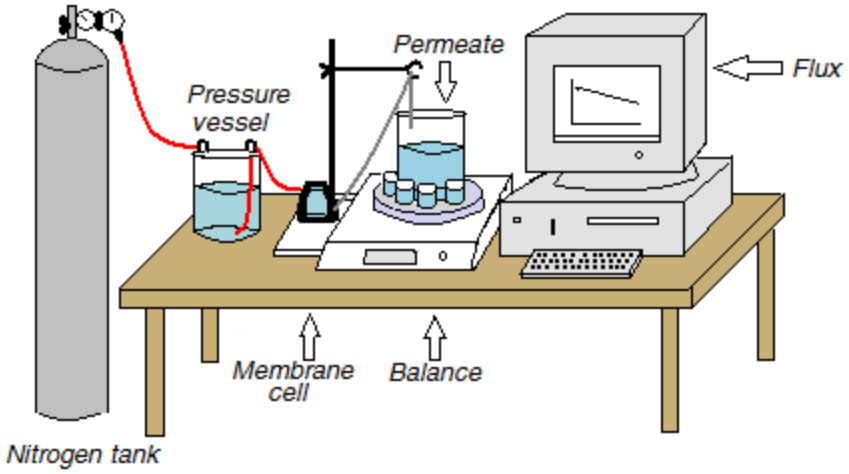

Figure 4.2. The lab-scale ultrafiltration setup.

Methylene blue filtrations with PAC and alternative adsorbents had feed solution concentrations of 0.9 mg/L unless otherwise indicated and were run at a constant flux of 500 L/m^2/h (lmh), which was achieved with manual pressure adjustments as needed. In this study, adsorbent additions occurred as pulse inputs for all filtrations, and carbon coatings were made by adding the adsorbent directly to the membrane cell, which was filled with the feed solution. Permeate samples were collected in glass vials and analyzed with a UV/Vis spectrophotometer (Varian Cary 50 Bio) at 666 nm, with the method detection limit calculated as 4 ppb. Because of a comparatively low precision with analysis of the permeate samples, methylene blue experiments were performed in triplicate.

For the filtrations with atrazine as the target contaminant, feed solutions were made by transferring stock solution to 1-2 L of distilled or deionized water. Feed solution concentrations were 15 ppb except for the filtrations that were intended to determine the effect of varying concentration. Controls were run to ensure that the model contaminant

did not adsorb to the equipment. Permeate samples were collected in 20 mL polyethylene vials. Liquid scintillation counting (Wallac 1415) was used for detection of ^{14}C-atrazine in the permeate samples, which were composed of 10 mL of sample and 10 mL of liquid scintillation cocktail (UltimaGold XR). The count time was 10 minutes per sample, and the detection limit was calculated as 0.07 ppb.

It was discovered that the first atrazine batch (10 mCi/mmol) was contaminated by an unknown, tritium-labeled compound, which originated at the lab where it was produced. The contamination affected several of the filtrations, which are tabulated in the results and discussion section, and for the other atrazine filtrations the new atrazine batch (160 mCi/mmol) was used. Several filtrations affected by the contaminated stock solution were redone with the new stock solution to assess the magnitude of the deviations. In addition, selected filtrations were run in duplicate to verify the accuracy of the results.

4.3.2 Stirred Vessel Filtrations

For the filtrations simulating a stirred tank configuration, a 250-mL Erlenmeyer flask containing a stir bar was incorporated between the pressure vessel and the membrane cell, and the carbon was added to the flask before the filtration. Some adsorption of carbon in the tubing connecting the stirred vessel to the membrane cell was noted, which may have caused experimental errors, though tubing length was minimized to help prevent such errors.

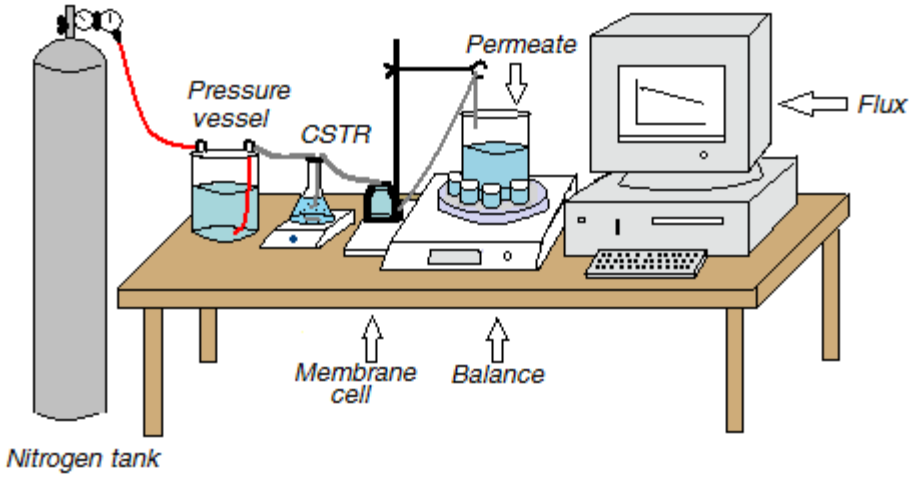

Figure 4.3. The lab-scale stirred vessel ultrafiltration setup. The Erlenmeyer flask represents a completely stirred tank reactor (CSTR).

4.3.3 Adsorption Isotherms

Methylene blue solutions of varying concentrations were contacted with the four adsorbents using a carbon mass of 1-2 mg and a volume of 140 mL in glass bottles. Bottles were mixed on a rotary tumbler in the dark for two days, which was determined to be sufficient for reaching equilibrium based on batch kinetics tests (*73, 74*). MWCNT, NGP, and S-PAC samples were centrifuged prior to analysis to remove the carbon that was capable of settling. Controls without methylene blue were run to determine the absorbance by the carbon that did not settle during centrifugation.

For atrazine, initial concentrations were varied, and about 1 mg of adsorbent was added to each glass bottle containing 250 mL of solution. Mixtures were mixed on a rotary tumbler in the dark for one week, which has been shown to be a suitable time period for attaining adsorption equilibrium for atrazine using batch kinetics tests (*37, 75*). Because the UF membrane with 0.1 µm pore size had only 3% atrazine retention, it was

acceptable to separate the adsorbents from the solutions using membrane syringe filters rather than centrifugation, though membrane retention was taken into account in the calculations.

4.4 Flux Tests

Constant pressure filtrations consisting of four stages were run to determine the extent of membrane fouling by the adsorbents. The first stage was required to determine the flux for the blank membrane, and this was achieved with filtration of distilled water for 20 minutes at 3 psi. Membrane characteristics and apparatus are as described in Section 4.3.1. For the second stage, a specified mass of adsorbent was added to the membrane cell, and the flux decline was determined at 3 psi for 20 minutes of filtration after the carbon had settled on the membrane. Membrane backwashing was then performed by reversing the membrane direction in the membrane cell and filtering distilled water. This process was conducted at 35 psi for one minute, conditions that have been used for PAC/UF pilot-scale evaluations (*76*). The membrane was dipped in water to remove loose carbon and replaced in the membrane cell for the flux recovery, which involved 20 minutes of filtration at 3 psi.

CHAPTER FIVE

RESULTS AND DISCUSSION

5.1 Characterization of Adsorbents

5.1.1 Particle Size Distributions and Surface Areas

The average diameters for WPH PAC and S-PAC were determined to be 25 (± 14) μm and 0.23 (± 0.02) μm, respectively, and the PSDs are shown in Figure 5.1. For the F400 fractions, average particle sizes were 65 (± 16) μm and 170 (± 19) μm, and these fractions will be distinguished by their average particle sizes rather than their sieve sizes throughout this text.

The average particle sizes for the two F400 fractions were unexpectedly high, considering that the upper mesh sizes used for these fractions were 63 and 150 μm, respectively. Observation of the geometries of the particles under a microscope indicates that many of them have an oblong shape, with one dimension much larger than the other. This potentially enables a particle with a dimension larger than the mesh size to pass through the sieve. Therefore, using an arithmetic mean as the average particle size for modeling and other purposes may be inadvisable when high accuracy is required.

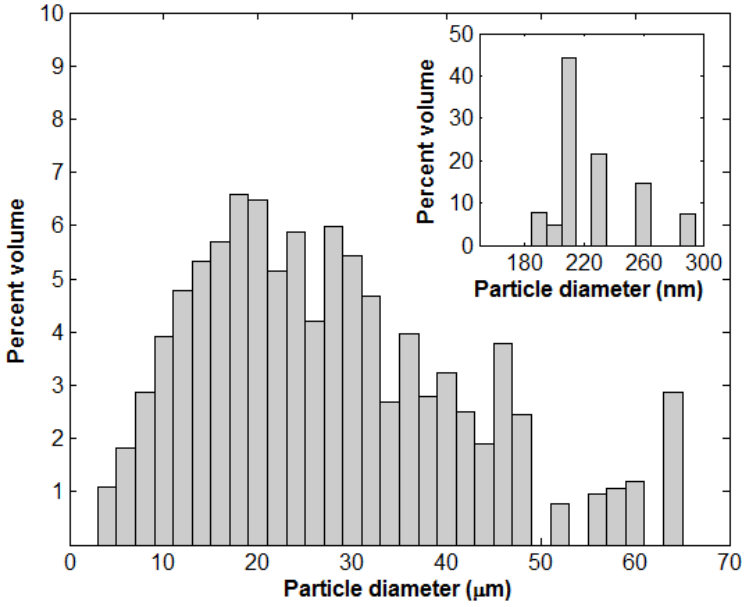

Figure 5.1. Particle size distributions of WPH PAC and S-PAC (inset).

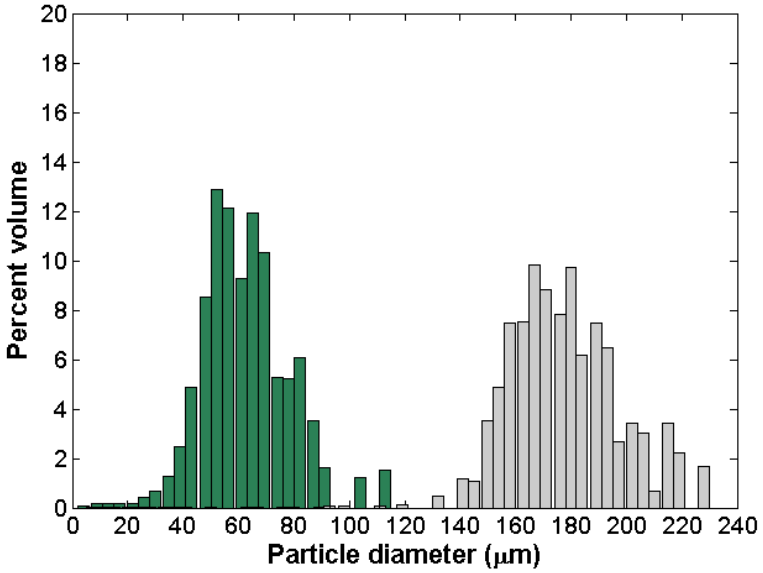

Figure 5.2. Particle size distributions for two carbon fractions produced from F400 GAC.

MWCNTs were reported by the manufacturer to be 10-20 μm in length. Other dimensions provided by the manufacturer are a 5-15 nm inner diameter and a 30-50 nm outer diameter, and the outer diameter has been measured as 29 (± 13) nm using transmission electron microscopy (*77*). Inspection with light microscopy showed that MWCNTs suspended in distilled water formed oblong aggregates in the 200 μm to several mm range. NGPs were reported by the manufacturer to have dimensions of less than 5 μm diameter and less than 1 nm thickness, though aggregation was also observed for this adsorbent. As a result of this analysis, MWCNTs, NGPs, and S-PAC were sonicated in vials for 10 minutes prior to use in filtrations. Full disaggregation was not achieved for the MWCNTs and NGPs, which is clear from Figures A-2 and A-3, but aggregate sizes were reduced.

Assuming spherical particles, approximations for the external surface area on the activated carbon adsorbents were determined. These approximations use the average particle size for calculation and do not include internal pore space. It was determined that S-PAC had an external surface area of 33 m^2/g, while for PAC the result was only 0.27 m^2/g. In addition, the total surface areas measured with nitrogen gas adsorption for each adsorbent are tabulated in Table 5.1.

Table 5.1. Adsorbent Surface Areas

Material	Surface Area (m^2/g)
MWCNTs	187 (± 1)
F400	948 [a]
NGPs	624 (± 4)
S-PAC	773 (± 3)
WPH PAC	900 (± 4)

[a] For F400 GAC (Ref. [*15*]).

5.1.2 Pore Size Distributions

Shown in Figure 5.3 are the pore size distributions for WPH PAC and the alternative adsorbents, and the summations of the micro and mesopore volumes are summarized in Table 5.2. As expected, the activated carbon adsorbents had a microporous structure, while CNTs and NGPs had primarily mesoporous volume. PAC and S-PAC had comparable micropore volumes, but S-PAC had a significantly higher mesopore volume, a finding that is compatible with previous measurements on the same adsorbent batch by another research group (*78*).

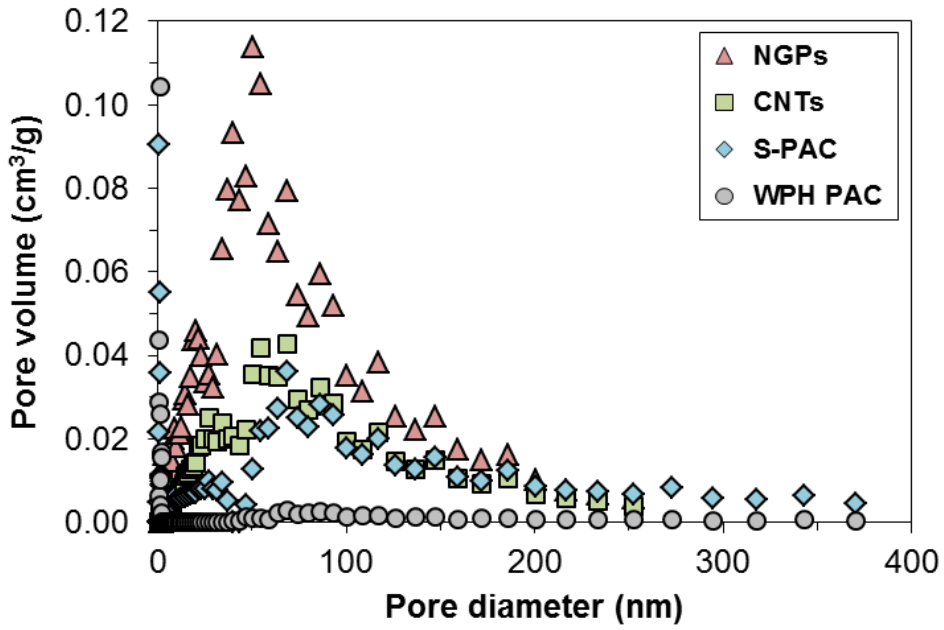

Figure 5.3. Pore size distributions of the adsorbents.

Table 5.2. Pore Size Classifications

Material	Micropore Volume (cm^3/g)	Mesopore Volume (cm^3/g)
MWCNTs	0.009	0.365
NGPs	0	1.108
S-PAC	0.230	0.257
WPH PAC	0.257	0.020

5.1.3 FTIR Analysis and Oxygen Content

FTIR analysis of the adsorbents showed several small peaks for PAC and S-PAC. The spectra were overlaid and are shown in Figure 5.4 with likely peak identifications. The activated carbon adsorbents are associated with functional groups containing oxygen (Figure 2.2), and the spectra for these materials do indicate the presence of oxygen.

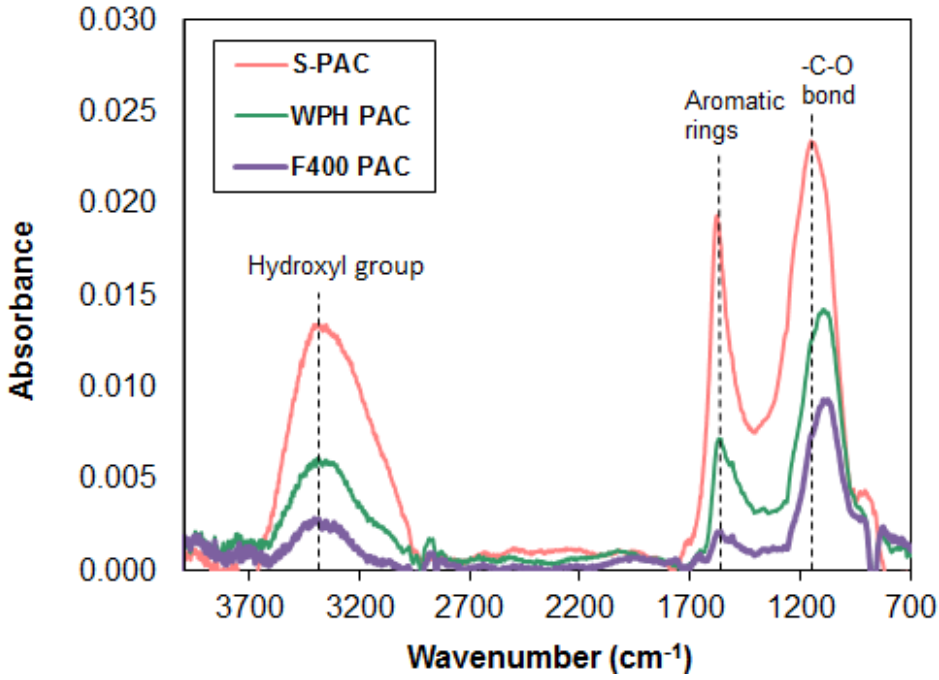

Figure 5.4. FTIR spectra of activated carbon adsorbents, labeled with likely functional group identifications.

The FTIR technique is capable of responding to functional groups only on the particle surface, so groups in the internal pores are not identifiable with the method. Therefore, total oxygen content was determined with elemental analysis, and results are presented in Table 5.3. The oxygen content for the NGPs was reported by the manufacturer to be 2.1%, which is compatible with the experimental results. Although the S-PAC was produced from the WPH PAC, its oxygen content was about 4% higher. F400 PAC and F400 GAC had very similar results of around 4% oxygen, though previous work on F400 elemental composition yielded a measurement of 10% (*79*). As stated in Chapter 2, oxygen groups are expected to reduce adsorption effectiveness for hydrophobic contaminants because of increased hydrophilicity on the carbon surface,

though electrostatic interactions between the positively charged methylene blue and negatively charged oxygenated groups may be favorable for adsorption.

Table 5.3. Oxygen Contents of the Adsorbents

Adsorbent	% Oxygen (Sample 1)	% Oxygen (Sample 2)
F400 GAC	3.62	4.71
F400 PAC [a]	4.23	2.98
MWCNTs	1.49	1.48
NGPs	2.24	1.80
S-PAC	8.33	9.05
WPH PAC	4.28	4.21

[a] Particle size 170 μm.

5.1.4 Zeta Potential

To draw conclusions about the net external surface charges on the adsorbents, zeta potential measurements were obtained. The tests were conducted at the approximate pH of the filtration feed solutions, which showed variability among measurements but fell in the range of 5.5 to 7.0. Table 5.4 summarizes the zeta potentials of the adsorbents and the pH values at which they were obtained.

Table 5.4. Zeta Potential Measurements

Adsorbent	pH	Zeta Potential (mV)
MWCNTs	7.05	-37.9 (± 6.9)
F400 PAC	5.98	-30.6 (± 4.1)
NGPs	6.78	17.2 (± 5.7)
S-PAC	6.35	-31.9 (± 4.8)
WPH PAC	6.43	-42.7 (± 3.9)

Note: Zeta potential entries are based on the average of 5 replicate measurements at an adsorbent concentration of 0.1 mg/mL.

Studies on the surface characteristics of coal-based PAC revealed a zeta potential of -30 to -40 mV in the pH range of 6 to 7 (*16*), which correlates well with the results in the above table. For adsorption of cationic dyes, such as methylene blue, a low zeta potential of less than -30 mV, corresponding to an overall negative surface charge, is desirable (*80*). It has been noted that the use of electrophoretic mobility as an indicator of zeta potential may not be accurate for characterizing the total surface charge of activated carbons because of their porous texture (*10*). However, this method is useful for determining overall charge on the external surface area.

Some features of the results for the alternative adsorbents are notable. Unlike the other adsorbents, the NGPs had a zeta potential above zero, indicating a positive net surface charge. S-PAC was expected to have the same zeta potential as the WPH PAC from which it was formed, since the microgrinding process used to produce S-PAC was not expected to affect surface chemistry. However, the experimental results indicate that WPH PAC had a slightly lower zeta potential than S-PAC, measured at an essentially equivalent pH.

5.1.5 Adsorbent Monolayers

Calculations were done to determine the mass of PAC required to form a monolayer on the membrane, assuming spherical particles with the average diameter. The calculations also assume that the arrangement of particles constitutes a simple rhombic layer (*81*), which is shown in Figure 5.5 and corresponds to a bed void fraction of 0.37. A MATLAB program for this procedure was created and is included as Appendix B-2.

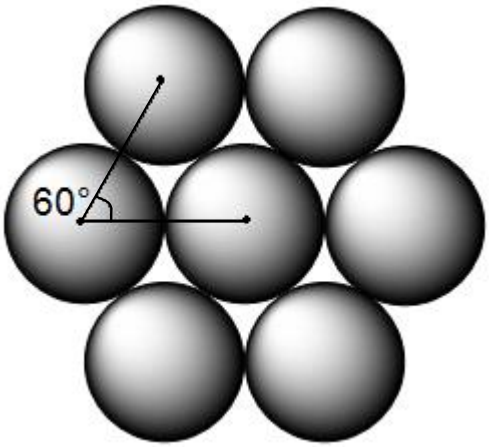

Figure 5.5. Aerial view of carbon particles, constructed using the arrangement that was assumed for monolayer mass calculations. Adapted from ref. [81].

Table 5.5 summarizes the calculated monolayer masses of the five activated carbon adsorbents used throughout this project. Monolayer calculations are useful for determining what fraction of the membrane surface is covered by an adsorbent of a particular particle size. An apparent particle density of 0.90 g/mL was assumed for all activated carbon adsorbents. This value was calculated based on the apparent powder density for F400 GAC, 0.52 g/mL, which was provided by Calgon Carbon Corporation. Apparent powder density accounts for volume supplied by the particle skeleton as well as

the interparticle and intraparticle pores, while the apparent particle density is based on the skeleton and only the internal particle pore volume (*82*).

Table 5.5. Calculated Masses for Membrane Monolayers

Adsorbent	Average Particle Size (µm)	Mass of Membrane Monolayer (mg)
F400 GAC	1400	260
F400 PAC	65	13
F400 PAC	170	34
S-PAC	0.23	0.045
WPH PAC	25	4.9

5.2 Adsorption Isotherms

The experimental results of the isotherm tests were fit to the Langmuir and Freundlich models (*83*). The Freundlich equation is given by

$$q_e = K_F C_e^{1/n} \tag{16}$$

in which q_e is the solid-phase concentration at equilibrium, C_e is the liquid-phase concentration at equilibrium, and K_F and n are the Freundlich constants. The Langmuir equation is

$$q_e = \frac{q_0 K_L C_e}{K_L C_e + 1} \tag{17}$$

with q_0 and K_L as the Langmuir constants.

5.2.1 Methylene Blue

As shown in Figure 5.6, the Langmuir equation more accurately modeled the results for most of the adsorbents, especially in the upper range of equilibrium

concentrations. The trends seen with the isotherm tests are compatible with approximate total removal in the filtrations with the coated membranes. With a small particle size that enables better access of adsorbate to pores, S-PAC showed the highest adsorption capacity. The MWCNTs were not expected to have a large adsorption capacity because of their low surface area and lack of microporosity compared to the other materials. Although NGPs lack micropores as well, they have a 3× higher BET surface area than the CNTs.

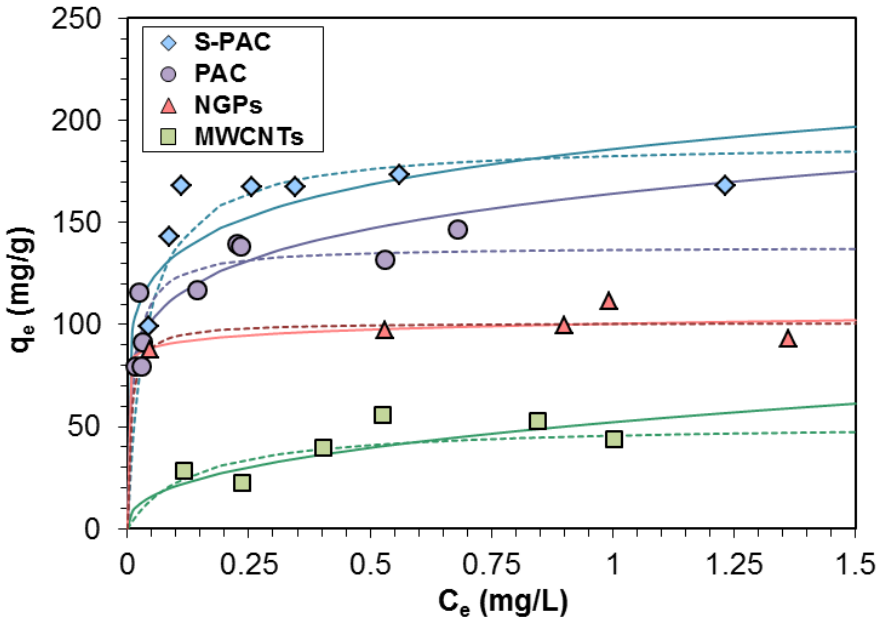

Figure 5.6. Isotherms for methylene blue with different carbonaceous adsorbents showing Freundlich (solid lines) and Langmuir (dashed lines) model fits.

Table 5.6. Methylene Blue Isotherm Coefficients

Adsorbent	Freundlich Model			Langmuir Model		
	K_f, (mg/g)(L/mg)$^{1/n}$	$1/n$	R^2	q_0, mg/g	K_L, L/mg	R^2
F400 PAC[a]	154.5	0.10	0.43	163.8	20.4	0.55
MWCNTs	52.2	0.34	0.60	51.5	7.8	0.46
NGPs	100.4	0.04	0.40	101.0	141.4	0.48
S-PAC	185.9	0.14	0.55	189.4	26.4	0.88
WPH PAC	158.7	0.15	0.77	138.1	80.4	0.74

[a] 170 μm particle size.

A previous study found the Langmuir constant q_0 to be 46.2 mg/g for methylene blue and CNTs (*84*), which is comparable to the results presented here. For equilibrium concentrations up to the gram-per-liter level, the Langmuir adsorption capacity, q_0, has been reported as 417 mg/g on F400 carbon (*73*). On a mg-per-m^2 basis, the adsorbents in this study had very similar adsorption affinities for methylene blue (Figure 5.7), indicating that surface area is the primary determinant for methylene blue adsorption.

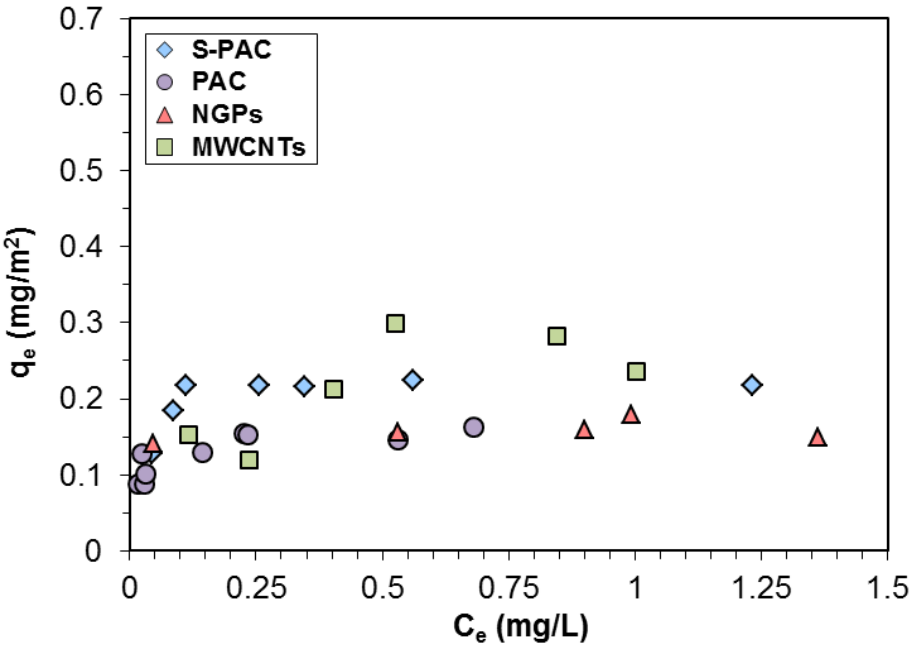

Figure 5.7. Isotherms for methylene blue adsorption, normalized to adsorbent surface area (m^2/g).

5.2.2 Atrazine

Table 5.7 includes the Freundlich and Langmuir isotherm coefficients for atrazine adsorption on PAC and the alternative adsorbents; these tests were conducted with the new batch of atrazine. In contrast to the methylene blue isotherms, PAC had a greater adsorption capacity for atrazine than S-PAC. Because the S-PAC was produced from PAC, they were thought to bear the same chemical surface characteristics. Therefore, it is unclear why the adsorption capacity trends for PAC and S-PAC differed between atrazine and methylene blue, though the use of lower concentrations for atrazine compared to methylene blue or differences in porosity may have affected the results. The R^2 values in Table 5.7 were low for the CNTs and NGPs, indicating that the Freundlich and Langmuir isotherm models may not be suitable for these adsorbents.

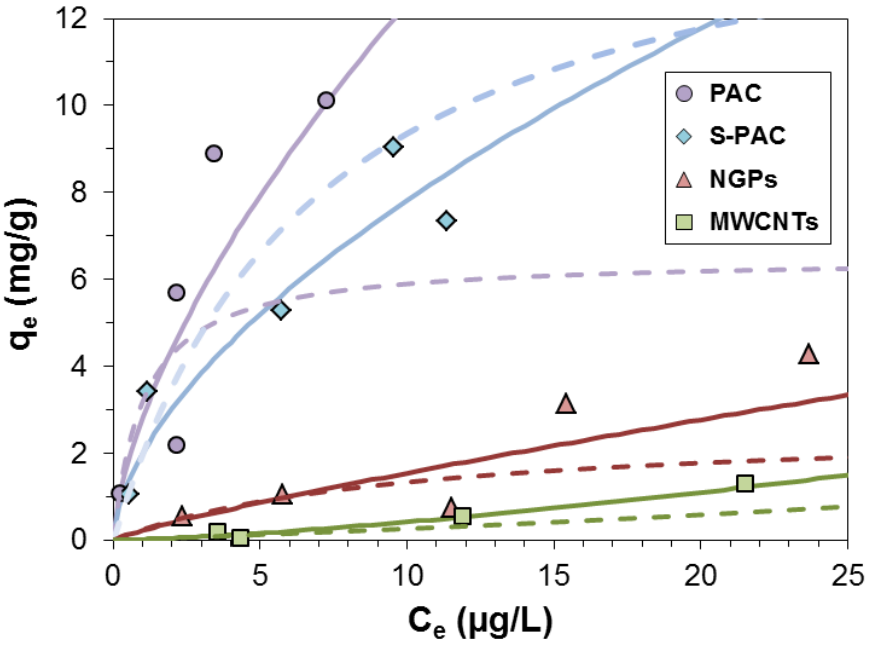

Figure 5.8. Isotherms for atrazine with different carbonaceous adsorbents showing Freundlich (solid lines) and Langmuir (dashed lines) model fits.

Table 5.7. Atrazine Isotherm Coefficients

Adsorbent	Freundlich Model			Langmuir Model		
	K_F, (mg/g)(L/µg)$^{1/n}$	$1/n$	R^2	q_0, mg/g	K_L, L/µg	R^2
MWCNTs	0.02	1.40	0.80	-2.44	-0.01	0.39
NGPs	0.22	0.84	0.70	2.66	0.10	0.67
S-PAC	2.06	0.59	0.89	15.87	0.14	0.94
WPH PAC	2.83	0.65	0.81	6.51	0.96	0.86

Normalizing the data to surface area did not affect the appearance of the isotherms significantly, though CNT adsorption capacity did improve slightly on the surface-area-adjusted scale. This observation indicates that there is a factor other than

surface area that affected adsorption. Yan et al. (*85*) observed that the equilibrium adsorption capacities of SWCNTs and MWCNTs differed on a surface-area-normalized basis, and they inferred that surface chemistry was responsible for the differences. Correspondingly, surface chemistry may contribute to differences noted for the adsorbents in this study. The general consensus in the literature is to classify atrazine as a molecule susceptible to hydrophobic interactions (*86-88*), though some attest that it is influenced by polar mechanisms as well (*89*). Therefore, it would seem that the higher oxygen contents detected with the activated carbon adsorbents would contribute to reductions in the effectiveness of atrazine adsorption.

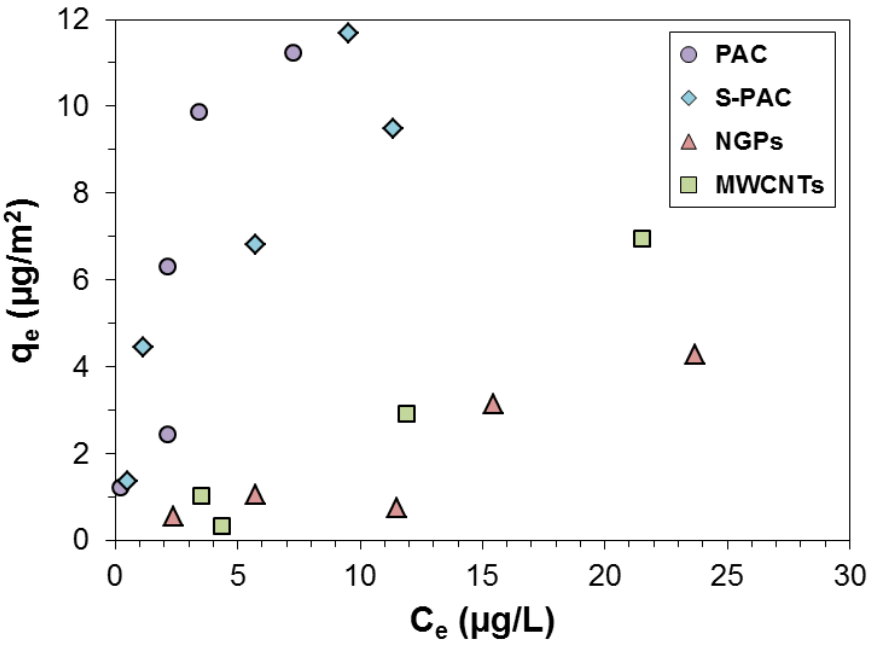

Figure 5.9. Isotherms for atrazine adsorption, normalized to adsorbent surface area (m^2/g).

Alternatively, the molecular sizes and optimal pore sizes for adsorption of the two model contaminants may contribute to the noted differences in adsorption capacity

among the carbonaceous materials. Since atrazine is a smaller molecule that may access smaller micropores, the significantly larger micropore volume for the activated carbon adsorbents compared to the CNTs and NGPs may account for the larger adsorption capacities of PAC and S-PAC. As a larger molecule, methylene blue may not be capable of accessing the small micropores and may be less affected by the disparities in micropore volume among the adsorbents.

5.3 Methylene Blue Retention in Coated Membrane Filtrations

The HSDM and LDF model were applied to the breakthrough curves for the carbon coated membranes, but the models are not applicable to the stirred vessel setup or the uncoated membrane filtrations. For this reason, Sections 5.5-5.6 include selected figures with the HSDM and LDF model applied, and the figures in Sections 5.3 and 5.4 display trendlines to guide the eye rather than models. All methylene blue filtrations with PAC and the alternative adsorbents were run with a feed solution concentration of 0.9 mg/L.

5.3.1 Effect of Coating Mass

Carbon coated membranes were shown to be viable for consistent removal of methylene blue. Figure 5.10 shows removal for 1 and 3-mg (2.9 and 8.7 g/m^2) coated membranes using WPH PAC as the adsorbent. There was an improvement in methylene blue retention compared to the uncoated membrane, with the membrane contributing to about 20% of the removal. Using a 3-mg coating, the system was capable of removing nearly 100% of the methylene blue initially.

The calculated monolayer mass for PAC was 5 mg (14.5 g/m^2). However, it is likely that both 1 and 3-mg PAC coatings sufficiently covered the membrane surface because the broad PSD in Figure 5.1 indicates the presence of smaller particles. In addition, the membranes appeared gray with no white space visible, implying full surface coverage. Despite these observations, it is likely that successful full-scale implementation of the membrane coating adsorption technique will be more easily achieved with adsorbent applications greater than the calculated monolayer mass.

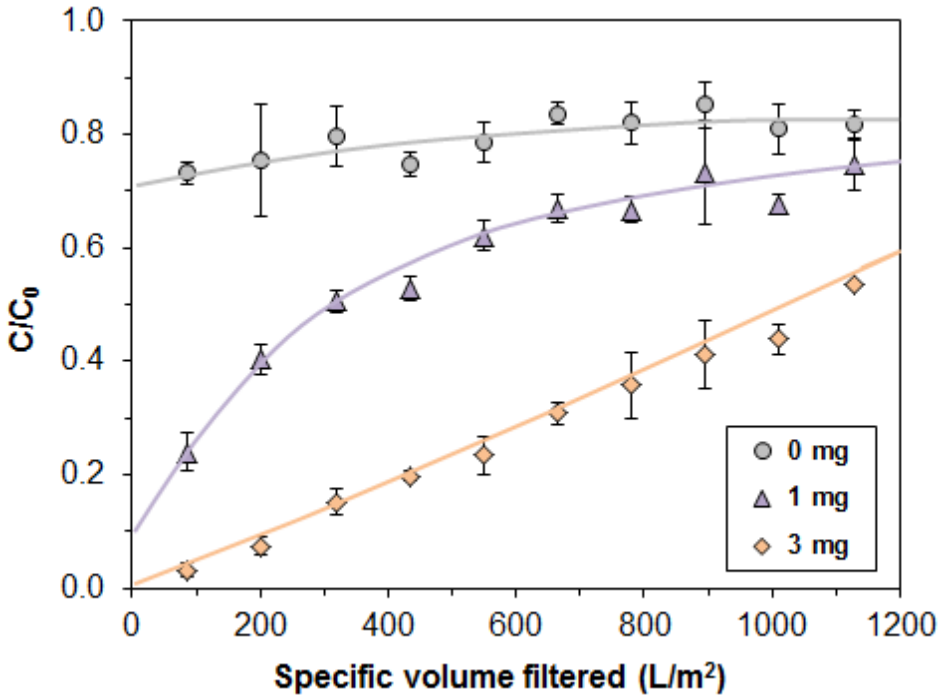

Figure 5.10. Methylene blue removal by UF membranes coated with 1 and 3 mg of WPH PAC (2.9 and 8.6 g/m^2), with permeate concentrations (C) normalized to the feed solution concentration (C_0). Removal by the uncoated membrane is shown for comparison, and the solid lines in the figure correspond to trendlines.

5.3.2 Comparison of PAC, S-PAC, MWCNTs, and NGPs

The membrane coated with 1 mg of S-PAC (Figure 5.11) showed better initial methylene blue retention than the membrane coated with 1 mg of PAC (Figure 5.10). The large external surface area of S-PAC is hypothesized to be the leading cause of the differences apparent for the breakthrough curves for PAC and S-PAC, considering that the calculations described in Section 5.1.1 revealed an external surface area for S-PAC that was 122 times higher than that of PAC on a per-gram basis. The reduced particle size of S-PAC corresponds to a high immediate contaminant removal but a steep breakthrough curve because of the lower pore volume and limited internal adsorption sites. For PAC, pores are deeper because of the higher particle volume. Therefore, pore diffusion progresses throughout the filtration, and the breakthrough curve is more gradual.

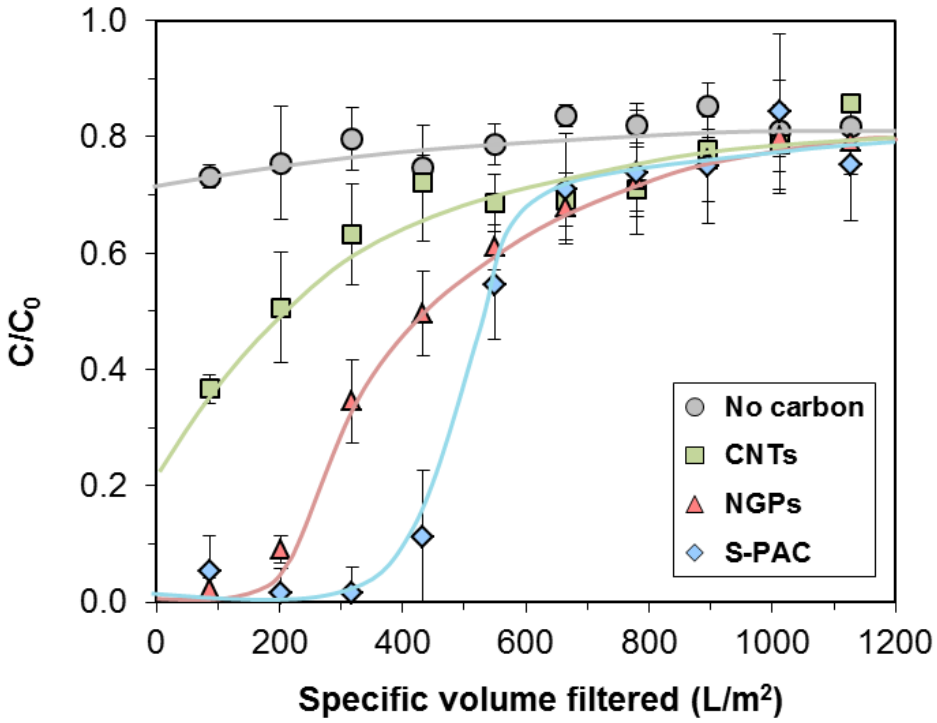

Figure 5.11. Methylene blue removal by 1 mg (2.9 g/m^2) of alternative adsorbents with a flux of 500 lmh. The solid lines in the figure are trendlines.

Research has shown that the resistance to solute mass transfer decreases with decreasing particle size (*90*), which also likely contributed to faster adsorption kinetics for S-PAC. An additional factor is the greater number of layers on the membrane for S-PAC. The calculated monolayer mass was only 50 μg, which implies that the 1-mg S-PAC coating in Figure 5.11 corresponded to a multilayer coating on the membrane. This enhanced surface coverage compared with PAC may have contributed to the better initial retention of methylene blue for the S-PAC coated membrane. One final contributor to the rapid adsorption on S-PAC relates to its higher mesopore volume compared to PAC (Table 5.2), a beneficial attribute because mesopores may serve as transport pores (*78*).

The adsorption curves for MWCNTs and NGPs in Figure 5.11 illustrate that neither of these adsorbents removed methylene blue from water as rapidly as S-PAC. A comparison with Figure 5.10 reveals that MWCNTs were slightly less effective than PAC. Methylene blue, with dimensions of 14.3 × 6.1 × ~ 4 Å, adsorbs in micropores, though there is disagreement about the minimum pore size required (*67*). MWCNTs consist of pores that fall in the meso- and macropore ranges, though it has been observed that aggregates can form voids acting as micropores for adsorption (*27*). The experimental pore size data in Table 5.2 do indicate a small volume of micropores. Nevertheless, it is likely that the micropore deficiency and lower surface area contributed to the inferior adsorption capabilities of MWCNTs.

Studies on the use of functionalized graphene oxide for the adsorption of methylene blue revealed that electrostatic interactions between the oxidized surface and cationic dye led to favorable adsorption (*31, 32*). However, the graphene used in this project is non-functionalized and had a low oxygen content compared to the activated carbons, so it is likely that its adsorption effectiveness seen in Figure 5.11 originated from some other attribute. The NGPs had an intermediate surface area of 624 (± 4) m^2/g but a mesopore volume four times that of S-PAC, so their rapid adsorption kinetics could be a result of having more easily accessible adsorption sites, dictated by the prevalence of mesopores.

To verify the adsorption kinetics observed using the carbon coatings on the membranes, batch adsorption tests were conducted. Results are shown in Figure 5.12 for the four adsorbents used for the coated membrane filtrations. The general trends observed

with the batch kinetics tests are in agreement with the kinetics trends noted earlier in this section for the coated membrane filtrations. As predicted, S-PAC showed the fastest removal of methylene blue, with a concentration reduction of more than 20% within 2 minutes. The NGPs and PAC displayed similar kinetics profiles, which may have been influenced by the tendency for the NGPs to float, a characteristic that could have resulted from low density or hydrophobicity. The flotation likely contributed to insufficient mixing in the batch tests, but because the membrane filtrations were done under pressure, the flotation of the NGPs was not an issue for the coated membrane filtrations.

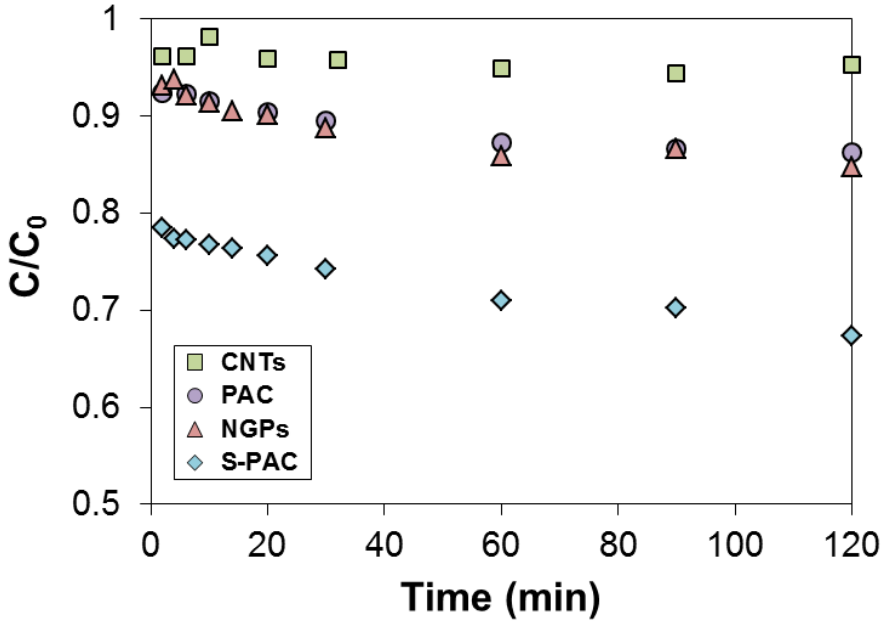

Figure 5.12. Batch kinetics adsorption tests for methylene blue and various adsorbents. Initial methylene blue concentration was 0.9 mg/L, and the carbon dose was 1 mg/L. The contents of the beakers were stirred at 200 rpm.

5.3.3 Stirred Vessel versus Coated Membrane

The hydraulic residence time in a carbon membrane coating is on the millisecond scale. For example, a 5-mg (14 g/m^2) PAC coating subjected to an influent flow rate of

500 lmh has a contact time of about 200 milliseconds. Despite the low contact time, carbon coatings displayed improved methylene blue removal kinetics over the conventional adsorption method consisting of a stirred reactor, as shown in Figures 5.13a and 5.13b. It is hypothesized that the carbon coating on the membrane improves opportunities for adsorbate-carbon contact, thereby improving retention. However, this initial improvement in retention is offset by a faster methylene blue breakthrough. At 1200 L/m^2, the total adsorption in the S-PAC coating was estimated to be 170 mg/g, and for the S-PAC in the stirred vessel it was calculated as 100 mg/g. It is likely that the removal in the stirred vessel was lower because it had not yet reached its adsorption capacity. This is apparent in the figure, since the permeate sample at 1200 L/m^2 for the stirred flask was of lower concentration than that of the uncoated membrane.

Hypothetical MCLs for contaminants are shown in the figures, which illustrates that a carbon coating may have the ability to maintain permeate concentrations below the MCL for a longer filtration period than carbon in a stirred tank. Situations requiring a large reduction in contaminant concentration may be more efficiently handled with a membrane coating, since the amount of time, t_2, in which the coating removes the contaminant below the MCL is longer than t_1, the filtration period during which the carbon in the stirred vessel maintains concentrations below the MCL. This situation is depicted in Figure 5.13a, while Figure 5.13b shows the expected scenario for a higher MCL, for which a stirred vessel configuration may be more advantageous from a carbon usage perspective.

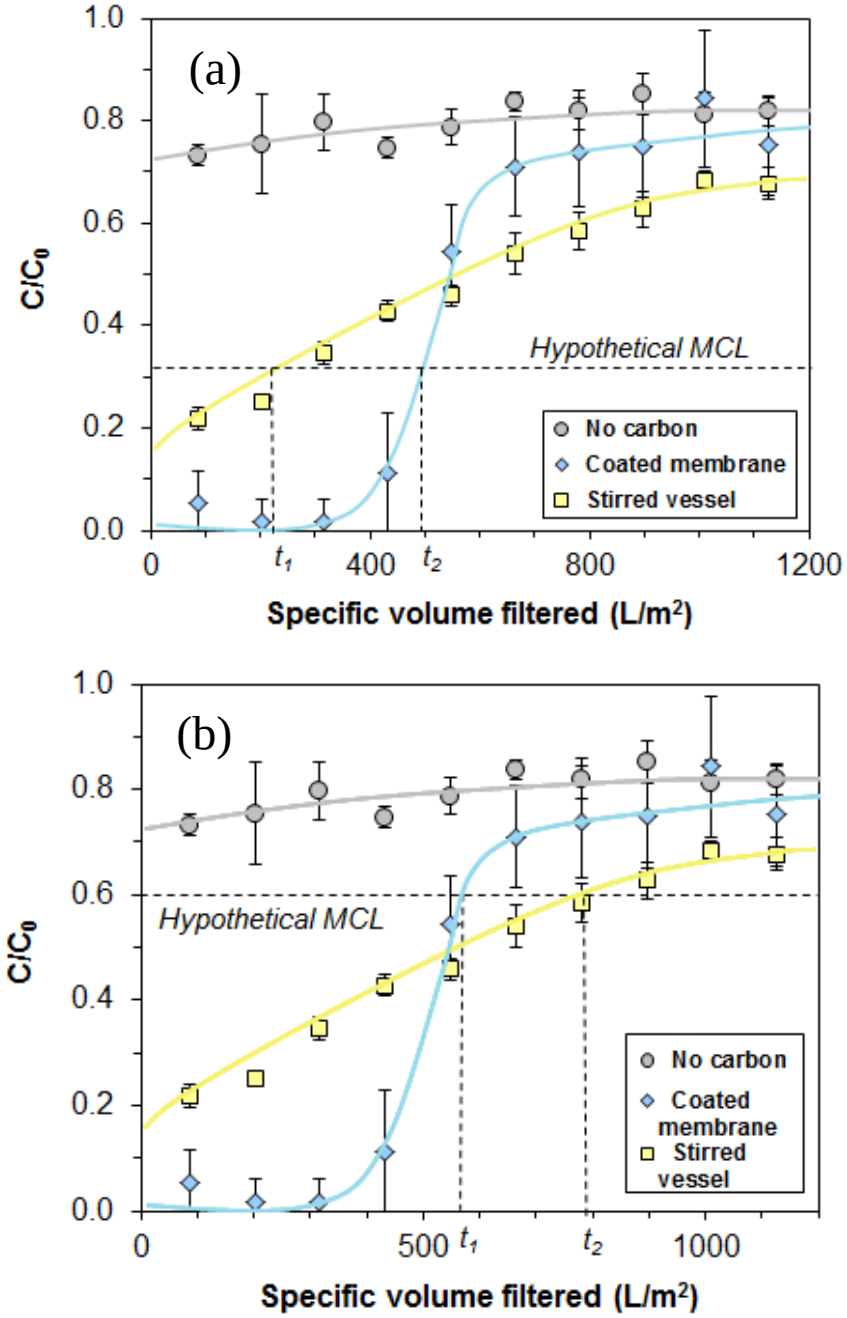

Figure 5.13. Comparison of methylene blue removal by a carbon coated membrane and a stirred vessel setup using 1 mg of S-PAC at 500 lmh, with the solid lines indicating trendlines. The residence time for the S-PAC in the stirred vessel configuration was calculated as 1.3 hours. Different hypothetical MCLs are shown in (a) and (b), with corresponding carbon usage periods, denoted by t_1 and t_2.

These results suggest that the adsorbent addition point in the filtration system may be tailored to meet the contaminant removal needs dictated by MCLs or other criteria. This type of manipulation pertaining to the carbon addition method may enable treatment plants to minimize their carbon usages rates (CURs), thereby reducing overall cost. However, there are other variables not addressed here that may need to be assessed, including adsorbent recirculation and competitive adsorption with NOM.

5.4 Atrazine Retention in Coated Membrane Filtrations

As described in the materials and methods section, the atrazine stock solution was found to be contaminated by an unidentified, tritiated compound. Therefore, a clarification is needed to explain which of the data discussed in this section were affected by the contamination. Table 5.8 provides a summary of the results influenced by the contaminated solution. To evaluate the extent of contamination, a few of the filtrations were redone with the new batch of atrazine, and these results are shown in Figure 5.14. Without the contaminant present, larger concentration reductions for atrazine were noted in the permeate.

The difference of normalized permeate concentrations (C/C_0) between filtrations conducted with contaminated feed solution and those with the new feed solution were calculated. These filtrations were originally run in duplicate, so an average of the permeate concentration for each sample point was used as the basis for comparison. An average improvement of 0.15 (C/C_0 units) was found for the 2-mg (5.8 g/m^2) PAC coatings, and for S-PAC the difference was 0.25 on average.

Table 5.8. Summary of Atrazine Results

Figure	Affected by Contamination?
5.8-5.9	No
5.14-5.18	Yes
5.19-5.21	No
A-11	Yes

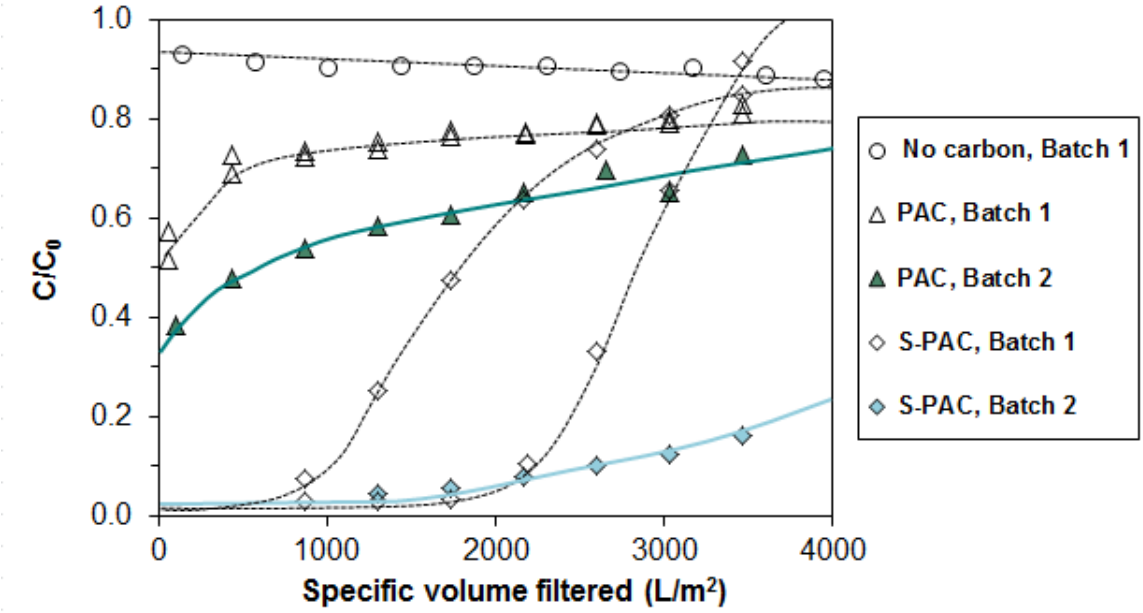

Figure 5.14. Comparison of atrazine retention by membranes coated with 2 mg (5.8 g/m^2) of WPH PAC and S-PAC, with a flux of 2000 lmh. "Batch 1" represents filtrations done using the original atrazine feed solution, which was found to be contaminated with a tritiated compound. "Batch 2" refers to filtrations conducted with the replacement feed solution. Retention by the uncoated membrane is shown for comparison, and the solid lines indicate trendlines.

Based on these results, it is clear that the activated carbon retained a substantial portion of the unidentified contaminant. However, retention by the uncoated membrane decreased from 10% (Figure 5.14) to 3% (data not shown) with the new batch of atrazine.

It is possible that atrazine was influenced by intermolecular interactions with the tritiated contaminant that was adsorbed on the membrane, leading to improved atrazine retention in the uncoated membrane filtration. It is likely that these trends apply to all of the results for the filtrations run with the first batch of atrazine. Comparable to the methylene blue results, the improvement in atrazine retention for S-PAC compared to PAC in Figure 5.14 is a result of its smaller particle size. As with Section 5.3, the solid lines in this figure correspond to trendlines, as is the case for Figures 5.15 and 5.17-5.21.

5.4.1 Effect of Flux

Figure 5.15 illustrates that a fourfold decrease in flux caused a significant improvement of atrazine retention in the membrane coatings, with a 25-mg (72 g/m^2) coating removing all atrazine from the feed solution throughout the filtration at 500 lmh. It is likely that an increase in residence time of adsorbate in the carbon coating contributed to improvements in removal with the transition from 2000 to 500 lmh. A 10-mg (29 g/m^2) coating run at 500 lmh showed similar adsorption characteristics to a 25-mg coating at 2000 lmh when plotted on the scale of time, though it should be noted that there is a lower permeate output in a set period of time with a lower flux.

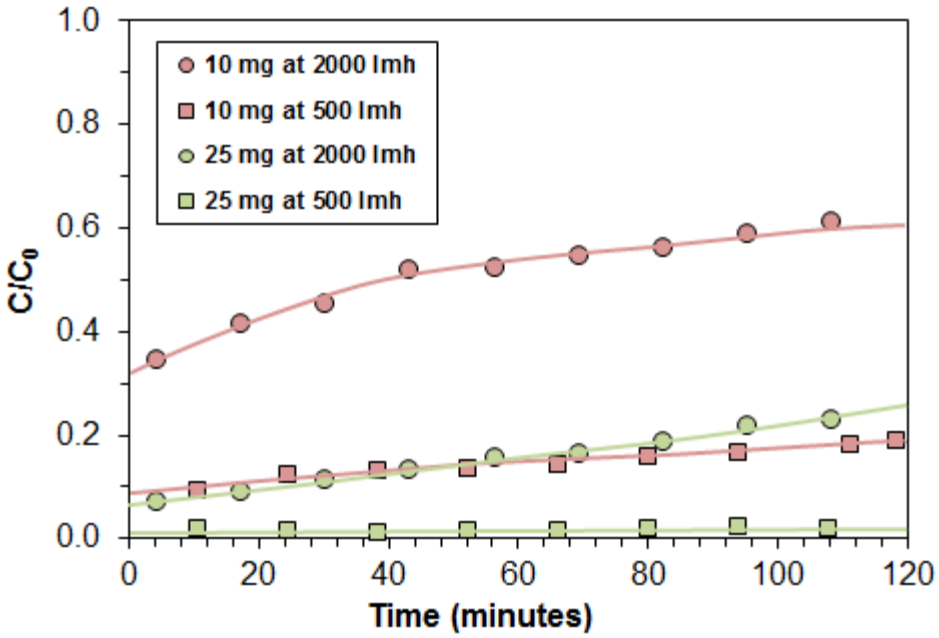

Figure 5.15. Effect of flux on atrazine removal by membranes coated with two different masses of 65 µm F400 PAC, with the solid lines indicating trendlines. These filtrations were done with the atrazine solution that was later found to be contaminated by an unknown, tritiated compound.

5.4.2 Effect of Feed Solution Concentration

Figure 5.16 shows that a 20× increase in feed solution concentration resulted in no significant change in atrazine retention, with permeate concentrations normalized to the feed solution concentration. Findings from a previous study indicate that an increase in feed solution concentration causes a faster and steeper breakthrough profile (*49*). The higher concentration is associated with an increased adsorption capacity, as shown in the isotherm in Figure 5.8, but the capacity is reached more quickly. Despite these observations, no significant correlation between feed solution concentration and breakthrough profile was observed in these results. It is likely that concentration

increases at the ppb level are not sufficient to cause a notable difference in adsorption kinetics.

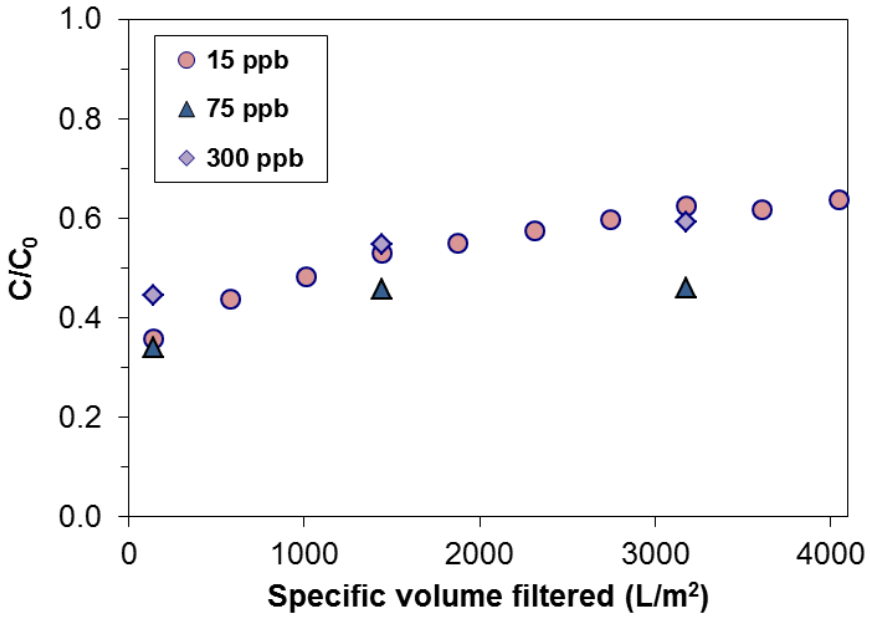

Figure 5.16. Effect of feed solution concentration on removal of atrazine using membranes coated with 10 mg of 65 µm F400 PAC at a flux of 2000 lmh. These filtrations were run with the atrazine solution that was later found to contain an unknown, tritiated compound.

5.4.3 Effect of Adsorbent Type and Size

Figure 5.17 shows that NGPs and S-PAC retained atrazine better than PAC in 2.5 mg applications (7.3 g/m^2). In fact, none of the S-PAC samples yielded statistically significant radioactivity measurements, indicating that the coating successfully removed all influent atrazine. For methylene blue, retention by the NGP coating was nearly as effective as the S-PAC coating, but for atrazine there was a notable difference. Aside from feed solution concentration differences, this could be caused by structural characteristics of the adsorbates and adsorbents. For example, atrazine is a smaller

molecule than methylene blue, which enables it to more rapidly diffuse and access smaller micropores present in the S-PAC but not found in the NGP structure. As with the methylene blue filtrations, adsorbent surface coverage on the membrane is likely to be an additional key factor.

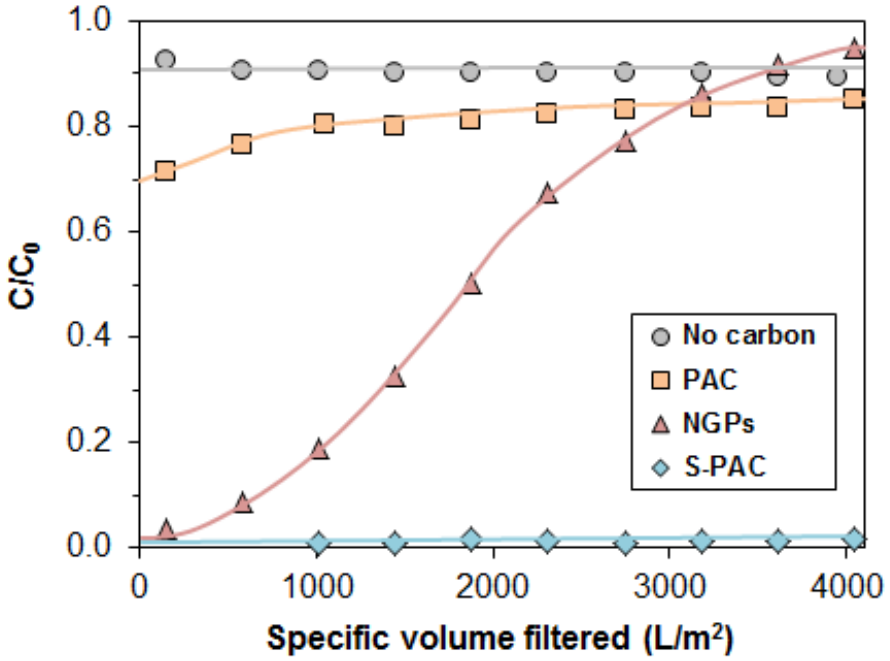

Figure 5.17. Atrazine removal by membranes coated with 2.5 mg of adsorbent, with a flux of 2000 lmh. The solid lines correspond to trendlines. F400 PAC of average particle size 65 µm was used, while S-PAC was generated from WPH PAC. These filtrations were conducted with an atrazine solution that was later found to contain an unidentifiable, tritiated compound.

An additional comparison of the adsorbents is provided in Figure 5.18, which shows results for filtrations with PAC of two particle sizes, as well as MWCNTs and S-PAC. The 1-mg S-PAC coatings initially removed more atrazine from the feed solution than the 25-mg PAC coatings, which reinforces the previous assertions that particle size and possibly mesoporous structure are key determinants for adsorption kinetics.

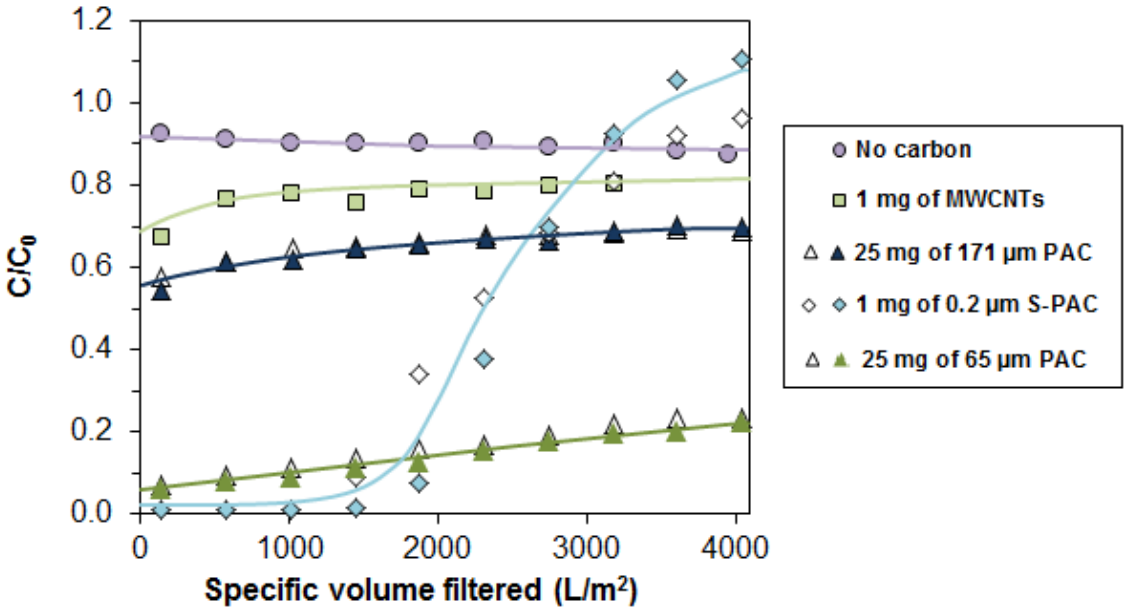

Figure 5.18. Atrazine removal by membranes coated with F400 PAC, S-PAC, and MWCNTs, with a flux of 2000 lmh. The solid lines indicate trendlines, and the filtrations were done with the atrazine solution that was later found to be contaminated by an unknown, tritiated compound.

The measured permeate concentrations for S-PAC exceeded the feed concentration near the end of the filtrations, which is an unexpected result. It is possible that the S-PAC was passing through the membrane because of its small particle size, resulting in the detection of adsorbed atrazine molecules by the liquid scintillation counter. This situation would produce an erroneously high concentration, leading to C/C_0 values greater than one. Alternatively, the tritiated contaminant may have been competing with atrazine for sorption sites on the carbon particles. If the contaminant had a stronger sorption affinity than atrazine, it could have induced desorption of atrazine molecules, leading to increases in permeate concentrations. This explanation is more reasonable than the membrane passage of S-PAC, as further filtrations (Figure 5.19) with

the uncontaminated atrazine did not yield normalized permeate concentrations in excess of one.

5.4.4 Stirred Vessel versus Coated Membrane

Figure 5.19 shows that, for each of the alternative adsorbents, retention of atrazine in the membrane coating was superior to that in the stirred vessel. As before, MWCNTs displayed lower retention compared to the other materials. In fact, while the S-PAC coating showed atrazine retention near 100% at the beginning of the filtration, the MWCNT coating had only about 15% removal.

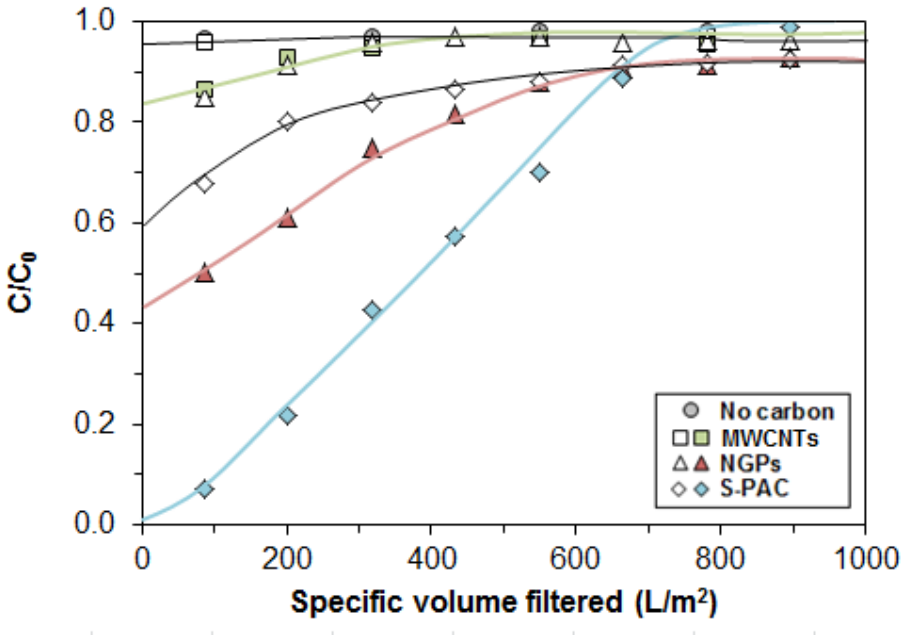

Figure 5.19. Comparison of atrazine retention in the stirred vessel (open symbols) and coated membrane (solid symbols). The flux was 500 lmh, and the mass application was 0.5 mg (1.4 g/m^2). Trendlines were applied to the data and are shown in the figure.

A notable feature of the atrazine breakthrough profiles in Figure 5.19 that is not present in the methylene blue results of Figure 5.13 is the significant improvement in total retention in the membrane coating compared with the stirred vessel. A conjecture for

the science behind this phenomenon is described and illustrated in Section 2.3.2. In short, the liquid-phase concentration in contact with the membrane coating is higher than the liquid-phase concentration present in the stirred tank. Because a higher concentration corresponds to a higher adsorption capacity on the isotherm, the membrane coatings have the potential to remove more contaminant before necessitating replacement. The effect is more significant for lower concentrations, since isotherm curves are steeper at lower concentrations. Consequently, the methylene blue filtrations at higher feed solution concentrations did not show noticeable differences in total contaminant removal between the stirred vessel and membrane coating, while the atrazine filtrations at 26× lower concentrations did reveal differences.

In addition to the filtrations with the alternative adsorbents, a comparison of the stirred vessel and membrane coating techniques was done with WPH PAC at a dose of 10 mg (29 g/m^2), and results are shown in Figure 5.20. The coated membrane displayed retention near 100% throughout the filtration, while the stirred vessel configuration showed lower retention. The curve for the stirred vessel setup has a U-shape, which is characteristic of pulse dosages to stirred tanks (*91*). In the early stage of the filtration, the feed solution ahead of the stirred tank has lower contact with the adsorbent, and permeate concentrations are relatively high. Decreases in permeate concentration as the filtration progresses are likely caused by the accumulation of PAC on the membrane surface, which effectively enables contact between the contaminant and adsorbent in both the stirred tank and membrane coating. The permeate concentrations then begin increasing again as adsorption capacity is approached. The U-shaped curve is not apparent in the

figures for the alternative adsorbents, which may be a result of the lower mass of adsorbent used.

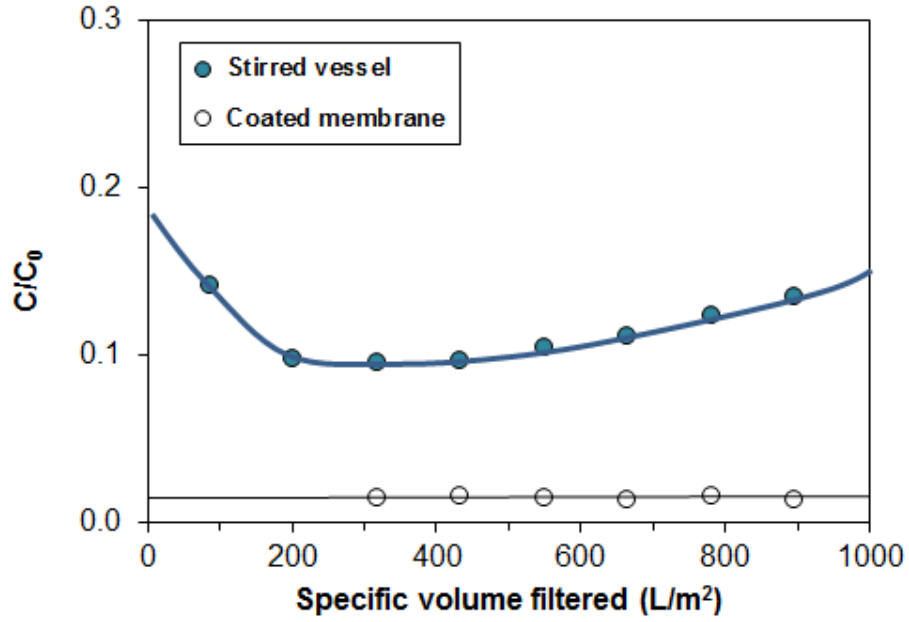

Figure 5.20. Atrazine removal by 10 mg (29 g/m^2) of WPH PAC comparing adsorption in a stirred flask and a membrane coating with a flux of 500 lmh. Trendlines were applied to the data.

5.4.5 Comparison of Atrazine and Methylene Blue

To determine what effects adsorbate identity has on adsorption characteristics, separate filtrations were conducted with methylene blue and atrazine, with all filtration conditions equivalent and S-PAC as the selected adsorbent. Accounting for differences in retention by the membrane, it appears that methylene blue and atrazine exhibit approximately equivalent affinities for adsorption sites on the carbon particles. However, the initial retention of atrazine exceeded that of methylene blue, possibly a result of the faster diffusion associated with atrazine, the smaller of the two molecules. Methylene

blue has the advantage of bearing three aromatic rings for favorable π-π interactions at the carbon surface. Atrazine has only one aromatic ring, but it has an advantage of being a smaller molecule that can access smaller pores, which are associated with greater adsorption energies.

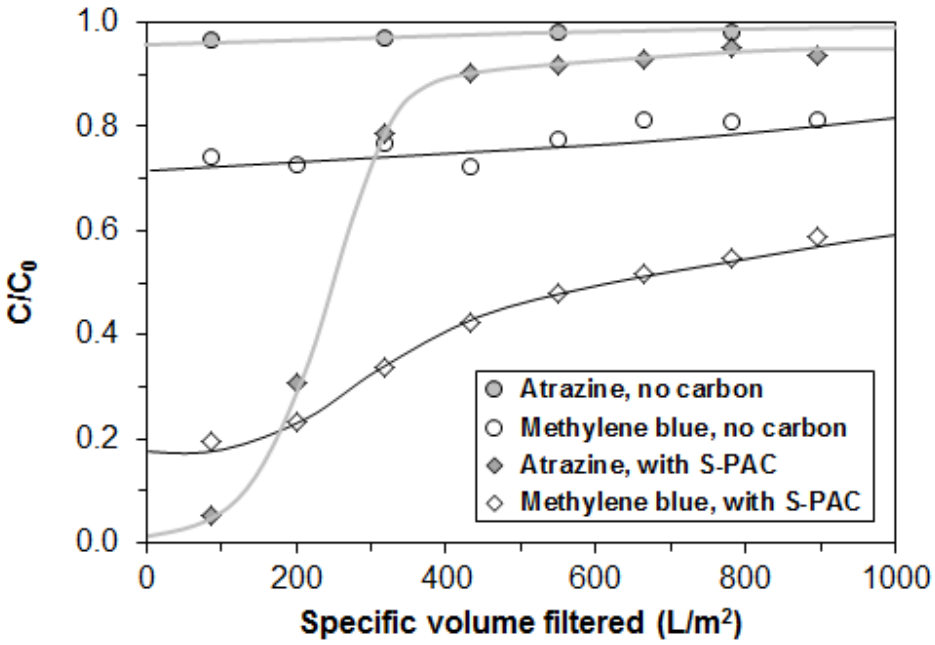

Figure 5.21. Filtration with 1 mg of S-PAC at 500 lmh and 0.9 mg/L feed solution concentration for both atrazine and methylene blue, with the solid lines indicating trendlines.

5.5 HSDM Application

The HSDM was applied to the experimental data sets with the intent of evaluating model accuracy and identifying the causes of deviations. The model was programmed in MATLAB, and the applicable programs are available in Appendices B-3 through B-7.

5.5.1 Verification with Packed Columns

Two different approaches were used to determine if the HSDM was properly programmed in MATLAB. The first was a verification using sample parameters taken from the literature source that provided the equations for the model (*54*). Shown in Figure 5.22a and Figure 5.22b are the breakthrough curves from the literature and the MATLAB model, respectively. The figures correspond to filtration of phenol through F400 GAC columns of 65 cm depth. As the curves look very similar, it was concluded that the programming was correct, and the model was verified as applicable for deep-bed GAC column data.

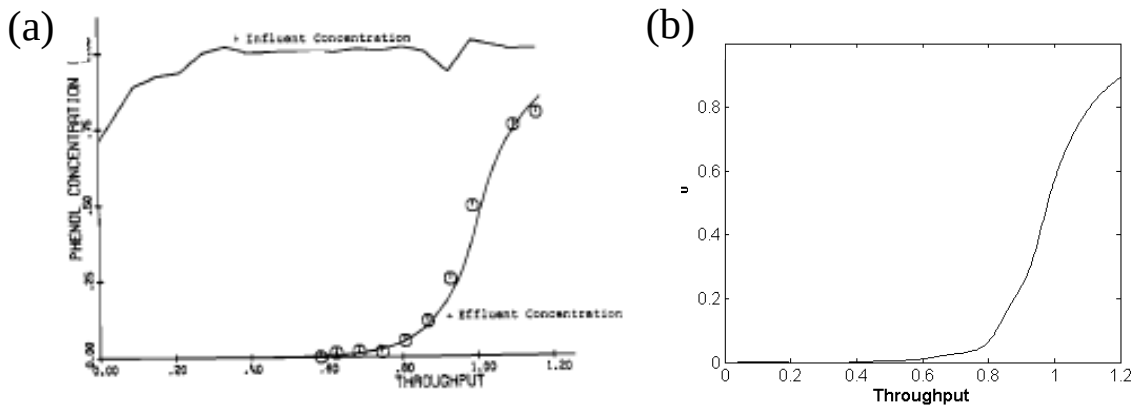

Figure 5.22. (a) Breakthrough curve for filtration of phenol through a F400 GAC column (copied from ref. [54]). (b) HSDM output with identical parameters executed in MATLAB.

The second approach for analysis of the MATLAB model involved testing it for application to small-column adsorption data collected in the laboratory with methylene blue and F400 GAC. Langmuir isotherm coefficients were found in the literature (*73*), and they were verified experimentally using four bottles containing equilibrated

carbon/methylene blue mixtures. Filtrations were run with columns of 1-2 cm, and results are shown in Figure 5.23. It is notable that the model was adequate for the larger mass of 3.3 g, but for the smaller mass (0.9 g), deviations are apparent.

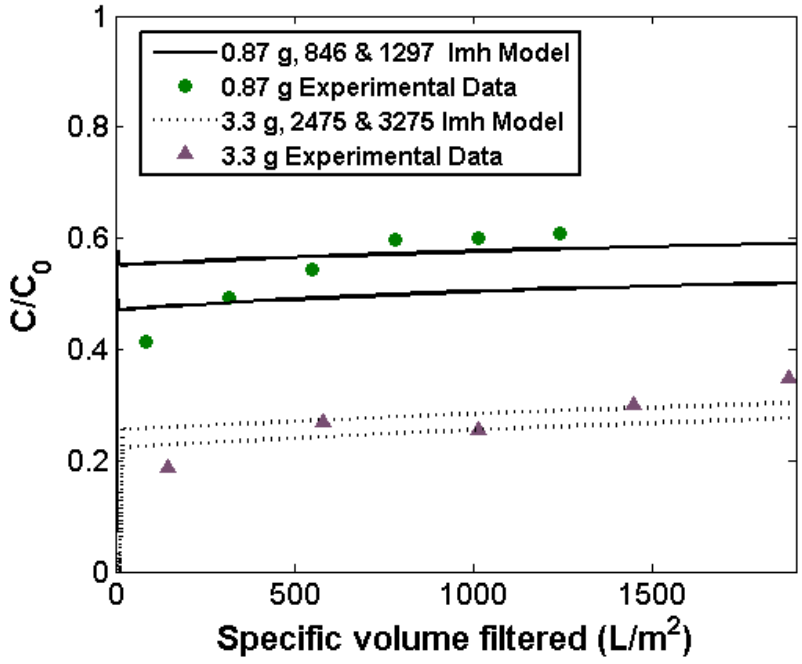

Figure 5.23. Model predictions and experimental results for filtrations of methylene blue through F400 GAC columns with two different masses. Feed solution concentrations were 3.4 mg/L in each case. Experimental flux values were unsteady, so ranges were applied to the model, and lines shown in the figures indicate model outputs using the average flux plus or minus the standard deviation. (In each case, the lower flux corresponds to the lower line in the graph.)

5.5.2 Application to Membrane Coatings

Using the HSDM for membrane coatings required that the retention of the adsorbate in the membrane be taken into account. Experiments were run to determine the relationship between concentration and retention in the membrane, with the results indicating that the removal in the membrane for both atrazine and methylene blue is a

percentage of the liquid-phase concentration, not a set amount of removal. The HSDM was applied to selected experimental filtration conditions, and the results are shown in Figures 5.24 and 5.25. An additional application to atrazine filtrations is included as Figure A-12.

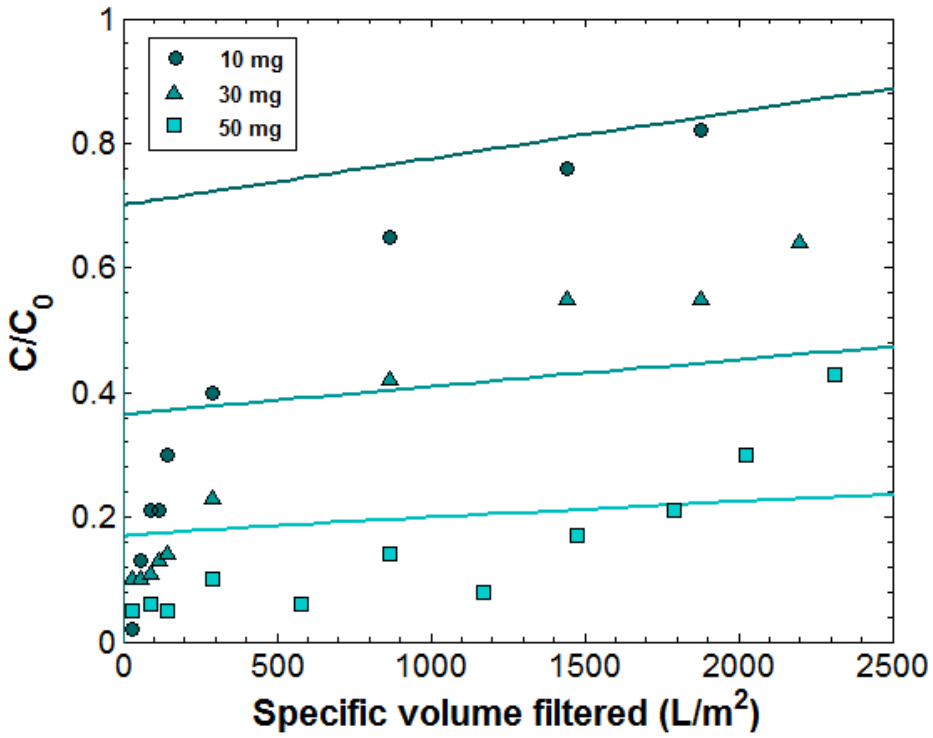

Figure 5.24. HSDM results for filtrations through membranes coated with three different masses of 170 µm F400 carbon. The flux was 1800 lmh, and methylene blue was the model contaminant with C_0 = 0.5 mg/L.

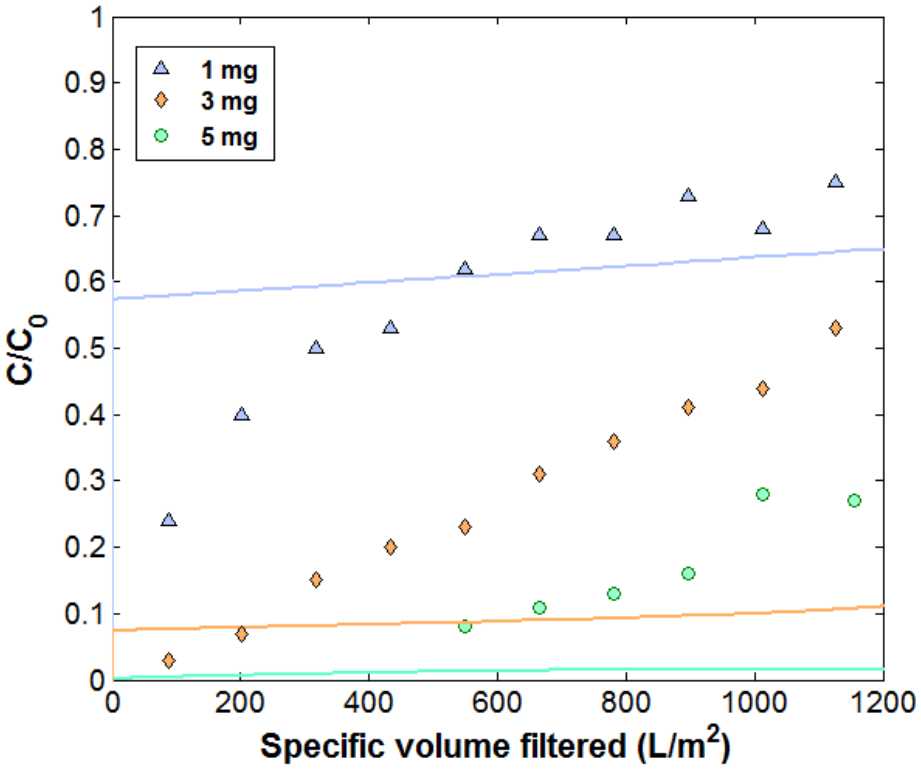

Figure 5.25. HSDM results for filtrations through membranes coated with three different masses of WPH PAC. The flux was 500 lmh, and methylene blue was the model contaminant with C_0 = 0.9 mg/L.

It is clear from Figures 5.24 and 5.25 that the HSDM did not function well for membrane coatings. In addition, the model program predicted an immediate breakthrough for S-PAC coatings, which was not observed experimentally. Possible sources of deviations are as follows:

1. The carbon layers were sufficiently thin, such that the porosity estimation of 0.37 described in Section 5.1.5 was inaccurate.

2. The use of an average particle size rather than incorporation of the entire particle size distribution was inadequate, since particle size affects the shape of the breakthrough curve.
3. The surface diffusion coefficients obtained with the Sontheimer correlation were inaccurate.
4. The built-in differential equation solver using the Runge-Kutta method in MATLAB produced rounding errors.
5. The carbon mass applications were too small, such that the mass transfer zone was not large enough for model application.
6. The adsorbents were not evenly distributed on the membrane surfaces.

The first point in the list was addressed by applying an adjusted porosity to the model when the deposited mass was less than that needed to form a monolayer on the membrane. In such a case, the program finds the porosity using Eq. 6, estimating the bed volume from the membrane surface area and particle size of the adsorbent. Items 2 and 3 in the above list are addressed in the following sections. Attempts were not made to rectify the potential problems identified in items 4 and 5, since they would require more radical adjustments to the model and its programming. Visible inspection of the membranes did not reveal heterogeneities in the distribution of the activated carbon coatings on the membranes, so the sixth item in the list was not addressed.

5.5.3 Effect of Particle Size Distribution

Because Figures 5.1 and 5.2 depict broad PSDs, it was hypothesized that particle size variability contributed to model deviations. In particular, particles that are smaller than the average diameter incorporated in the model may have caused lower experimental permeate concentrations in the first few minutes of filtration than those that were predicted from the model, since small particles are associated with fast adsorption kinetics. Figure A-13 shows sample breakthrough curves that emphasize the significance of particle size on retention characteristics. To enable the model to account for PSD, the following rationale was used, and program adjustments were made:

- The membrane surface was divided into theoretical fractions based on the relative percentages of each particle size group given by the PSD.
- The model parameters were adjusted to direct a portion of the influent flow through each theoretical membrane segment coated with the fractional mass of adsorbent given by the PSD.
- The total contaminant concentration in the permeate was calculated by summing contributions associated with each particle size fraction.

Following the above procedure, it was found that the PSD affected the modeled contaminant retention negligibly. Consequently, using an average particle size as intended by the original model was adequate for encompassing the differences in adsorbent size characteristics.

5.5.4 Adjustment of the Surface Diffusion Coefficient

The surface diffusion coefficient was identified as a parameter that affects model output significantly. This observation was verified with the use of the LDF model (described in Section 5.6), which showed that intraparticle diffusion rather than external mass transfer governed the rate of adsorption for the filtrations with WPH PAC coatings. Because the Sontheimer correlation has been described as a means of acquiring only a rough estimation of the surface diffusion coefficient, it was considered possible that the inaccuracy in this parameter may be a primary source of errors.

Implementing an adjusted surface diffusion coefficient in the model was successful in fitting the model output to the experimental data points in Figure 5.26. However, the surface diffusion coefficient used was about 100 times lower than the value of 7×10^{-11} cm^2/s predicted by the Sontheimer correlation, and the use of the smaller value could not be justified. Typical values found in the literature are comparable to the number predicted by the Sontheimer correlation, and the coefficient computed with the correlation yielded well-fitted curves for the F400 GAC results in Figure 5.23.

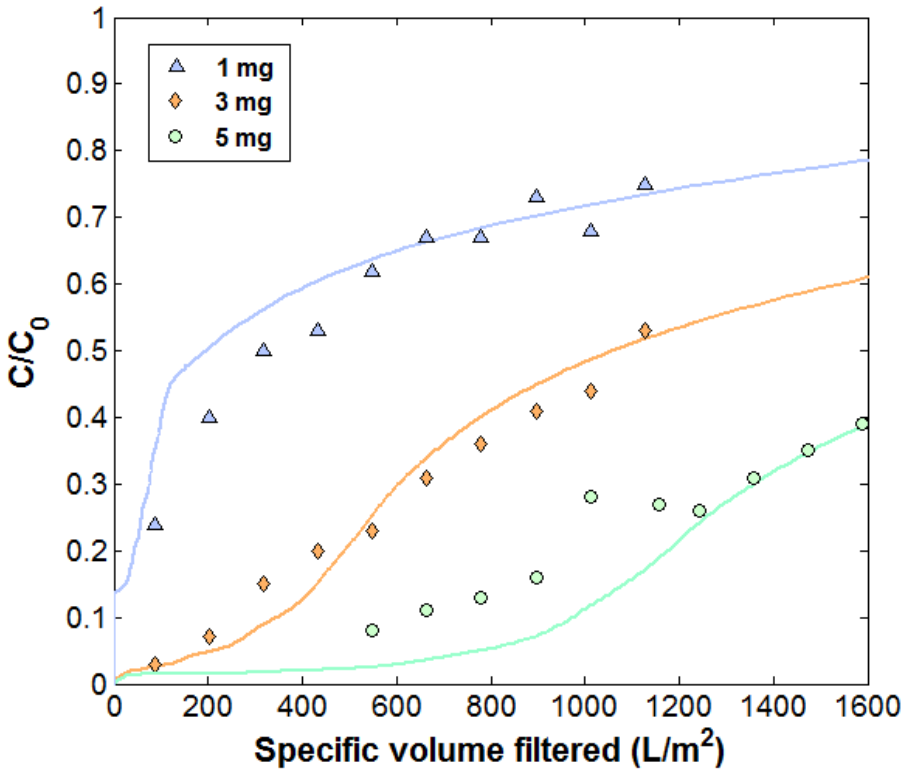

Figure 5.26. HSDM results for WPH PAC filtrations through coated membranes with a flux of 500 lmh using methylene blue as the model contaminant. For these model applications, a surface diffusion coefficient of 7×10^{-13} cm^2/s was used, with all other parameters kept the same as those applied in Figure 5.25.

5.6 LDF Model Application to Membrane Coatings

As in the HSDM applications, the removal of the contaminant by the membrane was taken into account for the results reported in this section. Shown in Figure 5.27 are the results of the LDFC and LDFQ model applications to filtrations with methylene blue and F400 PAC membrane coatings. For the LDFC model applications, an average R^2 value of 0.78 (± 0.13) was achieved, and a comparable value of 0.79 (± 0.14) was calculated for the LDFQ.

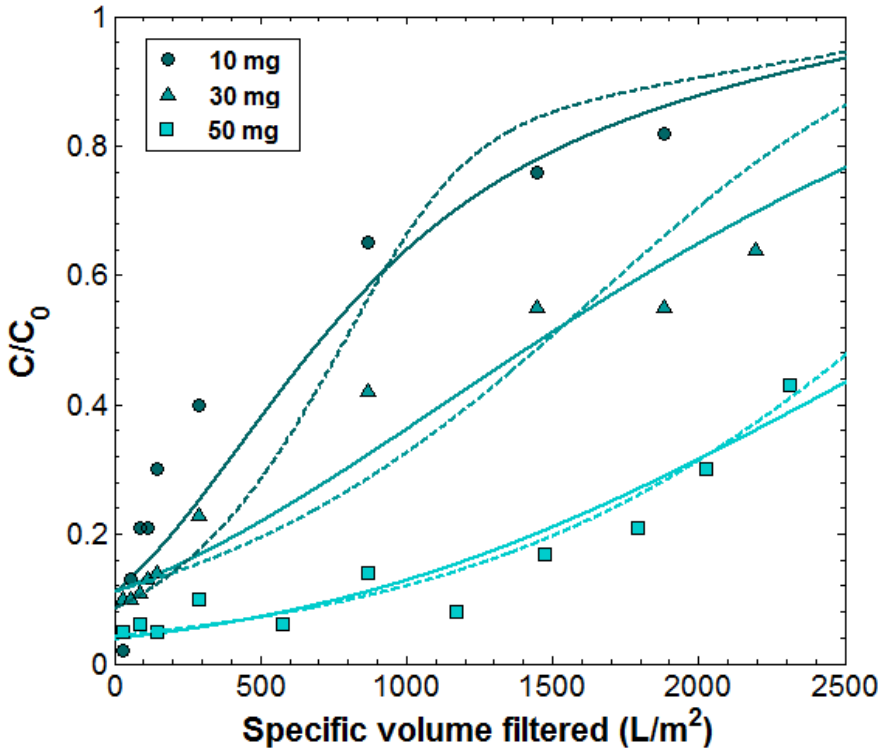

Figure 5.27. LDFQ (solid lines) and LDFC (dashed lines) model fits for filtrations with three different masses of 170 µm F400 PAC at a flux of 1800 lmh with methylene blue as the model contaminant and C_0 = 0.5 mg/L.

A quantitative assessment of the model fits to the data for the WPH PAC coatings (Figure 5.28) illustrates that the LDFQ model is more suitable for the results. Calculated R^2 values were 0.93 (± 0.05) for LDFQ and 0.82 (± 0.09) for LDFC. Consequently, the surface diffusion mechanism was likely more important than film transfer for these filtrations. This in turn is a result of the rapid convective flow in the system compared to the slower surface diffusion into the pores of the adsorbent particles.

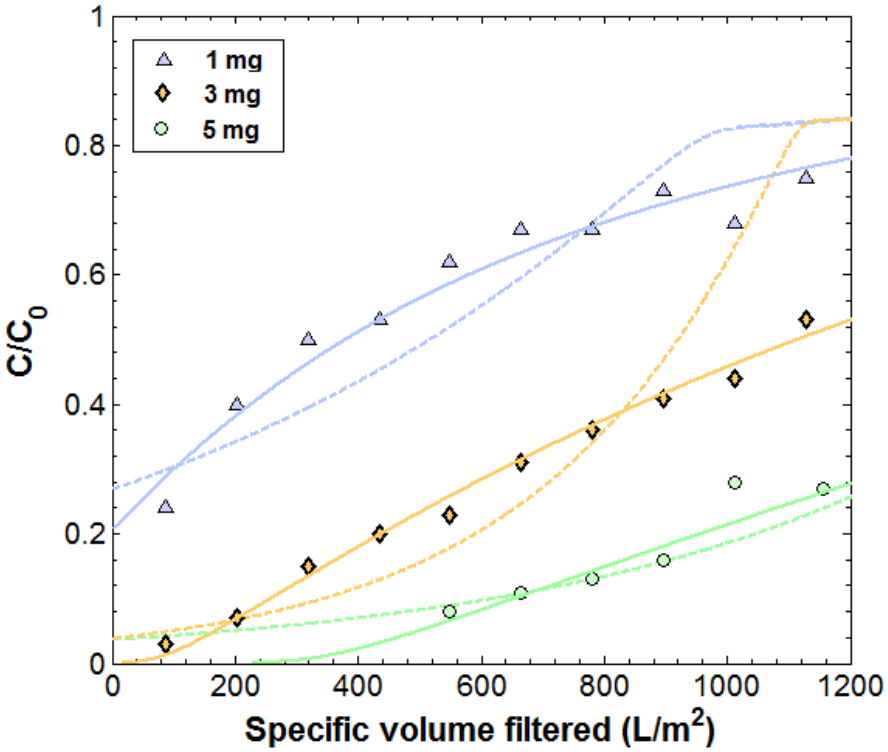

Figure 5.28. LDFQ (solid lines) and LDFC (dashed lines) model fits for WPH PAC filtrations with methylene blue at a flux of 500 lmh and C_0 = 0.9 mg/L.

5.7 Membrane-Carbon Cross-Linking

The application of polyDADMAC to membranes had minimal effect on the adherence of PAC or S-PAC to the membrane surface. For some trials, the polymer actually seemed to impede carbon adherence. Furthermore, polymer coated membranes exhibited poor permeability as evidenced by drastic flux declines. The application of polymers as cross-linkers in coated membrane filtrations needs to be studied further to evaluate the best membrane-polymer combinations and application concentrations to maximize adsorbent adherence and minimize flux reduction.

5.8 Flux Measurements

5.8.1 Flux Reductions

A representative data set from the flux reduction experiments is graphed in Figure 5.29, which shows results from a 3-mg S-PAC coating test. The figure indicates the reference flux through the uncoated membrane as well as the reduction observed with the addition of the adsorbent and the recovery after backwashing. In Figure 5.30, the average normalized fluxes after 1-mg carbon additions are shown for the various adsorbents along with the appearances of the coated membranes. The addition of PAC, MWCNTs, and NGPs resulted in only slight flux reductions (less than 4% each), but S-PAC was more detrimental (17% reduction) for a 1-mg coating. It is apparent that although the small S-PAC particles had fast adsorption kinetics, they caused the greatest filtration resistance.

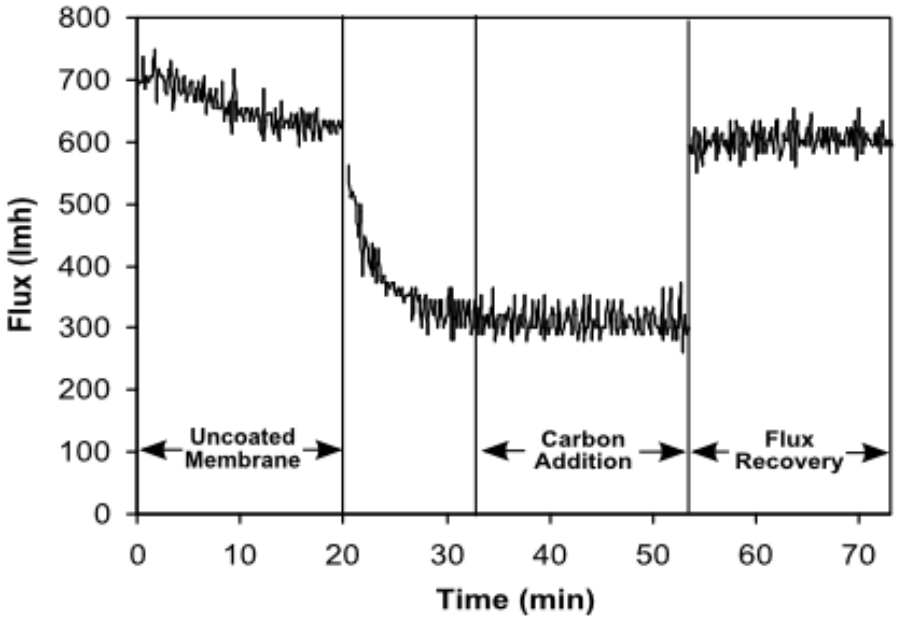

Figure 5.29. Flux measurements for a 3-mg S-PAC coating showing each stage of the flux experiments. In the region between the uncoated membrane filtration and the carbon addition, the carbon was depositing on the membrane. The flux recovery was measured after backwashing.

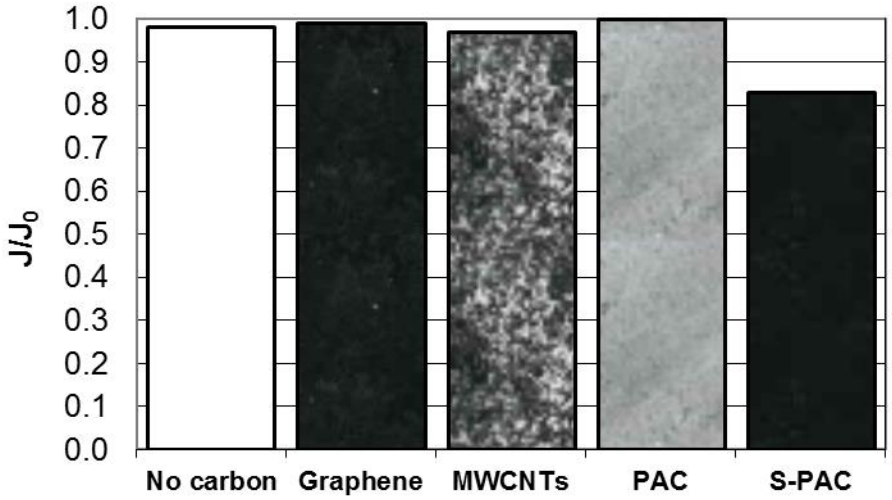

Figure 5.30. Flux reductions associated with the addition of 1 mg of adsorbent to the membrane. The flux values were normalized to the reference flux for the membrane before carbon application, and the fill patterns of the bars were formed from scanned images of the coated membranes. Values are based on averages over 20 minutes of filtration.

The Kozeny-Carman model shown in Eq. 15 was applied to the PAC and S-PAC results, assuming a porosity of 0.37. For PAC, the model predicted less than 1% flux decline for carbon applications of 1, 30, and 50 mg, which is consistent with experimental results. However, for full-scale systems, other variables influence the degree of fouling. For example, a study on PAC/UF with hollow-fiber membranes revealed that particles tend to clog fibers at the inlet of the module (*41*).

Filtrations with seven different mass applications of S-PAC to the membranes were conducted to draw conclusions about the applicability of the model to S-PAC coatings and to demonstrate the propensity for this adsorbent to reduce flux. Application of the model with the 230 nm average S-PAC particle diameter collected from the particle size analyzer overestimated the flux declines, as shown in Figure 5.31. A better

fit was found using the model with a particle diameter in the 400-500 nm range. The deviations may be due to re-aggregation after sonication to produce a larger effective particle size during the filtration, or to a cake porosity larger than 0.37.

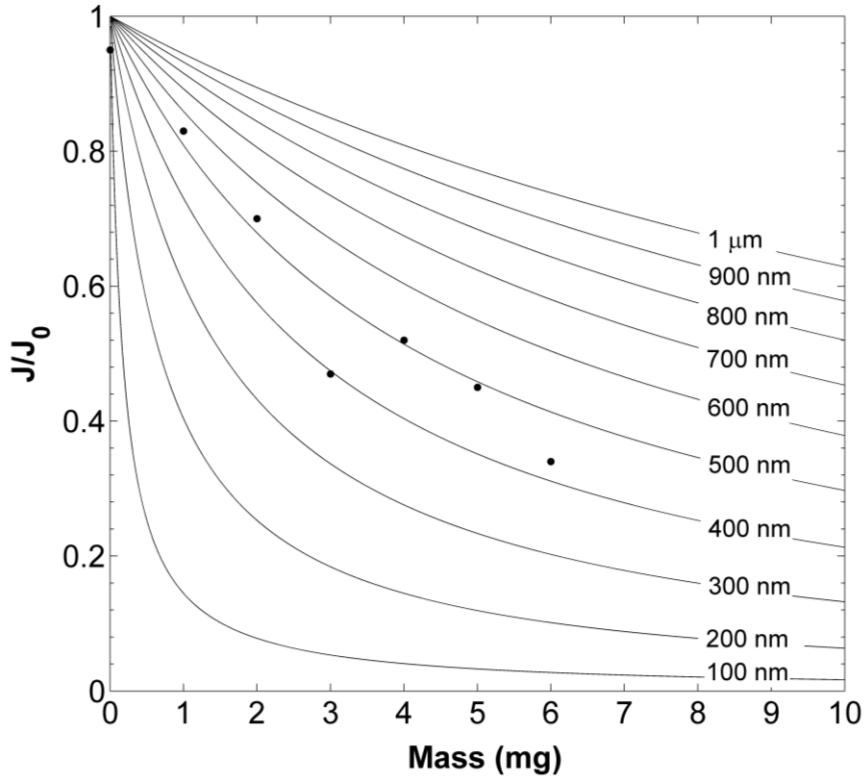

Figure 5.31. Normalized experimental flux values for seven different mass applications of S-PAC (data points). The results of the Kozeny-Carman model (solid lines) are shown for varying particle diameters, which are listed at the right.

In another study, NOM was contacted with S-PAC for comparison with PAC, and trans-membrane pressure was monitored (*92*). The authors observed that the system with S-PAC actually showed less fouling because of its stronger flocculation ability and increased propensity for removal of NOM, a membrane foulant. Consequently, although the results of this project imply that S-PAC may negatively impact filtration efficiency,

other conditions need to be taken into account in an evaluation of the application of S-PAC to water treatment.

5.8.2 Flux Recoveries

Previous work has implied that higher-pressure filtration causes membrane compaction, leading to anomalous flux values (*93*). For this reason, an uncoated membrane test was run as a control, with the results in Figure 5.30 indicating that the application of 35 psi backwash pressure for one minute reduced the flux by only 3%, which might be attributable to the normal flux decline rather than membrane compaction.

After backwashing, flux recovery exceeded 90% in each case, even for S-PAC applications of up to 6 mg, which had decreased the flux by 66% during the carbon application. However, the S-PAC membranes remained visibly fouled as noted by their black color (Figure 5.32). No correlation was noted between S-PAC application mass and flux recovery, and the average recovery for six trials from 1-6 mg was 92 ± 3%. These observations imply that some physically irreversible pore clogging or surface attachment occurred, and that this process is independent of mass application. In addition, the potential for S-PAC to pass through the UF membrane completely is a possibility because the average S-PAC particle size is close to the average pore size of the UF membrane, an observation that is reinforced by Figure A-9.

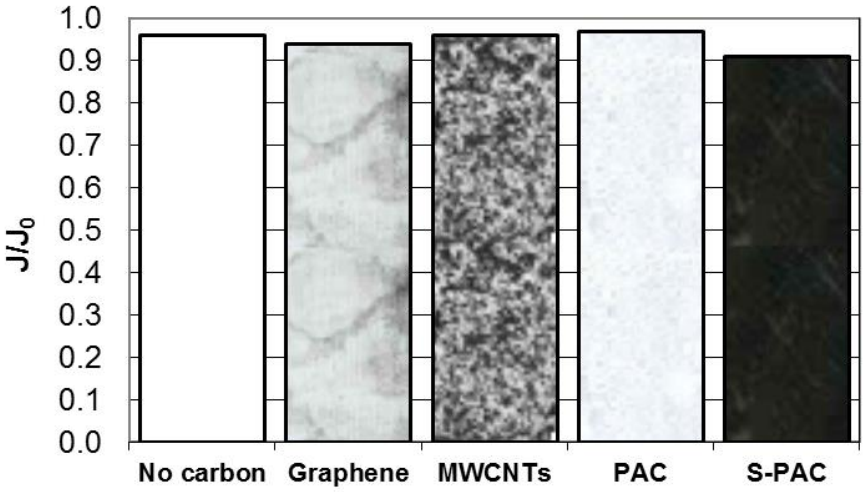

Figure 5.32. Flux recoveries for 1-mg coated membranes after backwashing, normalized to the reference flux for the membrane before carbon application. The fill patterns of the bars were formed from scanned images of the backwashed membranes.

Because S-PAC showed the best contaminant removal properties but the most extensive membrane fouling, it was considered desirable to attempt to improve the flux characteristics of S-PAC filtrations. This motivated the construction of layered coatings using multiple adsorbents. To test this technique, NGPs were applied to the membrane as a 1-mg coating before assembling a 2-mg layer of S-PAC, with NGPs selected as the lower layer because of their platelet structure and ability to maintain flux. A schematic of the intended construction is shown in Figure 5.33.

Figure 5.33. A representation of a layer-by-layer assembly of adsorbents. Figure not drawn to scale, and although the manufacturer of the NGPs describes them as platelets, they may in actuality adopt more spherical shapes as a result of aggregation.

No change in flux decline or flux recovery was observed compared to the 2-mg S-PAC coatings without an intermediate NGP layer. It is possible that the S-PAC particles were small enough to pass through the NGP layer and foul the membrane. If S-PAC is to be applied to full-scale systems, additional work may be needed to resolve the issue of significant flux impediment seen with applications even at low masses.

CHAPTER SIX

CONCLUSIONS AND FUTURE WORK

6.1 Conclusions

6.1.1 Assessment of Objectives

Objective 1. ***Compare the suitability of different carbonaceous materials for adsorption of methylene blue and atrazine in membrane coatings***. For methylene blue, adsorption effectiveness as determined by kinetics during filtrations was S-PAC > NGPs > PAC > MWCNTs, though S-PAC and NGPs showed similar breakthrough profiles. For atrazine, retention in the S-PAC coating was markedly superior to the coatings with the other adsorbents, likely a result of mesoporosity and particle size.

Objective 2. ***Determine the effect of varying filtration parameters on contaminant retention*****.** Changes in feed solution concentration at the ppb level showed no noticeable differences in the breakthrough profiles for atrazine. A decrease in flux improved atrazine removal because of increased contact time between adsorbate and adsorbent during the filtration, and increasing carbon dose produced an expected increase in contaminant removal for both methylene blue and atrazine.

Objective 3. ***Use a stirred vessel setup for comparison with the coated membrane approach***. In the stirred vessel configuration, breakthrough was slower. The methylene blue results imply that the appropriateness of using a stirred tank or a membrane coating depends on the magnitude of contaminant concentration reduction needed. For atrazine, the membrane coating showed greater retention with all adsorbents. The differences

between the methylene blue and atrazine results likely stem from the differing feed solution concentrations.

Objective 4. ***Develop a predictive model for contaminant adsorption in the carbon layer.*** The HSDM was not well suited for the prediction of adsorption in thin adsorbent layers. However, good agreement was obtained between the empirical LDF model and the experimental results.

Objective 5. ***Evaluate the contribution to membrane resistance resulting from application of a carbon coating and determine the extent of flux recovery.*** Model predictions and experimental results for PAC demonstrate that applications at the membrane coating scale (< 300 g/m^2) caused negligible flux reductions. Similarly, NGPs and MWCNTs only slightly reduced the flux. S-PAC caused significant reductions, even at low mass applications, though 88% or higher flux recovery was achieved after backwashing.

Objective 6. ***Attempt to improve coating adherence to the membrane with the use of polyDADMAC***. Unfortunately, polyDADMAC was unable to contribute to improvements in carbon adhesion on the membrane, and for some tests, the carbon did not adhere to the membrane at all. Furthermore, flux tests with polymer-coated membranes revealed dramatic reductions in flux associated with the application of the polymer.

Objective 7. ***Evaluate the advantages and disadvantages of the different adsorbents.*** Table 6.1 provides a qualitative summary of the filtration characteristics of the four adsorbent types tested in this project.

Table 6.1. Evaluation of the Adsorbents

Adsorbent	Overall Contaminant Removal	Adsorption Kinetics	Flux Decline	Flux Recovery
MWCNTs	Low	Slow	Low	High
NGPs	Intermediate	Intermediate	Low	High
S-PAC	High	Fast	High	Intermediate
WPH PAC	Intermediate	Slow	Low	High

Note – entries in table are based on relative comparisons among these four adsorbents only.

Filtrations with S-PAC coated membranes were shown to be the most effective for rapid contaminant removal, but S-PAC was hindered by its tendency to reduce the flux significantly. NGPs, with good contaminant removal and low flux reduction, are likely to be well-suited for membrane applications. Because of low surface area and possible incompatibilities relating to adsorbate size and pore size, MWCNTs were inferior to the other alternative adsorbents.

6.1.2 Practical Implications

The fast adsorption kinetics seen with S-PAC coatings can be advantageous in a scenario in which an immediate contaminant removal is required. However, the superior adsorption capability of S-PAC compared with PAC and the other adsorbents is coupled with substantial flux resistance resulting from the small particle size, which could lead to increased energy requirements. A balance among flux resistance, adsorption capacity, and adsorption kinetics is desirable for optimizing filtration efficiency.

If S-PAC is produced in slurry form, a separate tank in the filtration system will need to be allocated for containment of the S-PAC slurry to be added to the influent water for the membrane coatings. The additional tank is not needed for PAC applications

because PAC may be added in powder form. For full-scale implementations of carbon coatings, an analysis of the cost for use of an adsorbent will need to be conducted, accounting for CUR, adsorbent price, space and energy requirements, and improvements or reductions in membrane life expectancy associated with adsorbent applications.

6.2 Future Work

Based on the favorable results of this project, it would be beneficial to expand the scope of the membrane coating method. For example, it would be useful to assess the stability of carbon coatings in cross-flow filtrations, and a lab-scale hollow fiber membrane setup may be constructed. Ensuring that the adsorbent coats the membrane evenly will potentially be a challenge encountered. Additional investigations for improving the adherence of carbon on the membrane may be needed before the technique can be implemented successfully in full-scale systems.

In addition, there is potential for small-particle adsorbents like S-PAC to pass through the membrane. This is an important point to address because it is not desirable to have particles loaded with adsorbed contaminants entering drinking water supplies. Furthermore, the influence of NOM on the efficacy of membrane coatings was not addressed in this study and would be useful for additional assessment of the carbon coating technique, especially since a previous study concluded that NOM eliminates the issue of flux decline in S-PAC filtrations (*92*). Finally, improvements to the adsorption model are needed, and a model may be developed for MWCNTs and NGPs as well.

APPENDICES

Appendix A

Additional Figures

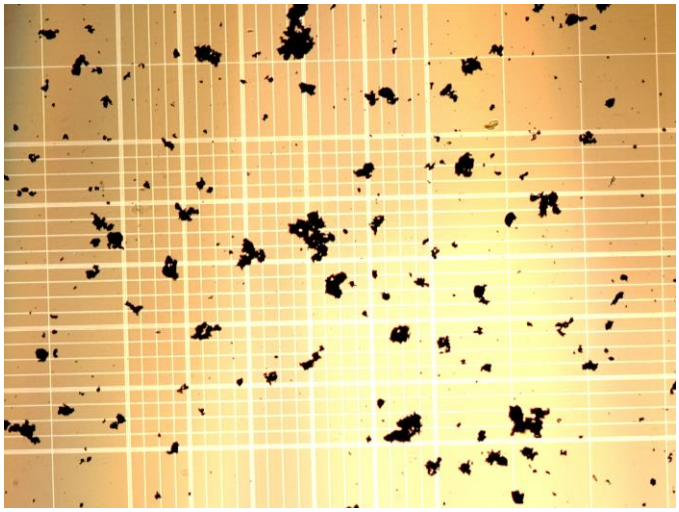

Figure A-1. WPH PAC on a hemocytometer viewed at 4× magnification under a microscope.

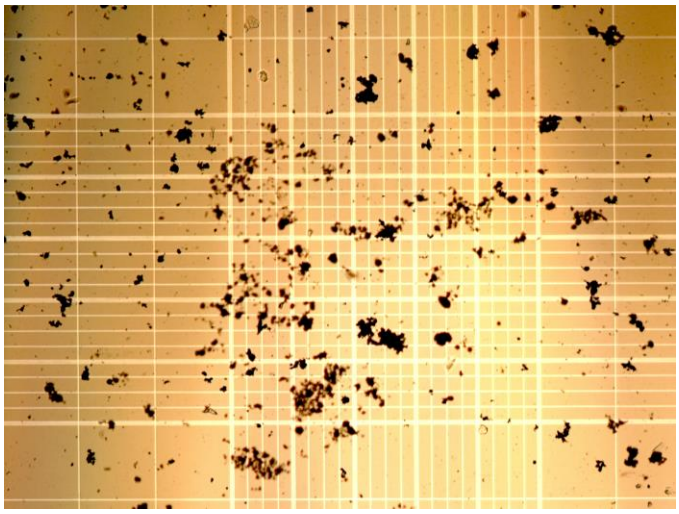

Figure A-2. Sonicated NGPs on a hemocytometer viewed at 4× magnification under a microscope.

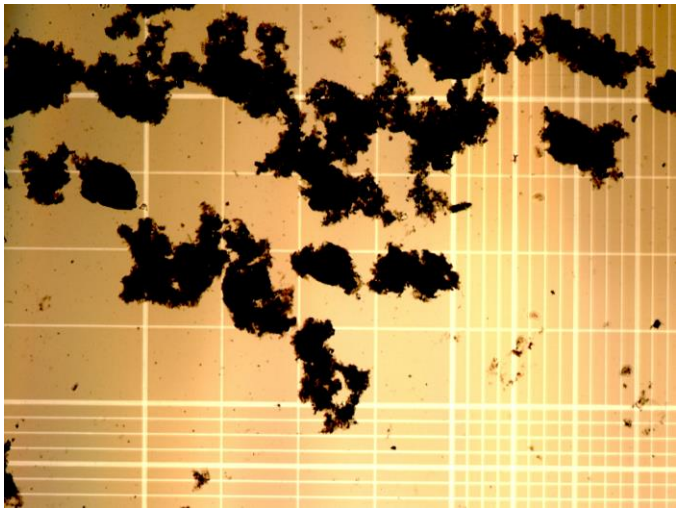

Figure A-3. Sonicated MWCNTs on a hemocytometer viewed at 4× magnification under a microscope.

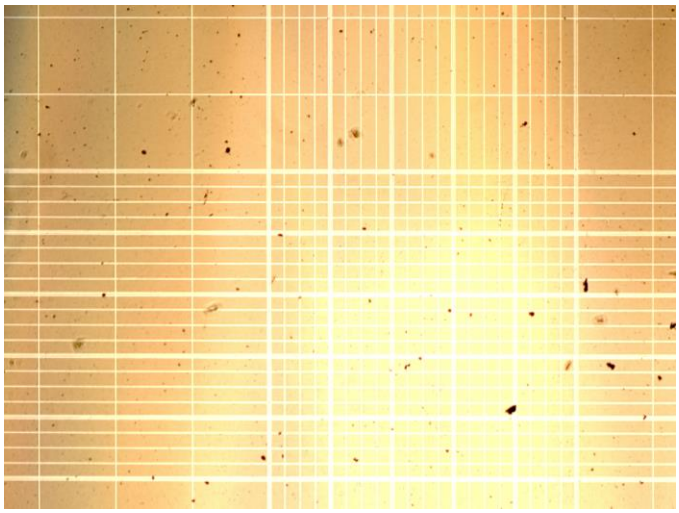

Figure A-4. Sonicated S-PAC on a hemocytometer viewed at 4× magnification under a microscope.

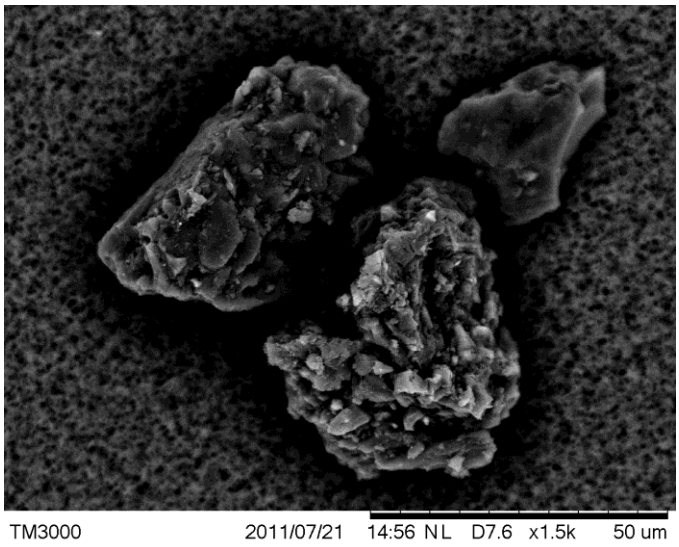

Figure A-5. SEM image of F400 PAC seen at 1,500× magnification on a PVDF membrane with pore size 0.1 μm.

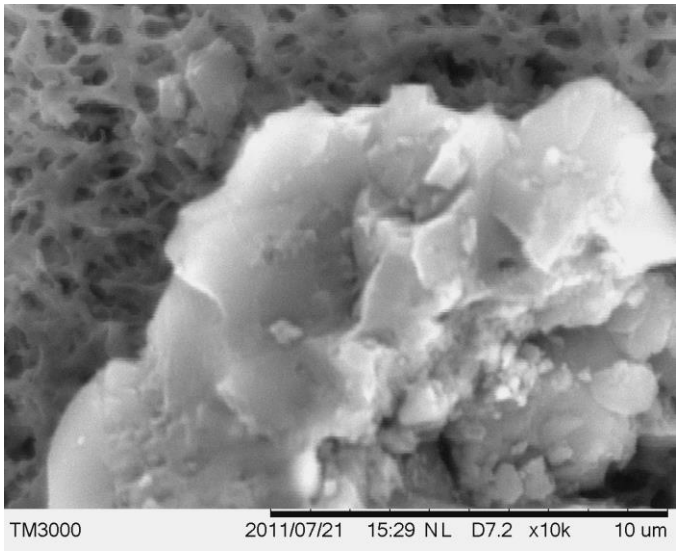

Figure A-6. SEM image of a WPH PAC particle seen at 10,000× magnification on a PVDF membrane with pore size 0.1 μm.

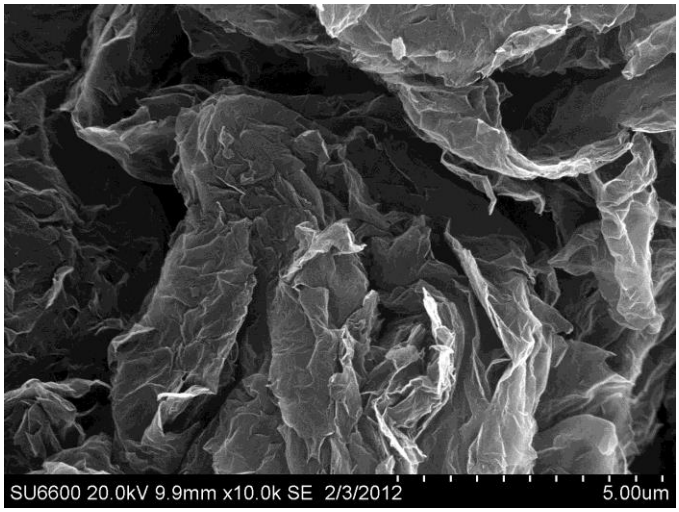

Figure A-7. SEM image of NGPs at 10,000× magnification on a PVDF membrane with pore size 0.1 μm.

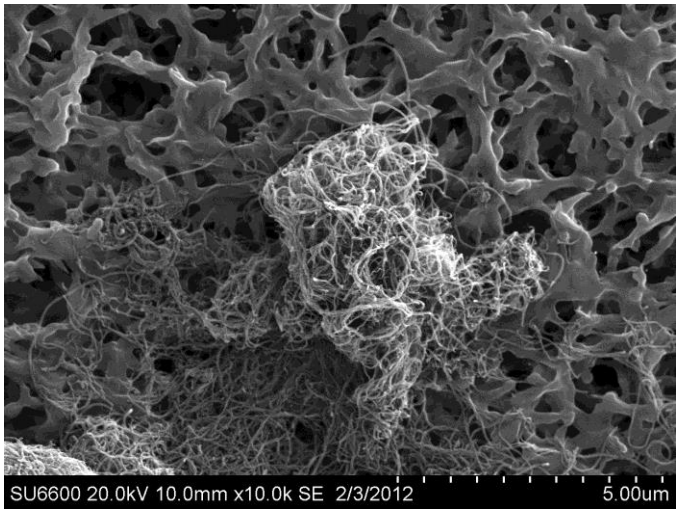

Figure A-8. SEM image of MWCNTs at 10,000× magnification on a PVDF membrane with pore size 0.1 μm.

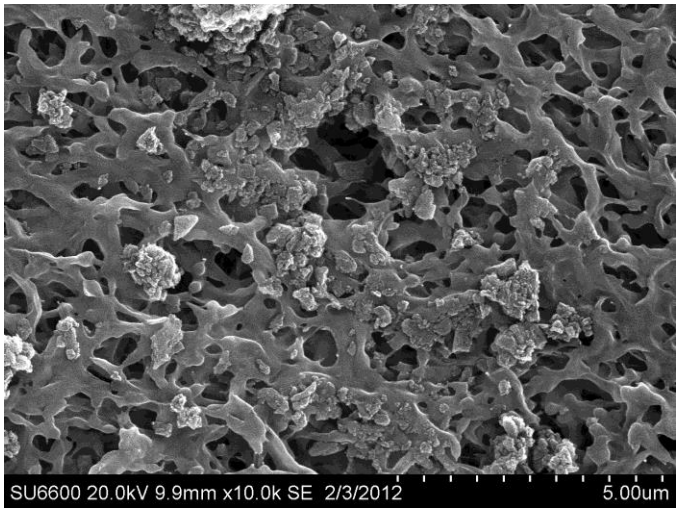

Figure A-9. SEM image of WPH S-PAC viewed at 10,000× magnification on a PVDF membrane with pore size 0.1 μm.

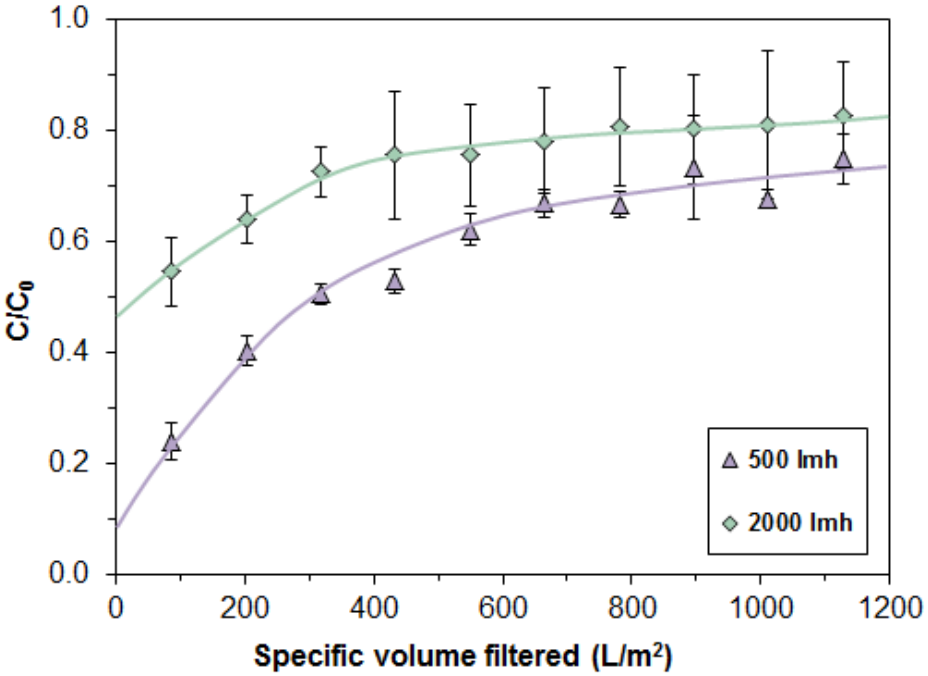

Figure A-10. Effect of flux on methylene blue removal by membranes coated with 1 mg (2.9 g/m^2) of WPH PAC. The solid lines in the figure represent trendlines.

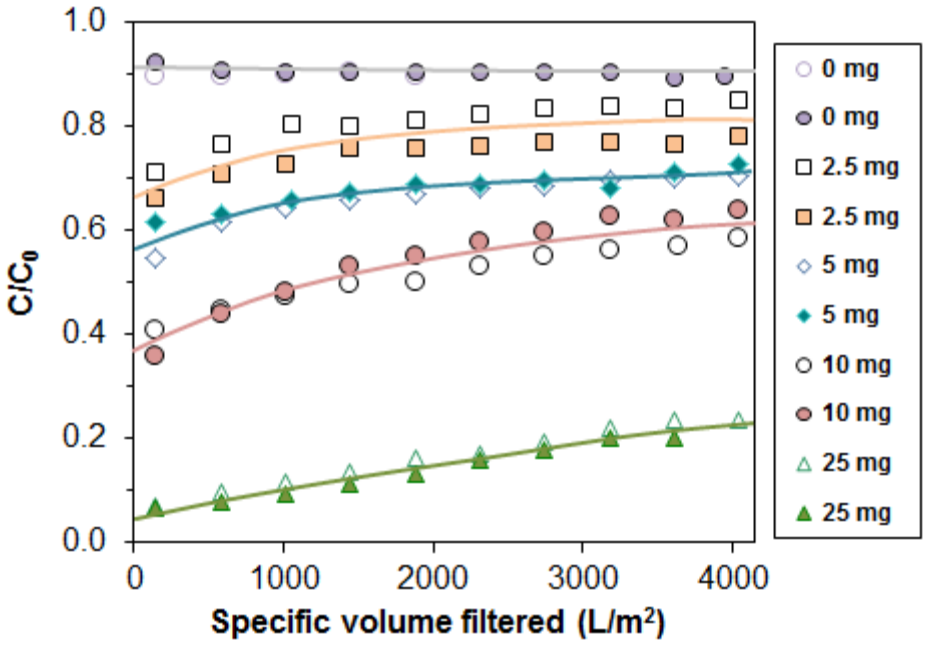

Figure A-11. Atrazine removal by membranes coated with different masses of 65 µm F400 PAC with a flux of 2000 lmh. The solid lines in the figure correspond to trendlines, and these filtrations were done with an atrazine solution that was later found to be contaminated by an unknown, tritiated compound.

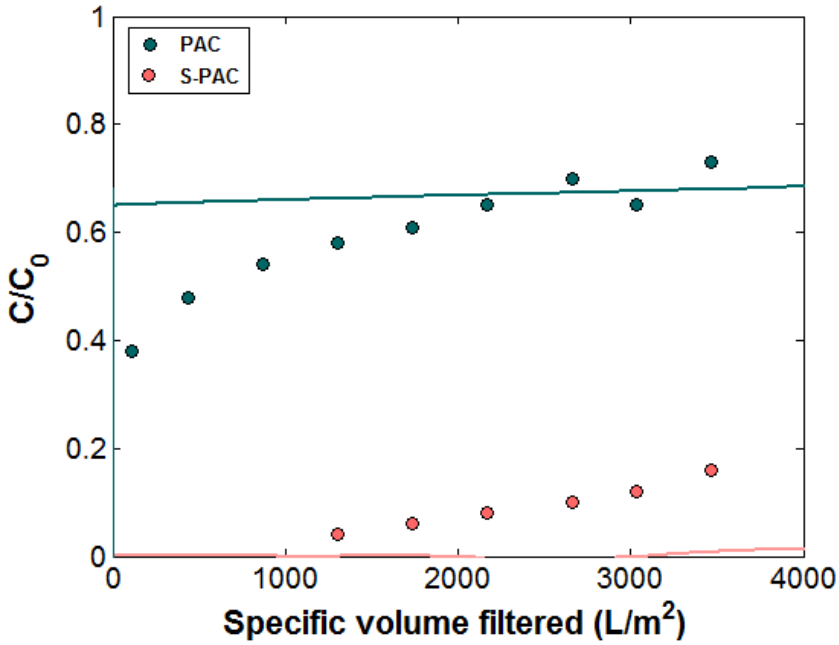

Figure A-12. HSDM application for atrazine retention in 2-mg S-PAC and PAC membrane coatings, with a flux of 2000 lmh.

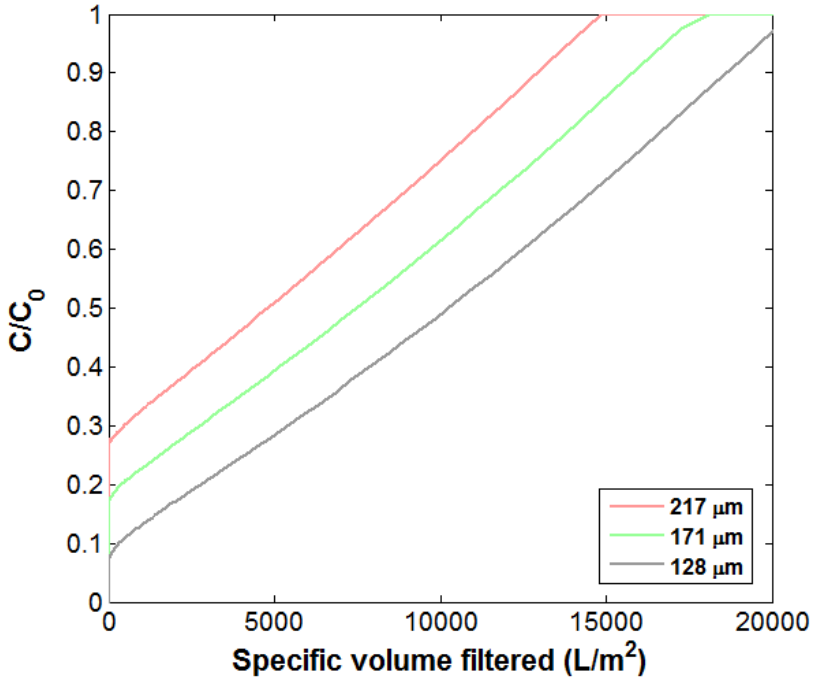

Figure A-13. Simulated HSDM breakthrough curves for methylene blue retention in 50 mg F400 PAC coatings with average particle size 170 µm, as well as 130 µm and 210 µm (± 25% of average particle size).

Appendix B

MATLAB Programs

In the following MATLAB programs, parameters that may be changed are underlined and in bold.

Appendix B-1: Particle Size Distribution Program

This script is designed to categorize particles in groups based on particle diameter. It requires images obtained on a hemocytometer under a microscope. The lightness setting on the microscope may need to be set higher for the program to recognize all particles. A calibration must be done to convert from particle area in pixels given by the program to area in metric units. Note that MATLAB often displays images at a reduced magnification, which needs to be considered when calibrating the program.

```
clear all;
viewImages = 1;
[filename pathname] = uigetfile('E:\17 um 6.2x 10x zoom 0.3 mg
per mL\.jpg','Select File','MultiSelect','on');
filename = cellstr(filename);
nThresh = 1;
totalVolumeMatrix = zeros(1,nThresh);
manualCount = zeros(1,length(filename));
autoCount = zeros(1,length(filename));
counts = zeros(length(filename),1);

for k = 1:length(filename);
file = char(filename(k));
I = imread([pathname file]);
level = 0.4;
% Decrease 'level' to detect lighter particles.
BW = im2bw(I,level);
M = bwlabeln(BW);
N = label2rgb(M,@lines);
BW2 = im2bw(N, level);
[B,L] = bwboundaries(BW2,'noholes');
stats = regionprops(L,'Area');
totalArea = 0;
```

```
for m = 1:length(stats);
totalArea = totalArea + stats(m).Area;
ParticleAreas(m) = stats(m).Area;

% To convert particle area (in pixels) to diameter (um), using
%calibration:
Diameter(m) = ((ParticleAreas(m)/3.14)^(0.5))*2*(enter conversion
factor);
end

% For sorting particle sizes into groups based on diameter:
max = max(Diameter);
min = min(Diameter);
numberofbars = 59;
barwidth = 5; % µm

% Second x-value (upper limit for 1st particle size group):
x = 10; % µm

for l = 1: numberofbars;
y = 0;
for j = 1:length(Diameter);
if Diameter(j)< x && Diameter(j) >= (x-barwidth);
y = y + 1;
end;
end;
BarData(l) = y;
x = x + barwidth;
end;
end

% Number of particles per size fraction:
sum = 0;
for j=1:length(BarData);
sum = sum + BarData(j);
end;

% X-values for sorting:
x = [5 10 15 20 25 30 35 40 45 50 55 60 65 70 75 80 85 90 95 100
105 110 115 120 125 130 135 140 145 150 155 160 165 170 175 180
185 190 195 200 205 210 215 220 225 230 235 240 245 250 255 260
265 270 275 280 285 290 295 300];  % µm

% Total volume for each size fraction:
for j=1:(length(BarData));
Volume(j) = BarData(j)*(4/3)*3.14*(((x(j+1)+x(j))/2/2))^3;  % µm^3
end;

% Total volume for all particles:
sum = 0;
for j=1:length(Volume);
sum = sum + Volume(j);
end;
```

```
% Percent volume of each size fraction:
for j=1:length(Volume);
PercentVol(j) = Volume(j)/sum * 100;
end;

% Graph output parameters:

% X-values for plotting purposes (Delete last number from x array
% used previously):
x = [5 10 15 20 25 30 35 40 45 50 55 60 65 70 75 80 85 90 95 100
105 110 115 120 125 130 135 140 145 150 155 160 165 170 175 180
185 190 195 200 205 210 215 220 225 230 235 240 245 250 255 260
265 270 275 280 285 290 295];
figure
bar(x, PercentVol, 'histc')
title 'Particle Size Distribution'
xlabel('Particle diameter (\mum)')
ylabel('Percent Volume')
% Axis limits:
axis([0, 300, 0, 50])
% Bar color:
colormap summer
% Tick marks:
set(gca, 'Xtick', [10 20 30 40 50 60 70 80 90 100 110 120 130 140
150 160 170 180 190 200 210 220 230 240 250 260 270 280 290]);

figure, imshow(label2rgb(L, @lines), 'InitialMagnification',67)
```

Appendix B-2: Monolayer Mass Program

This program determines the mass (µg) of carbon needed to form a single layer on the membrane, assuming spherical particles arranged in the configuration depicted in Figure 5.5. The corresponding interparticle porosity is also computed.

```
function [monolayer,porosity] = monolayer(dp,p,d)

%Inputs: dp = particle diameter (cm), p = apparent particle
%density (g/L), d = membrane diameter (m).

p = p/1000; % Density conversion to g/mL
Area = 3.14*(d/2)^2; % Membrane area, m^2
ESArea = 3^(1/2)*(dp/2/100)^2-3.14/2*(dp/2/100)^2; % Area of one
%interparticle void, m^2
PArea = 3.14*(dp/2/100)^2; % Cross-sectional area of one
%particle, m^2
np = Area/(ESArea+PArea); % Number of particles
V = (4/3)*3.14*((dp/2)^3); % Particle Volume, cm^3
monolayer = np*V*p*1e6; % Monolayer mass, µg
```

```
bedV = 3.14*(d/2)^2*dp/100; % Bed volume, m^3
porosity = (bedV-np*V/100/100/100)/bedV;

end
```

Appendix B-3: HSDM Script

This program is referenced in the graphing program in Appendix B-4. It includes Equations 7 through 9, rearranged to enable simplification with orthogonal collocation. The output is a matrix of liquid and solid-phase concentrations at the specified time points and locations throughout the adsorbent particle and carbon bed. The Mth column in the output matrix (with "M" being the number of collocation points in the carbon layer) is the reduced permeate concentration, C/C_0. Original equations may be found in ref. [48].

```
function [dCdt] = HSDM(t,C)

Parameters % Name of the script in Appendix B-7

i = [0.21535 0.42063 0.60625 0.76351 0.88508 0.96524 1];
% Collocation points in the particle (spherical coordinates)

[Ai,Bi,W] = ABsym(i); % Program in Appendix B-6

N = length(i)-1;

l = [0 0.03376 0.16939 0.38069 0.61930 0.83060 0.96623 1];
% Collocation points in the adsorbent bed (Cartesian coordinates)
M = length(l)-2;

[Al,Bl] = AB(l); % Program in Appendix B-5

dCdt = zeros(M+1+(N+1)*(M+2)+1,1);

for l = 2:M+2
sum = 0;
sum2 = 0;
for k=2:M+2
sum = sum+Al(l,k)*C(k-1);
sum2 = sum2+Bl(l,k)*C(k-1);
end;
```

```
dCdt(l-1) = -Dg*sum-Dg*Al(l,1)-3*Dg*Sts*(C(l-1)-
C(N*(M+2)+(M+1)+1)*qe/(K*(qO-C(N*(M+2)+(M+1)+l)*qe))/C0);
end;

g = 1;

for i = 1:N
for l = 1:(M+2)
for k = 1:N+1
index(N+1-(k-1)) = l+(M+1)+N*(M+2)-(k-1)*(M+2);
end;
sum(g) = 0;
for j=1:(N+1)
sum(g) = sum(g)+Bi(i,j)*C(index(j));
end;
dCdt(g+(M+1)) = E*sum(g);
g = g+1;
end;
end;

for l = 1:M+2
for k = 1:N
index(N-(k-1)) = l+(M+1)+N*(M+2)-k*(M+2);
end;
sum(l) = 0;
for j = 1:N
sum(l) = sum(l)+W(j)/W(N+1)*dCdt(index(j));
end;
if l == 1
dCdt(l+(M+1)+N*(M+2)) = Sts/W(N+1)*(C(M+1+(N+1)*(M+2)+1)-
(C(l+(M+1)+N*(M+2))*qe/(K*(qO-C(l+(M+1)+N*(M+2))*qe))/C0))-
sum(l);
else
dCdt(l+(M+1)+N*(M+2)) = Sts/W(N+1)*(C(l-1)-
(C(l+(M+1)+N*(M+2))*qe/(K*(qO-C(l+(M+1)+N*(M+2))*qe))/C0))-
sum(l);
end;
end;

dCdt(M+1+(N+1)*(M+2)+1) = 0;

end
```

Appendix B-4: HSDM Output Graphing Program

```
Parameters % Name of the script in Appendix B-7

options = odeset('reltol',1e-6,'BDF','on');
 [t1,C1] = ode15s(@HSDM,tspan,x0,options);

for i = 1:numel(t1)
t1(i) = t1(i)*Tao*Dg;
svf(i) = t1(i)/60/60*Flux;
if C1(i,M+1)*(8e-5*svf(i)+0.7455) < 1
C1(i,M+1) = C1(i,M+1)*(8e-5*svf(i)+0.7455); % Accounts for
% removal of contaminant by membrane.
else
C1(i,M+1) = 1;
end;
end;

figure;
plot(svf,C1(:,M+1))
ylabel('C/C_0');
set(gca,'FontSize',16);
xlabel('Specific volume filtered (L/m^2)');
set(gca,'FontSize',16);
x2 = 1000; % Upper limit of x-axis (L/m^2)
axis([0,x2,0,1]);
set(gca,'FontSize',12);
```

Appendix B-5: Subprogram for Asymmetric Orthogonal Collocation Coefficients

This program generates the A and B matrices used for the axial collocation points in the HSDM program (*59*).

```
function [A,B] = AB(x)

for j=1:length(x)
for i=1:length(x)
Q(j,i) = x(j)^(i-1);
C(j,i) = (i-1)*x(j)^(i-2);
D(j,i) = (i-1)*(i-2)*x(j)^(i-3);
C(1,1) = 0;
D(1,1) = 0;
D(1,2)
end;
end;
A = C/Q;
B = D/Q;
end
```

Appendix B-6: Subprogram for Symmetric Orthogonal Collocation Coefficients

This program generates the A, B, and W matrices used for the radial collocation points in the HSDM program (*59*).

```
function [A,B,W] = ABsym(x)

for i=1:length(x)
for j=1:length(x)
Q(j,i) = x(j)^(2*i-2);
C(j,i) = (2*i-2)*x(j)^(2*i-3);
D(j,i) = (2*i-2)*(2*i-1)*x(j)^(2*i-4);
end;
f(i) = 1/(2*i-2+3);
end;
A = C/Q;
B = D/Q;
W = f/Q;

end
```

Appendix B-7: Miscellaneous Parameters Script

These are the remaining variables needed to run the HSDM program.

```
M = 6; % Number of collocation points in carbon layer.
N = 6; % Number of collocation points in carbon particle.

% Initial conditions:
x0 = zeros(M+1+(N+1)*(M+2)+1,1);
x0(length(x0)) = 1;

MW = 284.1; % Molecular weight of solute, g/mol
p = 900; % Apparent particle density, g/L
C0 = 2.44e-6; % Feed concentration, mol/L

% Langmuir constants:
K = 80.4*1000*MW; % L/mol (80.4 L/mg)
qO = 138.1/1000/MW; % mol/g (138.1 mg/g)
qe = qO*K*C0/(K*C0+1);

dp = 24.75; % Particle diameter, µm
dp = dp/1e6*100; % Particle diameter, cm
Flux = 500; % lmh
ps = 1; % Density of solution, g/cm^3
MV = 0.347; % Molar volume of solute, m^3/kmol
vs = Flux/60/60*100/1000; % Superficial velocity, cm/s
m0 = 1000; % Applied mass, µg
```

```
d = 0.021; % Membrane diameter, m

% Liquid diffusion coefficient:
n = 0.96; % Water viscosity, centipoise (1 poise = 1 g/(cm*s))
n = n/1000*100/100; % Viscosity, kg/(m*s)
T = 295; % Temperature, K
MW2 = 18; % MW of water, g/mol
Dl = 1.17e-16*T*(2.6*MW2)^(0.5)/(n*(MV^(0.6)))*100*100; % cm^2/s

% Porosity & volume of carbon layer:
Vp = m0/1e6/p/1000; % Volume of particles, m^3
[m1,porosity] = monolayer(dp,p,d); % Monolayer mass, µg, &
% porosity
if m0 < m1
V = 3.14*(d/2)^2*ap*2/100; % Bed volume, m^3
Ep = (V-Vp)/V;
else
Ep = 0.37;
V = Vp/(1-Ep); % Bed volume assuming 0.37 porosity, m^3
end;

% Film transfer coefficient:
n2 = 0.0096; % Viscosity, poise [1 poise = 1 g/(cm*s)]
Sc = n2/(ps*Dl); % Schmidt number
R = ps*dp*vs/(n2*(1-Ep)); % Reynolds number
kf = 2.4*R^(-0.66)*vs/(Sc^0.58); % Film transfer coefficient,cm/s

% Solid-phase diffusion coefficient:
Ds = 5*Dl*Ep*C0/(p*qe); % cm^2/s

Area = 3.14*(d/2)^2; % Membrane area, m^2
F = Flux/1000*Area/60/60; % Flow rate, m^3/s
Dg = p*(1-Ep)*qe/(Ep*C0); % Solute distribution parameter
Tao = V/F; % Hydraulic resistance, s
E = Ds*Dg*Tao/((dp/2)^2); % Surface diffusion modulus
Sts = Tao*kf/(dp/2)*((1-Ep)/Ep); % Stanton number for solid phase
tspan = [0,10]; % Time span
```

Appendix B-8: LDF Model Script

This script may be used to evaluate the LDFQ or LDFC models.

```
R = 0.018; % Obtained from Eq. 11
Flux = 500;

% Enter data for regression:
x = [87 202 318 434 549 665 780 896 1012 1127]; % SVF, L/m^2
c = [0.24 0.4 0.5 0.53 0.62 0.67 0.67 0.73 0.68 0.75];  % C/C_0

for i = 1:numel(x)
t(i) = x(i)/Flux*60; % min
c(i) = c(i)/(8e-5*x(i)+0.7455); %Accounts for removal by membrane
if c(i) > 1
c(i) = 0.999; % Ensures that permeate values do not exceed 1.
end;
% For LDFQ:
c1(i) = (R/(1-R)*log(c(i))-1/(1-R)*log(1-c(i))-1);
% For LDFC:
% c1(i) = (1-(R*log(1-c(i))-log(c(i)))/(1-R));
end;

[r,m,b] = regression(c1,t);

t0 = b; % Characteristic time, min
slope = m; % Slope of the regression lines in Eq. 10, 12, and 13

n = 1000; % Number of points for model evaluation
c(1) = 0.001; % 1st point
for j = 2:n
    c(j) = c(j-1) + 1/n;
end;

for i = 1:numel(c)
% LDFQ Equation:
t(i) = t0 + slope*(R*log(c(i))/(1-R)-log(1-c(i))/(1-R)-1); % min
% LDFC Equation:
% t(i) = t0 + slope*(1-(R*log(1-c(i))-log(c(i)))/(1-R)); % min
svf(i) = t(i)/60*Flux; % L/m^2
if c(i) < 1
c(i) = c(i)*(8e-5*svf(i)+0.7455); % Accounts for removal by
% membrane
end;
end;

figure;
plot(svf,c);
axis([0,1200,0,1]);
ylabel('C/C_0');
xlabel('Specific volume filtered (L/m^2)');
```

REFERENCES

1. Macdonald, R.W.; Barrie, L.A.; Bidleman, T.F.; Diamond, M.L.; Gregor, D.J.; Semkin, R.G.; Strachan, W.M.J.; Li, Y.F.; Wania, F.; Alaee, M.; Alexeeva, L.B.; Backus, S.M.; Bailey, R.; Bewers, J.M.; Gobeil, C.; Halsall, C.J.; Harner, T.; Hoff, J.T.; Jantunen, L.M.M.; Lockhart, W.L.; Mackay, D.; Muir, D.C.G.; Pudykiewicz, J.; Reimer, K.J.; Smith, J.N.; Stern, G.A.; Schoeder, W.H.; Wagemann, R.; Yunker, M.B. Contaminants in the Canadian Arctic: 5 years of progress in understanding sources, occurrence, and pathways. *Sci. Total Environ.* **2000**, *254*, 93-234.

2. Focazio, M.J.; Kolpin, D.W.; Barnes, K.K.; Furlong, E.T.; Meyer, M.T.; Zaugg, S.D.; Barber, L.B.; Thurman, M.E. A national reconnaissance for pharmaceuticals and other organic wastewater contaminants in the United States – II) Untreated drinking water sources. *Sci. Total Environ.* **2008**, *402*, 201-216.

3. Sullivan, P.J.; Agardy, F.J.; Clark, J.J. *The Environmental Science of Drinking Water*; Elsevier: Burlington, MA, 2005.

4. O'Connor, J.T.; O'Connor, T.; Twait, R. *Water Treatment: Plant Performance Evaluations and Operations*; Wiley and Sons: Hoboken, NJ, 2009.

5. Reiter, L; Falk, H.; Groat, C.; Coussens, C.M., Eds. *From Source Water to Drinking Water*; The National Academies Press: Washington, D.C., 2004.

6. Fitzer, E.; Köchling, K.H.; Boehm, H.P.; Marsh, H. Recommended terminology for the description of carbon as a solid. *Pure Appl. Chem.* **1995**, *67*, 473-508.

7. Marsh, H.; Rodríguez-Reinoso, F. *Activated Carbon*; Elsevier Ltd.: Oxford, UK, 2006.

8. Okada, K.; Yamamoto, N.; Kameshima, Y.; Yasumori, A. Porous properties of activated carbons from waste newspapers prepared by chemical and physical activation. *J. Colloid Interf. Sci.* **2003**, *262*, 179-193.

9. Wu, F.C.; Tseng, R.L.; Juang, R.S. Adsorption of dyes and phenols from water on the activated carbons prepared from corncob wastes. *Environ. Technol.* **2001**, *22*, 205-213.

10. Sontheimer, H.; Crittenden, J.C.; Summers, R.S. *Activated Carbon for Water Treatment*; Fed. Rep. of Germany, 1988.

11. Bandosz, T., Ed. *Activated Carbon Surfaces in Environmental Remediation*, 1st Ed.; Elsevier Ltd.: New York, NY, 2006.

12. Yadav, A. Approaches to mitigate the impact of dissolved organic matter on the adsorption of synthetic organic contaminants by activated carbon. Thesis. Clemson University, Clemson, SC, 2007.

13. Shmidt, J.L.; Pimenov, A.V.; Lieberman, A.I.; Cheh, H.Y. Kinetics of adsorption with granular, powdered, and fibrous activated carbon. *Separ. Sci. Technol*. **1997**, *32*, 2105-2114.

14. Müller, E.A.; Gubbins, K.E. Molecular simulation study of hydrophilic and hydrophobic behavior of activated carbon surfaces. *Carbon* **1998**, *36*, 1433-1438.

15. Karanfil, T.; Kilduff, J.E. Role of granular activated carbon surface chemistry on the adsorption of organic pollutants. 1. Priority pollutants. *Environ. Sci. Technol.* **1999**, *33*, 3217-3224.

16. Julien, F.; Baudu, M.; Mazet, M. Relationship between chemical and physical surface properties of activated carbon. *Wat. Res.* **1998**, *32*, 3414-3424.

17. Seredych, M.; Hulicova-Jurcakova, D.; Lu, G.Q.; Bandosz, T.J. Surface functional groups of carbons and the effects of their chemical character, density and accessibility to ions on electrochemical performance. *Carbon* **2008**, *46*, 1475-1488.

18. Bourikas, K.; Kordulis, C.; Lycourghiotis, A. Differential potentiometric titration: Development of a methodology for determining the point of zero charge of metal (hydr)oxides by one titration curve. *Environ. Sci. Technol.* **2005**, *39*, 4100-4108.

19. Dastgheib, S.A.; Karanfil, T.; Cheng, W. Tailoring activated carbons for enhanced removal of natural organic matter from natural waters. *Carbon* **2004**, *42*, 547-557.

20. Ding, L.; Snoeyink, V.L.; Mariñas, B.J.; Yue, Z.; Economy, J. Effects of powdered activated carbon pore size distribution on the competitive adsorption of aqueous atrazine and natural organic matter. *Environ. Sci. Technol.* **2008**, *42*, 1227-1231.

21. Weber, W.J.; Voice, T.C.; Jodellah, A. Adsorption of humic substances: The effects of heterogeneity and system characteristics. *J. Am. Water Works Assoc.* **1983**, *75*, 612-618.

22. Ando, N.; Matsui, Y.; Kurotobi, R.; Nakano, Y.; Matsushita, T.; Ohno, K. Comparison of natural organic matter adsorption capacities of super-powdered activated carbon and powdered activated carbon. *Wat. Res.* **2010**, *44*, 4127-4136.

23. Heijman, S.G.J.; Hamad, J.Z., Kennedy, M.D.; Schippers, J.; Amy, G. Submicron powdered activated carbon used as a pre-coat in ceramic microfiltration. *Desalination and Water Treatment* **2009**, *9*, 86-91.

24. Iijima, S. Helical microtubules of graphitic carbon. *Nature* **1991**, *354*, 56-58.

25. Ajayan, P.M. Nanotubes from carbon. *Chem. Rev.* **1999**, *99*, 1787-1799.

26. Yang, K.; Xing, B. Desorption of polycyclic aromatic hydrocarbons from carbon nanomaterials in water. *Environ. Pollut.* **2007**, *145*, 529-537.

27. Zhang, S.; Shao, T.; Kaplan, S.; Karanfil, T. The impacts of aggregation and surface chemistry of carbon nanotubes on the adsorption of synthetic organic compounds. *Environ. Sci. Technol.* **2009**, *43*, 5719-5725.

28. Zhang, S.; Shao, T.; Selcen Kose, H.; Karanfil, T. Adsorption of aromatic compounds by carbonaceous adsorbents: A comparative study on granular activated carbon, activated carbon fiber, and carbon nanotubes. *Environ. Sci. Technol.* **2010**, *44*, 6377-6383.

29. Cho, H.; Smith, B.A.; Wnuk, J.D.; Fairbrother, D.H.; Ball, W.P. Influence of surface oxides on the adsorption of naphthalene onto mutliwalled carbon nanotubes. *Environ. Sci. Technol.* **2008**, *42*, 2899-2905.

30. Abergel, D.; Apalkov, V.; Berashevich, J.; Ziegler, K.; Chakraborty, T. Properties of graphene: A theoretical perspective. *Adv. Phys.* **2010**, *59*, 261-482.

31. Zhang, W.; Zhou, C.; Zhou, W.; Lei, A.; Zhang, O.; Wan, O.; Zou, B. Fast and considerable adsorption of methylene blue dye onto graphene oxide. *Bull. Environ. Contam. Toxicol.* **2011**, *87*, 86-90.

32. Ramesha, G.K.; Kumara, A.V.; Muralidhara, H.B.; Sampath, S. Graphene and graphene oxide as effective adsorbents toward anionic and cationic dyes. *J. Colloid Interf. Sci.* **2011**, *361*, 270-277.

33. Christensen, M., Ed. *Microfiltration and Ultrafiltration Membranes for Drinking Water – Manual of Water Supply Practices.* 1st Ed.; American Water Works Association: Denver, CO, 2005.

34. Kawamura, S. *Integrated Design and Operation of Water Treatment Facilities*; John Wiley and Sons, Inc.: New York, NY, 2000.

35. Williams, J.; Goel, R.; Flora, J.; Vidic, R. Investigating role of growing adsorbent bed in a dead-end PAC/UF process. *J. Environ. Eng.* **2005**, *131*, 1583-1588.

36. Yiantsios, S.J.; Karabelas, A.J. An experimental study of humic acid and powdered activated carbon deposition on membranes and their removal by backwashing. *Desalination* **2001**, *140*, 190-209.

37. Campos, C.; Mariñas, B.J.; Snoeyink, V.L.; Baudin, I.; Laîné, J.M. PAC-membrane filtration process. I: Model development. *J. Environ. Eng*. **2000**, *126*, 98-103.

38. Campos, C.; Mariñas, B.J.; Snoeyink, V.L.; Baudin, I.; Laîné, J.M. Adsorption of trace organic compounds in CRISTAL® processes. *Desalination* **1998**, *117*, 265-271.

39. Snyder, S.A.; Adham, S.; Redding, A.M.; Cannon, F.S.; DeCarolis, J.; Oppenheimer, J.; Wert, E.C.; Yoon, Y. Role of membranes and activated carbon in the removal of endocrine disruptors and pharmaceuticals. *Desalination* **2007**, *202*, 156-181.

40. Baudin, I.; Chevalier, M.R.; Anselme, C.; Cornu, S.; Laîné J.M. L'Apie and Vigneux case studies: First months of operation. *Desalination* **1997**, *113*, 273-275.

41. Oh, H.; Yu, M.; Takizawa, S.; Ohgaki, S. Evaluation of PAC behavior and fouling formation in an integrated PAC-UF membrane for surface water treatment. *Desalination* **2006**, *192*, 54-62.

42. Campinas, M.; Rosa, M.J. Assessing PAC contribution to the NOM fouling control in PAC/UF systems. *Wat. Res.* **2010**, *44*, 1636-1644.

43. Mozia, S.; Tomaszewcka, M.; Morawski, A. Studies on the effect of humic acids and phenol on adsorption-ultrafiltration process performance. *Wat. Res.*, **2005**, *39*, 501-509.

44. Thiruvenkatachari, R.; Shim, W.; Lee, J.; Aim, R.; Moon, H.; A novel method of powdered activated carbon (PAC) pre-coated microfiltration (MF) hollow fiber hybrid membrane for domestic wastewater treatment. *Colloids and Surfaces A.* **2006**, *274*, 24-33.

45. Ba, C.; Economy, J. Preparation and characterization of a neutrally charged antifouling nanofiltration membrane by coating a layer of sulfonated poly(ether ether ketone) on a positively charged nanofiltration membrane. *J. Membrane Sci.* **2010**, *362*, 192-201.

46. Kotov, N.A.; Haraszti, T.; Turi, L.; Zavala, G.; Geer, R.E.; Dékány, I.; Fendler, J.H. Mechanism of and defect formation in the self-assembly of polymeric polycation-montmorillonite ultrathin films. *J. Am. Chem. Soc.* **1997**, *119*, 6821-6832.

47. Park, S.; Wei, S.; Mizaikoff, B.; Taylor, A.E.; Favero, C.; Huang, C. Degradation of amine-based water treatment polymers during chloramination as *N*-nitrosodimethylamine (NDMA) precursors. *Environ. Sci. Technol.* **2009**, *43*, 1360-1366.

48. Crittenden, J.C.; Weber, W.J. Predictive model for design of fixed-bed adsorbers: Parameter estimation and model development. *J. Environ. Eng*. **1978**, *104*, 433-443.

49. Lua, A.C.; Jia, Q. Adsorption of phenol by oil-palm-shell activated carbons in a fixed bed. *Chem. Eng. J.* **2009**, *150*, 455-461.

50. Traegner, U.K.; Suidan, M.T. Parameter evaluation for carbon adsorption. *J. Environ. Eng.* **1989**, *115*, 109-128.

51. Wilke, C.R.; Chang, P. Correlation of diffusion coefficient in dilute solutions. A.I.Ch.E. **1955**, *1*, 264-270.

52. Brodkey, R.S.; Hershey, H.C. *Transport Phenomena: A Unified Approach*; McGraw-Hill: New York, NY, 1988.

53. Williamson, J.E.; Bazaire, K.E.; Geankoplis, C.J. Liquid-phase mass transfer at low Reynolds numbers. *Ind. Engng. Chem. Fundam.* **1963**, *2*, 126-129.

54. Crittenden, J.C.; Weber, W.J. Predictive model for design of fixed-bed adsorbers: Model verification. *J. Environ. Eng*. **1978**, *104*, 433-443.

55. Crittenden, J.C.; Wong, B.W.C.; Thacker, W.E.; Hinrichs, R.L. Mathematical model of sequential loading in fixed-bed adsorbers. *Water Pollut. Control*. **1980**, *52*, 2780-2794.

56. Smith, E.H. Modified solution of Homogeneous Surface Diffusion Model for adsorption. *J. Environ. Eng.* **1991**, *117*, 320-338.

57. Hand, D.W.; Crittenden, J.C.; Thacker, W.E. Simplified models for design of fixed-bed adsorption systems. *J. Environ. Eng.* **1983**, *110*, 440-456.

58. Heinemann, H.; Carberry, J.J., Eds. *Catalysis Reviews*; Marcel Dekker, Inc.: New York, NY, 1974.

59. Finlayson, B.A. *The Method of Weighted Residuals and Variational Principles*; Academic Press, Inc.: New York, NY, 1972.

60. Kim, B.R.; Schmitz, R.A.; Snoeyink, V.L.; Tauxe, G.W. Analysis of models for dichloramine removal by activated carbon in batch and packed-bed reactors using quasilinearization and orthogonal collocation methods. *Wat. Res.* **1978**, *12*, 317-326.

61. Zhang, X.; Zhao, X.; Hu, J.; Wei, C.; Bi, H.T. Adsorption dynamics of trichlorofluoromethane in activated carbon fiber beds. *J. Hazard. Mater.* **2011**, *186*, 1816-1822.

62. Sircar, S.; Hufton, J.R. Why does the linear driving force model for adsorption work? *Adsorption* **2000**, *6*, 137-147.

63. Worch, E. Fixed-bed adsorption in drinking water treatment: A critical review on models and parameter estimation. *J. Water Supply Res. T.* **2008**, *57*, 171-183.

64. Murillo, R.; García, T.; Aylón, E.; Callén, M.S.; Navarro, M.V.; López, J.M.; Mastral, A.M. Adsorption of phenanthrene on activated carbons: Breakthrough curve modeling. *Carbon* **2004**, *42*, 2009-2017.

65. Bhattacharjee, S.; Sharma, A.; Bhattacharya, P.K. A unified model for flux prediction during batch-cell ultrafiltration. *J. Membrane Sci.* **1996**, *111*, 243-258.

66. Jiang, H.; Adams, C.; Graziano, N.; Roberson, A.; McGuire, M.; Khiari, D. Occurrence and removal of chloro-s-triazines in water treatment plants. *Environ. Sci. Technol.* **2006**, *40*, 3609-3616.

67. Pelekani, C.; Snoeyink, V.L. Competitive adsorption between atrazine and methylene blue on activated carbon: The importance of pore size distribution. *Carbon* **2000**, *38*, 1423-1436.

68. Colombini, M.P.; Fuoco, R.; Giannarelli, S.; Pospisil, L.; Trskova, R. Protonation and degradation reactions of s-triazine herbicides. *Microchem. J.* **1998**, *59*, 239-245.

69. Disanto, A.R.; Wagner, J.G. Pharmacokinetics of highly ionized drugs II: Methylene blue—Absorption, metabolism, and excretion in man and dog after oral administration. *J. Pharm. Sci.* **1972,** *61*, 1086-1090.

70. Technical Factsheet on: Atrazine. http://water.epa.gov/drink/contaminants/basicinformation/historical/up...

71. Executive Summary Methylene Blue http://ntp.niehs.nih.gov/.

72. Meylan, W.M.; Howard, P.H. Atom/fragment contribution method for estimating octanol/water partition coefficients. *J. Pharm. Sci*. **1995**, *84*, 83-92.

73. Liu, M.Y.; Tsang, D.C.; Hu, J.; Ng, K.T.; Liu, T.; Lo, I.M. Adsorption of methylene blue and phenol by wood waste derived activated carbon. *J. Environ. Eng*. **2008**, *134*, 338-345.

74. Serpa, A.L.; Schneider, I.; Rubio, J. Adsorption onto fluidized powdered activated carbon flocs-PACF. *Environ. Sci. Technol.* **2005**, *39*, 885-888.

75. Campos, C.; Snoeyink, V.L.; Mariñas, B.; Baudin, I.; Laîné, J.M. Atrazine removal by powdered activated carbon in floc blanket reactors. *Wat. Res.* **2000**, *34*, 4070-4080.

76. Jack, A.M; Clark, M.M. Using PAC/UF to treat a low-quality surface water. *J. Am. Water Works Assoc.* **1998**, *90*, 83-95.

77. Apul O.G.; Shao, T.; Zhang, S.; Karanfil, T. The impact of carbon nanotube morphology on phenanthrene adsorption. *Environ. Toxicol. Chem.* **2012**, *31*, 73-78.

78. Dunn, S.; Knappe, D. Effect of powdered activated carbon base material and size on disinfection by-product precursor removal. Proceedings of the American Water Works Association 2011 Annual Conference and Exposition.

79. Chingombe, P.; Saha, B.; Wakeman, R.J. Sorption of atrazine on conventional and surface modified activated carbons. *J. Colloid Interf. Sci.* **2006**, *302*, 408-416.

80. Dai, M. The effect of zeta potential of activated carbon on the adsorption of dyes from aqueous solution. *J. Colloid Interf. Sci.* **1994**, *164*, 223-228.

81. Cumberland, D.J.; Crawford, R.J. *The Packing of Particles*; Elsevier Science Publishers B.V.: The Netherlands, 1987.

82. Webb, P.A. Volume and density determinations for particle technologists. www.particletesting.com/docs/density_determinations.pdf.

83. Droste, R.L. *Theory and Practice of Water and Wastewater Treatment*. John Wiley & Sons, Inc.: Canada, 1997.

84. Yao, Y.; Xu, F.; Chen, M.; Xu, Z.; Zhu, Z. Adsorption behavior of methylene blue on carbon nanotubes. *Bioresource Technol.* **2010**, *101*, 3040-3046.

85. Yan, X.M.; Shi, B.Y.; Lu, J.J.; Feng, C.H.; Wang, D.S.; Tang, H.X. Adsorption and desorption of atrazine on carbon nanotubes. *J. Colloid Interf. Sci.* **2008**, *321*, 30-38.

86. Celano, G.; Šmejkalová, D.; Spaccini, R.; Piccolo, A. Interactions of three s-triazines with humic acids of different structure. *J. Agric. Food Chem.* **2008**, *56*, 7360-7366.

87. Abu-Zreig, M.; Rudra, R.P.; Dickinson, W.T.; Evans, L.J. Effect of surfactants on sorption of atrazine by soil. *J. Contam. Hydrol.* **1999**, *36*, 249-263.

88. Lesan, H.M.; Bhandari, A. Contact-time-dependent atrazine residue formation in surface soils. *Wat. Res.* **2004**, *38*, 4435-4445.

89. Saffron, C.M.; Park, J.; Dale, B.E.; Voice, T.C. Kinetics of contaminant desorption from soil: Comparison of model formulations using the Akaike information criterion. *Environ. Sci. Technol.* **2006**, *40*, 7662-7667.

90. van Deemter, J.J.; Zuiderweg, F.J.; Klinkenberg, A. Longitudinal diffusion and resistance to mass transfer as causes of nonideality in chromatography. *Chem. Eng. Sci.* **1956**, *5*, 271-289.

91. Chang, S.; Waite, T.D.; Fane, A.G. A simplified model for trace organics removal by continuous flow PAC adsorption/submerged membrane processes. *J. Membrane Sci.* **2005**, *253*, 81-87.

92. Matsui, Y.; Hasegawa, H.; Ohno, K.; Matsushita, T.; Mima, S.; Kawase, Y.; Aizawa, T. Effects of super-powdered activated carbon pretreatment on coagulation and trans-membrane pressure buildup during microfiltration. *Wat. Res.* **2009**, *43*, 5160-5170.

93. Katsoufidou, K.; Yiantsios, S.G.; Karabelas, A.J. A study of ultrafiltration membrane fouling by humic acids and flux recovery by backwashing: Experiments and modeling. *J. Membrane Sci.* **2005**, *266*, 40-50.